Nanoindentation twin-sensitive measurements and strengthening model of HPT OFHC 99.99% purity copper

Elsevier Editorial System(tm) for Materials Science & Engineering A

Manuscript Draft

Manuscript Number: MSEA-D-20-01640R2

Title: Nanoindentation twin-sensitive measurements and strengthening model of HPT OFHC 99.99% purity copper

Article Type: Research Paper

Keywords: OFHC pure copper; Twinning; HPT; Nanoindentation; ISE; TEM.

Corresponding Author: Professor Marcello Cabibbo, PhD

Corresponding Author's Institution: università politecnica delle marche

First Author: Marcello Cabibbo, PhD

Order of Authors: Marcello Cabibbo, PhD

Abstract: Severe plastic deformation (SPD) techniques are among the most effective deformation modes of introducing a high rate and density of dislocations in metallic materials and alloys. The newly introduced dislocations have different characters. These were classified after Hansen and the Risœ group as statistically stored (SSD), also called incidental dislocations (ID), and geometrically necessary (GND) dislocations. As the strain cumulates some of these dislocations, namely the GNDs, are promoted to form very-low, low, and eventually high-angle boundaries. That is, new cell and grain structured are formed as the plastic deformation accumulate. Studies of the early stages of plastic deformation inducing microstructure modifications are properly carried out on pure metals as they strengthen only by the effect of dislocation, crystallite boundaries, and texturing of the metallic matrix. On this basis, the present work focuses on an electron microscopy study of the early plastic deformation stages induced in an OFHC 99.99% pure copper by high-pressure torsion (HPT). A threshold stress for the initiation of twinning formation within the Cu-grains was identified. Nanoindentation measurements were performed at different penetration depths. Thus, a correlation between the tip size-sensitive hardness evaluation (known as indentation size effect, ISE), occurring at the lower penetration depths, and the twinning formation during the early stages of HPT was found.

Cover letter

The present manuscript entitled: “Nanoindentation twin-sensitive measurements and strengthening model of HPT OFHC 99.99% purity copper” by Marcello Cabibbo (DIISM / Università Politecnica delle Marche, Via Brecce Bianche 12, 60131 – Ancona, Italy) focuses on early stages of plastic deformation induced in a high-purity copper by high pressure torsion (HPT).
The objectives and methodologies of the manuscript are within the aims and scopes of the journal. A discussion section deals with the role of twinning formation on nanoindentation ISE and with a strengthening model also discussed with previously published contributions. Most of the referenced published works together with some previously published papers by this author on SPD techniques appeared in Materials Science and Engineering A journal.

The manuscript is original and no part of it has been published before, nor is any part of it under consideration for publication at another journal.

The author also declares no conflicts of interest.

Yours, sincerely,
Prof. Marcello Cabibbo

Response letter to the Reviewer's comments

Author thanks the accurate overview and useful comments made by the Reviewer(s) as they allowed to improve readability and correct some misleading scheme and micrograph description.
With this regard, all the Reviewer's comments are here reported along with the author's replies and explanations.

In section 2.1: Rods usually have diameters instead of widths. The author should explain what "fully-annealed" means as opposed to just "annealed".
R: Fully-annealed meant a baking to the set temperature of 673K for 1 hour and slowly cooling to room temperature in a turned off furnace. Thence the following was added at the beginning of subsection 2.1- The material: "Rods of OFHC 99.99% pure copper had a 10 mm diameter and they were subjected to a fully annealing treatment. This consisted to baking the rods at 673 K for 1 h, followed by cooling in the turned off furnace, corresponding to a cooling to room temperature of 8 h."

Later it states: "As shown in Fig. 1, the annealed Cu showed a coarse grained structure with no significant present of free dislocations within the grains." The author should explain the difference between "free dislocations" and "dislocations".
R: For a sake of clarity the above mentioned sentence was rewritten and it now reads as: "As shown in Fig. 1, the annealed Cu showed a coarse grained structure with rare presence of few dislocations within the grains whose volume fraction was so low to do not form any sort of entanglement."

Later, just after eqt. 1a; the reviewer does not follow how the author gets eqt 1b from eqt 1a according to the wording of the above statement.
R: The description of Eqs. (1a) and 1(b) was rewritten as in the following:
Since in the present case the disc thickness does not dependent on the rotation angle $\omega = 2\pi N$, the resulting HPT shear strain, γ, can be calculated as [5], Eq. (1a):

$$\gamma = 2\pi Nr/t \qquad \text{Eq. (1a)}$$

where r is the distance from the disc center, ranging from 0 to the disc radius, R, t is the disc thickness. For large HPT strains, typically $\gamma > 0.8$, the resulting equivalent vön Mises strain can be written as [5,37], Eq. (1b):

$$\varepsilon_{eq} = \frac{2}{\sqrt{3}} ln\left[\left(\frac{1+\gamma^2}{4}\right)^{0.5} + \frac{\gamma}{2}\right] \qquad \text{Eq. (1b)}$$

On the other hand, for low HPT shear strain, γ, the resulting vön Mises strain can be expressed as [5,37], Eq. (1c):

$$\varepsilon_{eq} = \frac{\gamma}{\sqrt{3}} = \frac{2\pi Nr}{t\sqrt{3}} \qquad \text{Eq. (1c)}$$

Thence, in the present study, Eq. (1c) was the one used to model the shear deformation induced in the OFHC pure Cu.

Using eqt 1b and inputting in N=1/2 turn, the reviewer find that the equivalent strain is =1.812r. if r=5 mm (the maximum radius possible based on a 10 mm diameter disk) then the equivalent strain is 9.06. However, the author states that the maximum equivalent strain reached was 3.63. The author needs to provide details of how he came up with this maximum equivalent strain.
R: Author wish to thank the Reviewer for having found these misleading data referring to the schematic representation of Fig. 2. The HPT disc diameter was 10 mm, so the radius R appearing in the Fig. 2 should had read R = 5 mm, and the TEM disc extraction distance from HPT disc center should had read r = 2 mm. Both these data were corrected in the new update scheme now appearing in Fig. 2. Fig. 2 and Table 2 captions were modified accordingly and they now read as: "Fig. 2. To scale scheme of HPT showing the location of extraction of the TEM discs.", and "Table 2. Equivalent strain ε_{eq} obtained by the different HPT experimental parameters at N = 1/18 (lowest) to 1/2 turns (highest), at radial distances r = 2 mm (almost mid-radius) from disc thick-center."

The following statement also needs to be explained in more detail: "HPT was carried out by depressing the vertical anvils to a depth of 0.05 mm." what is this depth relative to?
R: This sentence now reads: “HPT was carried out by depressing the vertical anvils to a depth of 0.05 mm into the 1 mm-thick HPT discs.”

The reviewer suggests the author make figure 2 such that the TEM 3 mm diameter (in the text it states the TEM disks were 3 mm wide(?); is this a width or a diameter?) disk is drawn to scale with respect to the 10 mm diameter disk.
R: Author agrees with the Reviewer’ suggestion. This was corrected as: “The 3 mm TEM discs were ~1 mm-thick, this initial thickness was mechanically grinded…”. More important, all the schematic representation of Fig. 2 was modified to make it to scale and clearer to the reader. The scheme of Fig. 2 was modified to show the details drawn to scale.

For figure 3, the end of the caption states, "SAEDP with crystallographic spot selected is reported in the inset. The DF g-vector was g = [02-2] allow to show the dislocations and cell/grain boundary lines." This does not appear to be grammatically correct as written and therefore the reviewer does not understand what it means.
R: This sentence was rewritten and it now reads as: “Inset in b) is the indexed SAEDP. DF g-vector was g = [02-2]. By selecting this crystallographic plane the existing tangled dislocations and cell boundaries within the grains were almost entirely visible as they mostly lying in the [022] planes and (022) directions.”

In the experimental results section, the statement "It resulted that twinning formation within the Cu-grains started to occur from a HPT strain level of eq = 0.91." does not appear to be grammatically correct and should therefore be rewritten to help the reader understand the meaning of this sentence. The sentence following this should also be rewritten as one aspect that is unclear is at what shear deformation level is being referred to? The next sentence also needs to be rewritten as it is not understandable as written.
R: These three sentences were rewritten and they now reads: “The initial generation of twinning, lying within the Cu-grains, started from a HPT strain level of ε_{eq} = 0.91. From this strain level of HPT plastic deformation the OFHC Cu started to refine its grain structure. At the same time, twins started to cumulate within the refining grains. That is, the deformation process did change microstructure mechanism as it proceeded only by SSD and GND formation at the earliest strain levels ε_{eq} = 0.40 (Fig. 3(a)). From a strain ε_{eq} = 0.91 both SSD and GND eventually were promoted to form the first low-angle boundaries (cell boundaries) and new high-angle grain boundaries (Fig. 3(b)).”

In section 3.1, the author describes a statistical analysis and mentioned grain sizes. Perhaps the authors need to qualify such statements in more detail regarding the limited area viewed by the TEM foil.
R: This was addressed in the Table 3 caption as follows: “Table 3. Mean grain, d_g, and cell size, d_{cell}, of OFHC CU subjected to HPT at ε_{eq} = 0.40 to 3.63. These mean values were determined out of 3 different areas of the TEM thin discs accounting of some 0.56-to-0.74 mm^2 per each experimental condition.”

The means in which the author came up with the error bars in figure 6 need to be explained.
R: This was addressed in the Fig. 6 caption as follows: “Fig. 6. Plot of hardness, H, and reduced elastic modulus, Er, vs. cumulative HPT straining, ε_{eq} = 0.40 to 3.63. Error bars were determined by averaging the obtained values from the 64 individual nanoindentation measurements that were performed at each experimental condition.”

The figure 4 caption. The author should explain how the Cu crystal was oriented at [011] (can the author input a SAEDP as an insert here?) and also explain if these bf TEM images? The author needs to label the g vector.
R: TEM images of Fig. 4 are bright-field (BF) micrographs, thence the g-vector is not needed here. Orientation was oriented simply by tilting the thin foils as to show the lowest crystallographic Kikuchi bands

symmetry for +(022) and –(022) lines. The [011]-zone axis SAEDP was added as Figure 4(d) and Fig. 4 caption was modified to now reads as:" Fig. 4. Twinning formation induced by the HPT strain, ε_{eq} = 0.91, a); ε_{eq} = 1.81, b); ε_{eq} = 3.63, c). Cu crystals were oriented along [011]-zone axis to properly reveal the twin boundaries and lines; related indexed SAEDP is reported in d)."

For figure 11, the author needs to label the g vector on the image.
R: TEM images of Fig. 11 are bright-field (BF) micrographs, thence the g-vector is not needed here.

The author should state how many nanoindents were performed in this work and their repeatability. The author should explain at what equivalent strains all the nanoindents were made at.
R: The following was added in the Experimental section: "Each reported experimental datum is the average value obtained out of series of [8x8]-matrix of individual measurements spaced 250 µm apart, giving a total of 64 individual measurements per experimental condition."

The author should explain what technique was used to measure the composition of the pure Cu rod as listed in table 1.
R: Caption of Table 1 reports the supplier purity identification. This now reads as: "Table 1. Chemical composition of the OFHC 99.99% purity copper (wt.%x1000), as reported by the supplier (purity standard identified as DIN1706-NFA51050 / CuC1, source FRW^{TM})."

<u>All modifications and added sentences were outlined in yellow in the manuscript body text</u>.

Nanoindentation twin-sensitive measurements and strengthening model of HPT OFHC 99.99% purity copper

Marcello Cabibbo

DIISM / Università Politecnica delle Marche, Via Brecce Bianche 12, 60131 – Ancona, Italy.

Keywords: OFHC pure copper; Twinning; HPT; Nanoindentation; ISE; TEM.

Abstract. Severe plastic deformation (SPD) techniques are among the most effective deformation modes of introducing a high rate and density of dislocations in metallic materials and alloys. The newly introduced dislocations have different characters. These were classified after Hansen and the Risœ group as statistically stored (SSD), also called incidental dislocations (ID), and geometrically necessary (GND) dislocations. As the strain cumulates some of these dislocations, namely the GNDs, are promoted to form very-low, low, and eventually high-angle boundaries. That is, new cell and grain structured are formed as the plastic deformation accumulate. Studies of the early stages of plastic deformation inducing microstructure modifications are properly carried out on pure metals as they strengthen only by the effect of dislocation, crystallite boundaries, and texturing of the metallic matrix. On this basis, the present work focuses on an electron microscopy study of the early plastic deformation stages induced in an OFHC 99.99% pure copper by high-pressure torsion (HPT). A threshold stress for the initiation of twinning formation within the Cu-grains was identified. Nanoindentation measurements were performed at different penetration depths. Thus, a correlation between the tip size-sensitive hardness evaluation (known as indentation size effect, ISE), occurring at the lower penetration depths, and the twinning formation during the early stages of HPT was found.

1. Introduction

Ultrafine-grained (UFG) metallic materials and alloys are known to possess superior mechanical properties compared to the conventional grained counterparts **[1]**. In the last two-three decades a number of grain refining methods were proposed and developed. These include top-down approaches, such as severe plastic deformation (SPD), and bottom-up approaches starting from powder metallurgy processes **[2-4]**. As for the top-down approach, different SPD techniques showed reliable, cost-effective, and promising means for obtaining thermally stable ultra-fine, and sometimes nanometric size, grain structures of metals and alloys. The most relevant such techniques are high-pressure torsion (HPT), equal-channel angular pressing (ECAP), accumulative roll-bonding (ARB), accumulative press-bonding (APB), twist extrusion (TE), friction stir processing (FSP), cyclic extrusion-compression (CEC), repetitive corrugation and straightening (RCS), accumulative back extrusion (ABE) and hydrostatic extrusion (HSE), high-pressure sliding (HPS) (**[5-13]** and references therein).
The exceptional mechanical properties achieved by the UFG metals are due to both the sub-micron cell, grain size and the mobile dislocations inside the UFGs. In addition, low stacking fault energy (SFE) materials, such as copper-alloys and pure copper, also strengthen by twinning formation within the grains. It is generally agreed that UFG processes proceed from newly introduced tangled dislocations (TD) and cell boundaries (both very-low, VLABs, and low-angle boundaries, LABs) [**5-8,11,14-19**]. These are continuously introduced in the material and eventually induced to rearrange and form cell structures by SPD. Cells are in turns induced to increase their

misorientation angle to eventually become grain boundaries (high-angle boundaries, HABs) **[14-19]**. More specifically, the dislocations generated during plastic deformation are typically classified into two categories that reflect the sliding mobility attitude and the special arrangement they tend to follow. Thus, according to Huges *et al.* [**20**] one type of dislocations are called geometrically necessary dislocations (GNDs), and incidental dislocations (IDs), or statistically stored dislocations (SSDs). GNBs form between regions of different strain patterns to accommodate the strain induced lattice rotation. IDs (or SSDs) form by random trapping processes of dislocation during straining. These latter are stored within the already existing grains as a statistical necessary process of accommodating the local straining in the metallic material. Upon SPD different strain patterns can be activated in the material involving activation of different slip systems. This, in turns, generates differences in the partitioning of slip activity on the same slip systems of the newly introduced dislocations, and then differences in the level of equivalent strain acting in the deforming material. These differences in slip pattern ultimately promote dislocation interactions, namely between IDs, GNDs, and among IDs and GNDs, resulting in a significant energy reduction. That is, the evolution of IDs and GNDs to form cell and eventually grain boundaries is an energetic favoured process. The here described dislocation evolutionary process is in fact a statistically and thermodynamically most probable phenomenon which is activated and promoted in the metallic material by plastic and severe plastic deformation.

The dislocation strengthening mechanisms generate by the SPD are usually studied by using pure metals, such aluminum [**14,15,16,18,19,21,22**], nickel [**23-25**], copper [**11,26**], and the like [**27,28**]. In the present study a OFHC 99.99% pure copper was used to analyse the early stages of plastic deformation induced by HPT. The choice of using HPT was motivated by the almost continuous range of induced strains that it is able to induce simply by limiting the number and fraction of the metal rotations under pressure. In fact, HPT generates progressive plastic deformation levels for given number and fraction of turns, from the disc center, where it is minimum, to the disc periphery, where it is at its maximum. On the other hand, the level of induced strain strongly depends on the number of HPT rotations, *N*. In HPT the sample, in form of a thin disk, is placed between two large anvils and subjected to a high pressure and concurrent torsional straining. This way, the two meaningful parameters are the magnitude of the imposed pressure, *P*, and the number of revolutions applied to the sample, *N*. Since, the imposed strain chiefly depends on the distance from the center of the disc, the microstructure modifications imposed by HPT are greatly inhomogeneous, but continuous. For the present study, this latter aspect is considered as a key microstructure aspect to determine the minimum necessary strain level to form twinned grains in a fully annealed 99.99% pure copper.

In this sense, HPT is different from most of the other SPD processes where generally strain gradients are generated quite quickly, making almost impossible to determine the early stages of cell structure formation [**4-6,12,14,21**].

Strain gradients and strain hardening, as well as metal plastic properties, such yield stress, hardness, toughness, strongly depend on the dislocation density, ρ_{disl}. That is, when a material is plastically deformed the dislocation density increases, leading to strain gradients and metal strain hardening. The metallic material straining under plastic deformation is usually studied by electron microscopy techniques (electron back-scattered diffraction, EBSD, field-emission gun scanning electron microscopy, FEGSEM, transmission electron microscopy, TEM). Anyhow, this was also characterized by performing extremely small indentations (nanoindentations) in low defect density materials [**29,30**]. Moreover, whenever strain gradients are formed by indentations using either pyramidal or conical indenters, GNDs are generated into the material in order to accommodate the induced strain [**31,32**]. Since strain gradient increases by reducing the deformation scale (*i.e.*, small penetration depths) the density of GNDs and, consequently, the hardness of the material, increase when the size of the deformed region decreases. This quite important experimental factor that affect the process of indentation of metallic material is known as indentation size effect (ISE) [**32,33**]. With this regard, it was found that the ISE can be described by taking into account the two types of

dislocations introduced during plastic deformation. That is, ISE can be described by taking into account the statistically stored dislocations (SSDs) and the geometrically necessary dislocations (GNDs) [**34**].

Following pioneering studies by Nix and Gao [**32**] nanoindentation hardness overestimation for lower tip penetration depths is directly related to underestimation of the plastic zone volume. In their model, Nix and Gao assumed plastic zones assumed to be hemispherical with a radius equal to the contact radius, a. This hemisphere volume, V, is calculated as: $V = 2\pi h^3/(3\tan^3\varphi)$, where φ represents the angle between the indenter surface and the sample surface. The nanoindentation hardness, H, is thus expressed as: $H = 3\cdot\sigma = 3^{1.5}\alpha Gb(\rho_{SSD} + \rho_{GND})^{0.5}$, being α a constant, G the material shear modulus, b its Burgers vector, and ρ_{SSD}, ρ_{GND} the densities of SSDs and GNDs, respectively. Since, H_0 can be defined as the material hardness with no GNDs, this can be expressed as $H_0 = 3^{1.5}\alpha Gb(\rho_{SSD})^{0.5}$, and thence $H = [1+(\rho_{GND}/\rho_{SSD})]^{0.5} = [1+(h_0/h)]^{0.5}$, where h_0 is the length scale factor of a given material under indentation, and h is the indentation penetration depth. This approach is based on a hemispheric volume limited to the next neighbouring of the tip radius and the lateral tip edges. This indeed can depends on the type of tip used, that is a pyramidal Berkovich, a spherical, or a cube-corner geometry [**34**].

Anyhow, GNDs is known to spread beyond the hemisphere, and thence the plastic zone volume needs to be corrected. This was addressed later on by Durst *et al.* [**35,36**], where the radius of the plastic zone is assumed to be $f\cdot a$, with f ranging from 1 to 3.5, and simulated by finite element means. In polycrystals, hardness always increases with decreasing grain size. This behaviour can be explained by the well-known Hall-Petch (H-P) relationship, which is based on the interaction between dislocations and grain boundaries in grain structured metallic materials. Anyhow, whenever the grains are wide and/or the indentation penetration depth is shallow, the generation of SSDs and GNDs is strongly related to one or few grains. This means, that the indentation plastic zone in these cases has a local character.

In this study the role of twinning formation within plastically deforming grains on the nanoindentation grain size sensitive hardness and reduced Young's modulus measurements is addressed. In particular, the minimum necessary strain by HPT to induce twinning formation was identified and the role of the twin formation on the nanoindentation depth sensitive measurements was addressed.

2. Experimental procedures and Method

2.1. The material

Rods of OFHC 99.99% pure copper had a 10 mm diameter and they were subjected to a fully annealing treatment. This consisted to baking the rods at 673 K for 1 h, followed by cooling in the turned off furnace, corresponding to a cooling to room temperature of 8 h. The chemical composition of the 99.99% purity Cu is reported in **Table 1**. Discs 1.0 mm-thick were cut from the annealed bars. As shown in **Fig. 1**, the annealed Cu showed a coarse grained structure with rare presence of few dislocations within the grains whose volume fraction was so low to do not form any sort of entanglement.

2.2. High-pressure torsion (HPT) process

The fully-annealed OFHC 99.99% pure Cu in form of a disc of 10 mm-diameter and 1.0 mm-thick was subjected to HPT under quasi-constrained conditions at room temperature, thus avoiding material outflow during straining. Different strain levels were induced into the metals as to get a discrete close range of strain levels, *i.e.*, from ε_{eq} = 0.40-to-3.63, by processing HPT at following rotation number fractions: N = 1/18, 1/8, 1/6, 1/4, 1/3, 1/2 turns.

Fig. 2 is a scheme of the HPT strain deformation imposed to a typical disc sample, where the incremental shear strain is given by $d\omega/\omega$, being ω the angular rotation around the disc center.
Since in the present case the disc thickness does not dependent on the rotation angle $\omega = 2\pi N$, the resulting HPT shear strain, γ, can be calculated as **[5]**, Eq. (1a):

$$\gamma = 2\pi Nr/t \qquad \text{Eq. (1a)}$$

where r is the distance from the disc center, ranging from 0 to the disc radius, R, t is the disc thickness. For large HPT strains, typically $\gamma > 0.8$, the resulting equivalent vön Mises strain can be written as **[5,37]**, Eq. (1b):

$$\varepsilon_{eq} = \frac{2}{\sqrt{3}} ln\left[\left(\frac{1+\gamma^2}{4}\right)^{0.5} + \frac{\gamma}{2}\right] \qquad \text{Eq. (1b)}$$

On the other hand, for low HPT shear strain, γ, the resulting vön Mises strain can be expressed as **[5,37]**, Eq. (1c):

$$\varepsilon_{eq} = \frac{\gamma}{\sqrt{3}} = \frac{2\pi Nr}{t\sqrt{3}} \qquad \text{Eq. (1c)}$$

Thence, in the present study, Eq. (1c) was the one used to model the shear deformation induced in the OFHC pure Cu.
HPT was carried out by depressing the vertical anvils to a depth of 0.05 mm into the 1 mm-thick HPT discs. Torsion strain was exerted by rotating the upper anvil at a low rotation speed of 0.7 rpm (~4° sec^{-1}) under a pressure of 2.0 GPa.
TEM inspections and nanoindentation measurements were performed at the mid-section of the discs (that is, at a thickness $t \cong 0.5$ mm) and at mid-radius (5 mm) from the disc center. Thus, according to Eq. (1b), the resulting equivalent strain, ε_{eq}, is as listed in **Table 2**.
The reason to use HPT to perform the present study is based on the possibility to generate low incremental strain levels, starting form a minimum level of equivalent strain as low as $\varepsilon_{eq} = 0.40$.
To avoid any possible artefact during sample preparation, the ~1 mm-thick HPT processed discs were prepared for TEM inspections by chemical and electro-chemical means only. They were first punched to 3 mm TEM discs from the above-mentioned HPT disc position and indicated in **Fig. 2**. The 3 mm TEM discs were ~1 mm-thick, this initial thickness was mechanically grinded and then electrochemically thinned and symmetrically polished to a ~200 μm thickness using a solution of 30% of phosphoric acid 20% ethylic alcohol in 50% distilled water at room temperature and a voltage of 12V. Prior final thinning to electron transparency by precision ion-milling (PIPS), the 200 μm-thick discs were fixed by a commercially pure 0.5 mm-thick copper ring with 3 mm external diameter. Then, this was thinned by Gatan™ PIPS with a low dual incident beam whose angle was fixed to 2° respect to the disc surface, to minimize the possible artefacts coming from the disc preparation (*i.e.*, to minimize the dislocations possibly introduced during the ion-milling process).

2.3. Sample preparation for TEM and method

TEM inspections were carried out in a Philips™ C-20® working at 200 keV with a double-tilt specimen holder equipped with a liquid-nitrogen cooling stage. Inspections were performed at the middle height of the HPT discs.
Two-beam excitation conditions were selected for most of the TEM observation and dislocation characterizations. Dislocation density, $\rho_{disl.}$, was quantitatively evaluated by stereological methods, such as the Ham's interception method [**38**]. Thence, $\rho_{disl.}$ was calculated through the count of

interception points between the mesh and the existing dislocations, n_{disl}, in the TEM micrographs. This was evaluated by $\rho_{disl.} = 2n_{disl}/(l_{mesh}t_{TEM})$, were, l_{mesh} is the total length of the mesh, and t_{TEM} is the thickness of the TEM foil. Crystal thickness, t_{TEM}, was determined through the diffracted beam intensity variation under dual beam conditions, using converged electron beam diffraction (CBED) patterns. This way, by plotting the linear interpolation of data points in a $S^2/n_{fringes}^2$ vs. $n_{fringes}^{-2}$ graph, where S is the fringes spacing, and $n_{fringes}$ the number of counted fringes, t_{TEM}^{-2} was determined at y-axis line intercept. The error due to the invisible dislocations (i.e., the ones oriented as to have $b \cdot g = 0$, where b is the Burgers vector and g refers to the dislocation lying crystallographic plane) is within the experimental error of the foil thickness evaluation. Cell (LAB) and grain boundary (HAB) misorientation were measured by Kikuchi band patterns. The misorientation angle measurement procedure by Kikuchi pattern on TEM is fully described elsewhere in previous published works by this author [**14-16**]. TEM inspections were carried out by orienting the Cu-matrix as to have [001], [011]-crystallographic planes || I_{beam} (electron beam direction).

2.4. Nanoindentation measurements

Nanoindentation measurements were performed at same HPT disc height as the one set for TEM inspections. For the nanoindentation measurements, samples were prepared by the same chemical polishing methods used for the TEM disc preparation. A Hysitron™ Triboscope UBI-1® was used. Calibration procedures were followed according to [**39**]. A trapezoidal load function of 5 s loading, 15 s at the set load, and 5 s unloading was used, with a set load, P_{Max} = 10 mN, and at a constant loading rate of 0.25 mN/s. Nanoindentations were performed for each experimental conditions, that is for strain levels ε_{eq} = 0.40-to-3.63. Each reported experimental datum is the average value obtained out of series of [8x8]-matrix of individual measurements spaced 250 μm apart, giving a total of 64 individual measurements per experimental condition.
Data analysis was performed according to the Oliver-Pharr model [**40**]. Thus, the hardness, H, was evaluated as $H = P_{Max}/A$, with $A = K_{ind}h_c^2$ being the contact area, K_{ind} an indenter tip dependent coefficient (24.56 for Berkovich tip [**41**]), h_c the contact depth related to the maximum penetration depth, h_m, which is $h_c = h_m - \chi P_{Max}/S$, χ = 0.75 for Berkovich tip [**40**] and S the material stiffness. This latter, according to the Oliver-Pharr approach [**40,41**] is measured as unloading slope at the maximum penetration depth, h_m, and it is $S = Bm(h_m - h_r)^{m-1}$, where B is the unloading curve intercept at $P = 0$, m is the unloading slope, and h_r is the residual depth (the permanent plastic penetration depth on unloading). Moreover, following the Oliver-Pharr method, the reduced elastic modulus can be derived as $E_r = [(\pi/4)^{0.5}/\beta] \cdot [S/(A)^{0.5}]$, where β = 1.034 for Berkovich tips [**40**]. Thence, in the present case, $H = 0.041 \cdot P_{Max}/h_c^2$ and $E_r = 0.173 \cdot S/h_c$.

3. Experimental Results

3.1. Microstructure

Fig. 3 shows representative TEM micrographs of the microstructure evolution driven by the HPT shear deformation, from ε_{eq} = 0.40 to 3.63.
The initial generation of twinning, lying within the Cu-grains, started from a HPT strain level of ε_{eq} = 0.91. From this strain level of HPT plastic deformation the OFHC Cu started to refine its grain structure. At the same time, twins started to cumulate within the refining grains. That is, the deformation process did change microstructure mechanism as it proceeded only by SSD and GND formation at the earliest strain levels ε_{eq} = 0.40 (**Fig. 3(a)**). From a strain ε_{eq} = 0.91 both SSD and GND eventually were promoted to form the first low-angle boundaries (cell boundaries) and new high-angle grain boundaries (**Fig. 3(b)**). At this latter strain level twinning started to form, and thus

this further strengthening mechanism started to operate within the pure Cu microstructure. Thence, the strain level ε_{eq} = 0.91 can be considered a threshold-like, or a cut-off lower strain limit, to initiate a microstructure twin strengthening. At strain levels above it, ε_{eq} > 1.21, the pure copper plastically deformed under HPT straining by further generation of GNDs, that eventually form grain boundaries, and by the combining strengthening effect of grain refinement and twinning-induced generation (**Fig. 3(c)-to-(f)**). With this respect, **Fig. 4** shows the evolution of the twinning induced to form and cumulate by the HPT shear deformation, from ε_{eq} = 0.91 to 3.63.

Moreover, the OFHC Cu microstructure evolved rapidly already in the early stages of straining (**Fig. 4(a),(b)**). It resulted that at strain level within ε_{eq} < 1, the microstructure undergoes typical strain hardening associated with a significant generation of LABs and cell boundaries, as showed by **Fig. 4(b)**. The formation of LABs, and eventually some HABs, is accompanied by the concurrent formation of twin boundaries. Both these microstructure features contribute to generate arrays of ultrafine grains at the higher strain levels.

In **Fig. 3(c)** dislocation pile-up process is showed; in particular, this piling-up generated lattice distortion on both sides of the cell wall and evolves with the presence of the early formation of twinning. These twins nucleated at grain boundaries (GBs) to extend within the grain. The formation of these twins is responsible for the development of sharp grain boundaries, which in turns implies a substantial stress relief in the boundary surrounding areas.

As for the mean grain and cell size evolution with cumulative HPT straining, the statistical evaluation carried out by TEM inspections showed a continuous grain, and especially cell size reduction from ε_{eq} = 0.91 to 3.63 (**Table 3**). That is, the mean grin size, which in the annealed initial condition was d_g = 28 μm, reduced to 19 μm at ε_{eq} = 0.40, and down to 3.2 μm, at the maximum strain of ε_{eq} = 3.63. As for the cell size, these reduced from an initial mean value d_{cell} = 1100 nm, down to 360 nm, at ε_{eq} = 3.63.

It resulted that cell size reduction process induced by HPT appeared to slow down at $\varepsilon_{eq} \geq 1.21$, when twinning formation started to characterized the grain interior and start to act as further barrier against dislocations (actually both SSDs and GNDs) sliding motion.

3.2. Nanoindentation Hardness, H, and elastic modulus, E_r

Fig. 5 reports representative nanoindentation load-displacement curves, *P-h*, for a load *P* = 10 mN, of OFHC Cu subjected to HPT at ε_{eq} = 0.40, 0.91, 1.21, and 3.63. As expected the penetration depth, h_c, reduced with cumulative straining. Yet, the unloading slope of the *P-h* slightly increased from the minimum detected strain of ε_{eq} = 0.40 to ε_{eq} = 0.91. This did not changed as the strain rose up to the maximum tested strain of ε_{eq} = 3.63. Since the unloading slope is related to the material reduced Young's modulus, E_r, the observed slope increment means that the elastic modulus of the OFHC Cu slightly increased at ε_{eq} = 0.91. This in turns implies that the occurrence of twinning formation within the grains is somehow responsible for the material changes of elastic response.

Hardness, *H*, and reduced elastic modulus, E_r, were measured according to the Oliver-Pharr approach [**40,41**], and results were plotted in **Fig. 6** as a function of the HPT shear deformation. Accordingly, the metal *H* steadily increased from the minimum, ε_{eq} = 0.40, to the top strain level, ε_{eq} = 3.63, although at ε_{eq} = 2.42, a plateau-like value of H ≅ 1.15 GPa was reached. The reduced elastic modulus, E_r, appeared to follow quite closely the hardness incremental trend with cumulative straining. Moreover, a similar plateau-like was reached at ε_{eq} = 2.42, with values E_r ≅ 170 GPa. These results are in good agreement with some previously reported study on commercially pure and quite similar OFHC pure Cu [**11**].

4. Discussion

4.1.Microstructure evolution and twinning formation induced by HPT

Dislocation formation (SSDs and GNDs) and twin formation with cumulative straining are two key mechanisms of microstructure strengthening especially for pure metals, such as the here studied OFHC 99.99% purity Cu. In fact, it is known that whenever a metallic material is subjected to plastic deformation, the newly introduced dislocations are induced to slide, in addition deformation twinning is activated, and thence both accommodate the imposed plastic strain [**42**]. The mean factors governing these microstructure induced modifications include the material SFE, the grain size and crystallographic orientation [**43-45**]. Also the external loading conditions such as stress [**46**], strain [**47**], strain rate [**48,49**], and temperature [**48**] play a crucial role. Compared to conventional materials processing, SPD techniques impose severe shear strains producing unusual and quite high mechanical properties that are ultimately driven by the unique microstructure modifications and evolution [**50,51**]. In the present case, understanding the competitive relationship between SSDs, GNDs, the cell and grain boundary formation and the deformation twinning induced by the HT shear deformation was considered as a key factor for the description of the early stages of deformation occurring in pure bcc low SFE metals, such as copper.

In materials with medium to high SFE, GNDs and SSDs develop since the early stages of plastic deformation [**52,53**]. The role of GNDs is to accommodate the shear strain gradients throughout the microstructure. SSDs are formed by tangled dislocation random trapped under uniform localized deformation. These newly introduced dislocations easily slide by cross slip by which the formation of dislocation boundaries (both low- and high-angle) is favoured with cumulative strain. The mechanism of boundary formation out of chiefly GNDs is driven by a mutual trapping, rearrangement, and annihilation process [**53,54**]. In fact, it is known that the dislocation types that do contribute to the crystal lattice rotation are the GNDs [**54**].

On the other hand, for lower SFE metals, such as copper, the formation of initially few, and then more and more volume fraction of stacking faults and twinning is favoured with cumulative straining [**55**]. Under severe plastic deformation regimes, the twinned grains contribute to accommodate the plastic deformation as well as the refining grains do. Moreover, when twinned grains have a proper crystallographic orientation respect to the external load, multiple twinning systems are activated, leading to twin-twin intersection phenomena. These, in turns, become a further strengthening mechanism for the twinned metallic material [**55,56**].

Thence, in low SFE metals the reduced dislocation mobility make the twinning deformation a necessary-like mechanism for the material to rearrange the microstructure, by strengthening it, under the applied external load. In the present study this necessary-like microstructure mechanism of twinning formation under HPT was found to occur for a strain level as low as ε_{eq} = 0.91. No traces of twinning formation was found for lower equivalent strains, where the microstructure strengthening proceeded only by formation and evolution of SSDs, GNDs, cell walls and eventually of some GB. The role of the SSDs and GNDs referring to the continuous process of cell and grain refinement induced by the HPT deformation was twofold. On one side, it was that of a microstructure source of active line defects able to thickening the newly generated boundaries, either cell or grain; on another side, it was that of contributing to rise the boundary misorientation angle as they continuously formed by the HPT action. As soon as the twins started to be generated, they behaved as a further microstructure strengthening term that did not affected the grain refining process driven by the HPT cumulative deformation.

4.2.Indentation size effect (ISE)

In nanoindentation measurements, as the indentation depths get shallow, by reducing the applied load, the obtained hardness is known to increase accordingly. This indentation size effect (ISE) was

observed in metallic materials [**32-36**]. Nix and Gao proposed a model, also known as NG-model, that relates this ISE to the generation of GNDs, whose density is proportional to the inverse indentation depth [**32**]. The additional hardening due to the GNDs is a mere effect of an indentation tip-to-the beneath indentation plastically deformed volume interaction phenomenon. Thus, ISE is particularly evident and pronounced in soft annealed metallic materials, such as the present case of annealed OFHC 99.99 purity Cu. On the contrary, ISE is typically of minimal significance in hardened metallic materials. This behaviour is directly correlated to the inner length scale of the material due to the induced increased dislocation density driven by the cumulative flow stress.
The ISE phenomenon is known to be generated by additional hardening given by the GNDs. This penetration depth sensitivity of the nanoindentation measurements is mainly based on two factors. One, is a microstructure-based factor, which is constituted by the total line length of dislocations necessary to form the permanent indented profile; the second, is geometrical-based and is related to the overall extension of the material volume in which the dislocations are stored. Indeed, both factors are strongly related to the generation of stored and necessary dislocations, *i.e.* SSDs and GNDs. A study of the ISE occurring on the early stages of HPT is here presented. To do that, nanoindentation load was almost continuously reduced from 10 mN to loads as low as ~100 μN. The obtained hardness, *H*, increment due to the ISE, as a function of lowering penetration depths down to few hundreds of nanometer, for strain levels of ε_{eq} = 0.40-to-3.63 is reported in **Fig. 7**. It is worth to note that the measured *H* variation with lowering penetration depths followed different slopes depending on the strain level to which the pure copper was subjected. It appeared that from HPT strains ε_{eq} < 0.40 / 0.91. *H* followed an almost continuous incremental rate as the load and penetration depth lowered. Starting from ε_{eq} = 0.91 and up to ε_{eq} = 3.63, *H* increment by lowering the penetration depth followed an initial almost linear trend, to drastically rise for penetration depths lower than 900-800 nm. This different ISE trend is believed to be somehow determined by the reducing grain size and the concurrent formation of twinned grains.

4.3. Twinning formation role in ISE

An ISE-driven hardness increment of ~10% was observed at indentation depths ranging 1.8-to-0.9 μm, from as-annealed to HPT strain ε_{eq} = 3.63 (**Fig. 7**). This increment can be identified as the minimal deviation from the actual *H* evaluation due to the ISE phenomenon and is reported in **Fig. 8**. Thus, the measured depth range to reach a *H* variation by 10% from the asymptotical and actual value, obtained at higher penetration depth ranges, strongly depended on the strain level and, ultimately, on the induced grain/cell size reduction. The corresponding penetration depth value is also called length scale, h^*. That is, as reported in the plot of **Fig. 8**, a direct correlation exists between the occurrence of a significant ISE and the mean grain (and cell) size of the testing metallic material. Present result appears to be in good agreement to data reported by Nix and Gao in [**32**] derived by a linear fitting of $(H/H_0)^2$ vs. h_c^{-1} in pure Cu, where a value of length scale of ISE h^* = 1.60 μm was reported. Thence, the here obtained results showed the length scale, h^*, to rise with grain, cell size reduction, and with occurrence of twinned grains. That is, the ISE appeared to anticipate by refining the grained structure of pure Cu by cumulative HPT straining. To some extent, this issue was addressed and discussed by Yang and Vehoff [**34**] who studied ISE occurring in high-purity nanocrystalline Ni with different mean grain size obtained by plastic deformation techniques. Similarly, Lapovok *et al.* [**57**] reported a certain degree of ISE initiation dependency to the level of ECAP shear straining in pure Cu. They show ISE occurring with lower penetration depth as the ECAP shear straining cumulate and thus as the resulting mean grain refined. Similar trends for commercially pure Cu were reported in [**58**] by HPT, and in [**36**] by ECAP.
Fig. 8 shows *H* rising trend slopes for the two strain levels above mentioned, that is, for ε_{eq} < 0.91, and for 0.91 < ε_{eq} < 2.42. It thus resulted that the *H* increment was slow (0.93 GPaμm^{-1}) at the earliest stages of deformation, to double (1.84 GPaμm^{-1}) for strain levels by which grain started to refine and twins started to form within the grains. This would ultimately means that a direct

correlation between the rate and amplitude of ISE and the grained structure of pure copper exists. To better understand this ISE microstructure dependency, twin spacing, λ_{Twin}, was measured for strains $0.91 < \varepsilon_{eq} < 2.42$, that is for the strain levels where twins started to form ($\varepsilon_{eq} = 0.91$) and then filled the grained structures ($\varepsilon_{eq} = 2.42$). The statistical evaluation of twin spacing, carried out for strain levels $\varepsilon_{eq} = 0.91$-to-2.42 is reported in **Fig. 9**.

The twin spacing appeared not to evolve significantly with cumulative HPT strain. Mean twin spacing was $\lambda_{Twin} \cong 32 \pm 2$ nm irrespective of the strain level throughout the range $0.91 < \varepsilon_{eq} < 2.42$. The only clear aspect that differentiated the λ_{Twin} size distribution with HPT strain was the maximum twin spacing sizes that appeared to reduced form 80 nm, at $\varepsilon_{eq} = 0.91$, down to 60 nm, at $\varepsilon_{eq} = 2.42$.

Quite similar twin spacing sizes were also reported by Yang and Vahoff [**34**] in SPD high-purity nickel and by Saldana *et al.* [**59**] in SPD same OFHC 99.99 purity copper. In particular, Saldana *et al.* accounted on thermomechanical stability in ultra-fine grained copper with high density of twin boundaries. Nanoscale network of twins within the grains are generally induced to form by SPD processes. In this sense, the here reported formation and evolution of twins induced by the HPT cumulative strain was actually expected mostly on the basis of the relative low OFHC Cu SFE. Moreover, twin boundary formation promoted by SPD (HPT in the present case) are strongly affected by the generation and evolution with strain of SSDs and GNDs. In particular, the twins formed during SPD means can have a significant high aspect ratio, that is a high length to spacing ratio). This microstructure feature was widely observed in the present study and the corresponding morphological twin evolution with SPD strain was also reported by Wang *et al.* in a nanostructured pre Cu [**60**].

Fig. 10 shows a direct comparison between the twin spacing and grain/cell evolution with cumulative HPT straining. The general refining trend of both cells and grains was accompanied by a non-significant twin spacing variation, although twin volume fraction increased to a great extent in the strain range $\varepsilon_{eq} = 1.21$-to-2.42.

4.4. Strengthening model

It is well known how strength of a metallic material can be directly related to the microstructural features, such dislocations, cell and grain boundaries (and related mean size), and, limited to the low-to-medium SFE metals, to the twin boundaries (TB). The flow stress, namely the material yield stress, can be derived as contributions aggregate of the above-mentioned strengthening terms [**61,62**]. Apart from the grain boundary strengthening which is modelled by the Hall-Petch relationship, a number of models accounted on the strength contribution coming from cell boundaries. These can actually have a low-angle, but also a very low-angle character [**14**]. The first ones are typically boundaries with misorientation angle within ~4-14°, the second ones have typical misorientation of ~2-4° and always show Moiré fringes on TEM. For the first case, the strength contribution can be modelled as to be proportional to the square root of the density of dislocation stored inside the boundaries (essentially SSDs) [**61**]. The second case corresponds to the existing tangled dislocations (TDs) [**14,62,63**]. On the other hand, the occurrence of TB from strain levels of $\varepsilon_{eq} > 0.40$, makes necessary considering this further microstructure strengthening contribution [**64,65**]. Thence, the following relationship was proposed for modelling the OFHC Cu yield stress as determined by the nanoindentation hardness measurements, Eq. (2):

$$\sigma_y = \sigma_0 + \sigma_{disl.} + \sigma_{HP} + \sigma_{TB} \qquad \text{Eq. (2)}$$

where σ_0, $\sigma_{disl.}$ is the stress due to SSDs and GNDs, σ_{HP} is the stress given by the grained structure (calculated through the Hall-Petch relationship), σ_{TB} is the stress due to the twins (twin boundaries, TB).

The dislocation contribution is the linear combination of the SSDs and of the GNDs strengthening, and they are both directly dependent on the related densities. In particular, SSDs do form very low-angle and low-angle boundaries under plastic deformation, and thus their density is expressed as, Eq. (3):

$$\rho_{SSD} = f\rho_{wall} + (1\text{-}f)\rho_{TD} \qquad \text{Eq. (3)}$$

Where f is the fraction of the SSDs that do contribute to the wall (boundary) formation, ρ_{wall} is the density of the formed walls, and ρ_{TD} represents the density of the dislocations existing in the cell and grain interiors that did not form boundaries and that are generally referred as to tangled dislocations (TD). According to [**57**] the value of f can be determined as $f = 1\text{-}(1\text{-}\lambda_{wall}/d_{cell})^3$, λ_{wall} and d_{cell} being the mean wall (cell boundary) thickness and cell size, respectively.
Thence, the dislocation strengthening contribution, $\sigma_{disl.}$, can be calculated as, Eq. (4):

$$\sigma_{disl.} = M\alpha Gb[f\rho_{wall} + (1\text{-}f)\rho_{TD} + \rho_{GND}]^{0.5} \qquad \text{Eq. (4)}$$

where $M = 3.06$ is the Taylor factor [**66**], $\alpha = 0.33$ [**66**], $G = 48.2$ GPa is the shear modulus of pure copper [**66**], $b = 0.256$ nm is the copper Burgers vector [**61,65**].
Here the walls are actually considered as the continuously generated very-low and low-angle boundaries, *i.e.* the cell boundaries.
Onset of twinning occurs whenever the slip stress reaches the minimum necessary strain to activate the twinning. The present results showed that the minimum necessary strain level to initiate the twin formation was $\varepsilon_{eq} = 0.91$. Thence, whenever formed, the twins yield a further strengthening contribution given by their boundaries (twin boundary, TB), σ_{TB}. This strengthening contribution is modelled similarly to an Hall-Petch relationship but with a constant, K_{TB}, significantly higher than that pertaining the grain boundary strengthening, K_{HP}. Thus, according to Hansen [**61,67,68**], Armstrong and Worthington [**69**] and Meyers *et al.* [**42**], $K_{TB} = 0.28$ MPa·m$^{1/2}$, compared to $K_{HP} = 0.14$ MPa·m$^{1/2}$, and the corresponding strengthening contribution can be modelled as, Eq. (5):

$$\sigma_{TB} = K_{TB}\cdot d_g^{-1/2} \qquad \text{Eq. (5)}$$

By taking into account the actual fraction of twinned grains, f_{twin}, rising with cumulative HPT straining, the following strengthening model was here proposed, Eq. (6):

$$\sigma_y = \sigma_0 + M\alpha Gb\{[f\rho_{wall} + (1\text{-}f)\rho_{TD} + \rho_{GND}]^{1/2} + [(f_{twin}\cdot K_{TB} + (1\text{-}f_{twin})\cdot K_{HP}]d_g^{-1/2}\} \qquad \text{Eq. (6)}$$

The calculated values of f_{twin} are also reported in the plot of **Fig. 10**. Referring to Eq. (6), **Fig. 11** shows a representative TEM micrograph of the microstructure at $\varepsilon_{eq} = 2.42$ in which all the strengthening features are present, *i.e.* dislocation walls, tangled dislocations, geometrically-necessary dislocations, twin boundaries, and grain boundaries.
Dislocation density, namely ρ_{wall}, ρ_{TD}, ρ_{GND}, and fraction of wall boundaries, f, were determined by TEM stereology analyses (ASM EN-112). The mean data for each experimental condition, $\varepsilon_{eq} =$ 0.40-to-3.63, are reported in the following **Table 4**.
The dislocation density data obtained in the present study well agree to previously published results on severely plastic deformed pure copper by ECAP up to 16 passes [**70**]. On the other hand, Lapovok *et al.* [**70**] reported dislocation wall spacing four times lower than the cell size at the early stages of ECAP deformation. In the present case a typical spacing of the dislocation walls of almost one-order of magnitude lower than the cell spacing was found.

On the basis of the data reported in **Table 3**, for grain sizes, and **Table 4**, for dislocation densities and fraction of the dislocation walls, Eq. (6) gives a microstructure-based quantitative evaluation of the OFHC 99.99 purity Cu yield stress, as reported in **Table 5**.

The present approach founds a number of scientific support given by previously published works and models proposed for different pure metals and alloys. These include the early studies on the impact of heterogeneous nature and distribution of dislocations on the metal and alloy shear stress, which were evaluated by Mughrabi using a composite-like model [**71,72**]. Following the pioneering works by Mughrabi, several other authors applied and adapted the Mughrabi composite-like model to different metals, alloys, and plastic deformation techniques [**73-78**]. These previous works report and apply strengthening models essentially same as the one here presented and applied to the OFHC 99.99 purity Cu. Moreover, the present approach is also able to describe metals and alloys work hardening mechanisms up to flow-stress saturation, as exhaustively reported by Nes and co-workers in [**79**].

Table 5 also reports a direct comparison between the yield stress as obtained through Eq. (6), and the one derived from the nanoindentation hardness measurements, $\sigma_y^{nanoind}$. With this respect, a linear relationship is known to hold between hardness, H, and yield stress, given by $H = (\sigma_y/3)\cdot(0.1)^{m-2}$, where m is the Meyer's hardness coefficient [**80**]. With this respect several published works on different metallic materials and alloys reported a hardness-to-yield stress relationship with a narrow ratio interval of $\chi = H_V/\sigma_y$ = 2.7-3.1 [**81-83**]. In the cold-rolled metallurgical status this relationship was reported to essentially have the same ratio range of 2.8-3.1 [**80,81**]. A Meyer's hardness similar approach was recently used and applied to aluminum alloys by Tiryakioğlu in [**82**]. In this case a $\sigma_y = A\cdot H_V + B$ type relationship was used starting from a Meyer's hardness approach as: $\sigma_y = H_V /0.947\cdot C - \Delta\sigma_y$. This type of approach to determining yield stress from hardness measurements, namely nanoindentation measurements, was also used by the present author for a 6N-Al subjected to low strains by HPT [**21**]. On the other hand, Tekkaya [**83**] for cold-worked Cu-based alloys introduced a step-like variation of the yield stress-to-hardness ratio depending on the yield offset that can be taken into account. For yield offset of within 0.112% the following relationship was proposed and experimentally validated: $H_V = 2.475\cdot\sigma_y$, where H_V is the Vickers hardness number. This relationship was generalized in a form of $\sigma_y = 9.81\cdot H_V/2.475$ for yield offsets up to 0.2%. In any case, by converting the Vickers number to MPa, the two previously reported approaches (Tiryakioğlu's and Tekkaya's) can be expressed as $\sigma_y = 0.375\cdot H^{nanoind}$, that is $\chi = H_V/\sigma_y = 2.7$. Very recently, Song *et al.* [**84**] reported a rather wider variation for $\chi = H_V/\sigma_y$ = 3-4.5, this reduces down to $\chi \cong 3.24$ whenever the ultimate stress is considered instead of the yield stress. Other studies, such as the work by Zhang *et al.* [**85**] indicated values ranging 3.26-3.70 (with a mean value of $\chi = 3.5$) in pure copper subject to ECAP. In his work, Zhang *et al.* reported an overview of the factor influencing the χ ratio between H_V and σ_y for different copper alloys.

Thence, in the present study both values of $\chi = 2.9$ and $\chi = 3.5$ were taken into consideration for the identification of the more appropriate value able to meet the yield stress determined by the microstructure based model here described. It is worth to underline here that the χ = 2.9-2.8 was found to be an appropriate ratio between H_V and σ_y in metallic alloys, as well as pure metals, such aluminum ([**21,80-82**] and references therein).

The direct comparison of yield stress obtained by using both $\chi = H^{nanoind}/\sigma_y = 2.9$ and 3.5,showed a quite better agreement to the yield stress given by applying Eq. (6) with $\chi = 3.5$ rather than by using $\chi = 2.9$. Present results seem to indicate that a slight difference of the H/σ_y does exist whenever low-SFE metals (namely pure metals) or high-SFE metals subjected to SPD are considered.

To better understand this fitting ratio between the two yield stress values obtained by microstructure inspections and by indirect hardness measurements the Gao's approach was here reported and discussed. Gao's relationship between hardness and yield stress also includes the material elastic modulus, E, Eq. (7):

$$H^{nanoind} = \frac{2}{3}\sigma_y \left\{1 + \frac{3}{4}\left(\frac{1}{3}\frac{E_r}{\sigma_y}\cot(\alpha)\right)^n + \frac{1}{n}\left[\left(\frac{1}{3}\frac{E_r}{\sigma_y}\cot(\alpha)\right)^n - 1\right]\right\} \quad \text{Eq. (7)}$$

where α is the semi-angle of the indentation tip, and n is the work-hardening coefficient. This approach and equation was applied to the present case, where the reduced (local) elastic modulus was determined by the nanoindentation measurements and the semi-angle α = 65°, for a Berkovich tip. The work-hardening coefficient n can be set equals to the true strain at necking and it can be derived from nanoindentation assuming a 8-to-10% plastic strain acting during the indentation process ([**85,86**] and references therein). That is, the value of work-hardening in stress-strain curves for annealed copper was is used, n = 0.54. By putting the constant values of Eq. (7) and the obtained reduced elastic modulus values as obtained different experimental conditions here tested, the data reported in **Table 6** were obtained. **Table 6** shows a reasonably good agreement between the Gao's model data and the microstructure strengthening model for strain levels ε_{eq} > 1.21,while for lower strain levels the agreement was less evident. On the other hand, this approach seemed not to show a better result alignment to the data obtained by the strengthening model compared to simply considering the ratio $\chi = H_V/\sigma_y$ = 3.5.

5. Conclusions

In this study early stages of plastic deformation by HPT were characterized by electron microscopy inspections. A OFHC 99.99 pure copper was subjected to strain levels as low as ε_{eq} = 0.40-to-3.63. Mechanical properties were tested by nanoindentation and the indentation size effect phenomenon was correlated to the microstructure evolution induced by the cumulative straining.
The following major findings can be outlined.

1. A minimum necessary strain level to induce the formation of twins was found and it resulted to be ε_{eq} = 0.91;
2. The occurrence of twinning within the refining grains influenced the ISE as it contributed to change the hardness-to-penetration depth curves. That is, the ISE depended to some extent to the formation of twins in pure Cu. With this respect, the hardness rise due to the ISE accelerated with reducing cell and grain size and with occurrence of twins. At the same time, the penetration depth by which ISE started to occur reduced with twin formation and progressive generation within the refining grains;
3. A microstructure based strengthening model was proposed and all the meaningful strengthening contributions were taken into account. In particular, SSDs, dislocation walls, GNDs, grain boundaries and twin boundaries strengthening contributions were modelled. OFHC pure Cu yield stress given by the microstructure based model was directly compared to the yield stress as derived from the nanoindentation hardness.
4. Discussion on the different models of relationship between hardness and yield stress seemed to indicate that $\chi = H_V/\sigma_y$ = 3.5 was the more appropriate coefficient to be considered.

Declaration of Competing Interest

None.

Acknowledgements.

The author wish to thank Mr. M. Pieralisi for his assistance in performing the HPT tests.

References

[1] X.X. Huang, N. Hansen, N. Tsuji, Hardening by annealing and softening by deformation in nanostructured metals, Science 312 (2006) 249-251.
[2] I.A. Ovid'ko, R.Z. Valiev, Y.T. Zhu, Review on superior strength and enhanced ductility of metallic nanomaterials, Prog. Mater. Sci. 94 (2018) 462-540.
[3] M. Cabibbo, Nanostructured Cobalt Obtained by Combining Bottom-Up and Top-Down Approach, Metals 8(11) (2018) 962-971.
[4] I. Sabirova, M.Yu. Murashkin, R.Z. Valiev, Nanostructured aluminium alloys produced by severe plastic deformation: New horizons in development Mater. Sci. Eng. A 560 (2013) 1-24.
[5] A.P. Zhilyaev, T.G. Langdon, Using high-pressure torsion for metal processing: Fundamentals and applications, Progr. Mater. Sci. 53 (2008) 893-979.
[6] R.Z. Valiev, T.G. Langdon, Principles of equal-channel angular pressing as a processing tool for grain refinement, Progr. Mater. Sci., 51 (2006) 881-981.
[7] A. Vinogradov, Y. Estrin, Analytical and numerical approaches to modelling severe plastic deformation, Progr. Mater. Sci. 95 (2018) 172-242.
[8] Y. Cao, S. Ni, X. Liao, M. Song, Y. Zhu, Structural evolutions of metallic materials processed by severe plastic deformation, Mater. Sci. Eng. R 133 (2018) 1-59.
[9] B.L. Li, N. Tsuji, N. Kamikawa, Microstructure homogeneity in various metallic materials heavily deformed by accumulative roll-bonding, Mater. Sci. Eng. A 423 (2006) 331-342.
[10] Y. Xun, F.A. Mohamed, Refining efficiency and capability of top-down synthesis of nanocrystalline materials, Mater. Sci. Eng. A 528 (2011) 5446-5452.
[11] A.I. Almazrouee, K.J. Al-Fadhalah, S.N. Alhajeri, T.G. Langdon, Microstructure and microhardness of OFHC copper processed by high-pressure torsion, Mater. Sci. Eng. A 641 (2015) 21-28.
[12] M. Ebrahimi, C. Gode, Severely deformed copper by equal channel angular pressing, Progr. Nat. Sci.: Mater. Int.l 27 (2017) 244-250.
[13] N.Q. Chinh, T. Csanádi, J. Gubicza, T.G. Langdon, Plastic behavior of face-centered-cubic metals over a wide range of strain, Acta Mater. 58 (2010) 5015-5021.
[14] M. Cabibbo, Microstructure strengthening mechanisms in different equal channel angular pressed aluminum alloys, Mater. Sci. Eng. A560 (2013) 413-432.
[15] M. Cabibbo, A TEM Kikuchi pattern study of ECAP AA1200 via routes A, C, B_C, Mater. Character. 61 (2010) 613-625.
[16] M. Cabibbo, W. Blum, E. Evangelista, M.E. Kassner, M.A. Meyers, Transmission electron microscopy study of strain induced low- and high-angle boundary development in equal-channel angular-pressed commercially pure aluminum, Metall. Mater. Trans. A39 (2008) 181-192.
[17] C. Xu, Z. Horita, T.G. Langdon, The evolution of homogeneity in processing by high-pressure torsion, Acta Mater. 55 (2007) 203-212.
[18] G. Sakai, Z. Horita, T.G. Langdon, Grain refinement and superplasticity in an aluminum alloy processed by high-pressure torsion, Mater. Sci. Eng. A 393 (2005) 344-351.
[19] Y. Ito, K. Edalati, Z. Horita, High-pressure torsion of aluminum with ultrahigh purity (99.9999%) and occurrence of inverse Hall-Petch relationship, Mater. Sci. Eng. A 679 (2017) 428-434.
[20] D.A. Hughes, N. Hansen, D.J. Bammann, Geometrically necessary boundaries, incidental dislocation boundaries and geometrically necessary dislocations, Scripta Mater. 48 (2003) 147-153.
[21] M. Cabibbo, Minimum necessary strain to induce tangled dislocation to form cell and grain boundaries in a 6N–Al, Mater. Sci. Eng. A 77 (2020) 138420.
[22] I. Sabirov, M.Yu. Murashkin, R.Z. Valiev, Nanostructured aluminium alloys produced by severe plastic deformation: New horizons in development, Mater. Sci. Eng. A 560 (2013) 1-24.

[23] A. P. Zhilyaev, B.-K. Kim, J.A. Szpunar, M.D. Baró, T.G. Langdon, The microstructural characteristics of ultrafine-grained nickel, Mate. Sci. Eng. A 391 (2005) 377-389.
[24] G.B. Rathmayr, A. Hohenwarter, R. Pippan, Influence of grain shape and orientation on the mechanical properties of high pressure torsion deformed nickel, Mater. Sci. Eng. A 560 (2013) 224-231.
[25] K.S. Raju, M.G. Krishna, K.A. Padmanabhan, K. Muraleedharan, N.P. Gurao, G. Wilde, Grain size and grain boundary character distribution in ultra-fine grained (ECAP) nickel, Mater. Sci. Eng. A 491 (2008) 1–7.
[26] Q. Xue, I.J. Beyerlein, D.J. Alexander, G.T. Gray III, Mechanisms for initial grain refinement in OFHC copper during equal channel angular pressing, Acta Mater. 55 (2007) 655-668.
[27] A. Azushima, R. Kopp, A. Korhonen, D.Y. Yang, A. Yanagida, Severe plastic deformation (SPD) processes for metals, CIRP Annals 57 (2008) 716-735.
[28] R.Z. Valiev, Producing bulk nanostructured metals and alloys by severe plastic deformation (SPD), Nanostruct. Metals All. Chapter 1 (2011) 3-39.
[29] D. Lorenz, A. Zeckzer, U. Hilpert, P. Grau, H. Johansen, H.S. Leipner , Pop-in effect as homogeneous nucleation of dislocations during nanoindentation, Phys. Rev. B 67 (2003) 172101 1-4.
[30] A. Asenjo, M. Jaafar, E. Carrasco, J.M. Rojo, Dislocation mechanisms in the first stage of plasticity of nanoindented Au(111) surfaces, Phys. Rev. B 73 (2006) 075431 1-7.
[31] N.A. Fleck, G.M. Muller, M.F. Ashby, J.W. Hutchinson, Strain gradient plasticity: Theory and experiment, Acta Metall. Mater. 42 (1994) 475-487.
[32] W.D. Nix, H.J. Gao, Indentation size effects in crystalline materials: A law for strain gradient plasticity, Mech. Phys. Solids 46 (1998) 411-425.
[33] W. Liu, L. Chen, Y. Cheng, L. Yu, X. Yi, H. Gao, H. Duan, Model of nanoindentation size effect incorporating the role of elastic deformation, J. Mech. Phys. Solids 126 (2019) 245-255.
[34] B. Yang, H. Vehoff, Dependence of nanohardness upon indentation size and grain size – A local examination of the interaction between dislocations and grain boundaries, Acta Mater. 55 (2007) 849-856.
[35] K. Durst, M. Göken, G.M. Pharr, Indentation size effect in spherical and pyramidal indentations, J. phys. D: Appl. Phys. 41 (2008) 074005.
[36] K. Durst, B. Backes, M. Göken, Indentation size effect in metallic materials: Correcting for the size of the plastic zone, Scripta Mater. 52 (2005) 1093-1097.
[37] N.H. Polakowski, E.J. Ripling, Strength and Structure of Engineering Materials, Prentice-Hall, Englewood Cliffs, NJ, 1966.
[38] J. C. Russ, R., T. Dehoff, Practical Stereology, 2nd Ed. Springer Science & Business Media LLC New York, 2000.
[39] M. Cabibbo, P. Ricci, R. Cecchini, Z. Rymuza, J. Sullivan, S. Dub, S. Cohen, An international round-robin calibration protocol for nanoindentation measurements, Micron 43 (2012) 215-222.
[40] W.C. Oliver, G.M. Pharr, Measurement of hardness and elastic modulus by instrumented indentation: Advances in understanding and refinements to methodology, J. Mater. Res. 19 (2004) 3-20.
[41] J.H. Gong, H.Z. Miao, Z.J. Peng, Analysis of the nanoindentation data measured with a Berkovich indenter for brittle materials: effect of the residual contact stress, Acta Mater. 52 (2004) 785-793.
[42] M.A. Meyers, O. Vöhringer, V.A. Lubarda, The onset of twinning in metals: a constitutive description. Acta Mater. 49 (2001) 4025-4039.
[43] W.Z. Han, Z.F. Zhang, S.D. Wu, S.X. Li, Combined effects of crystallographic orientation, stacking fault energy and grain size on deformation twinning in fcc crystals, Phil. Mag. 88 (2008) 3011-3029.

[44] Y. Cao, Y.B. Wang, X.Z. Liao, M. Kawasaki, S.P. Ringer, T.G. Langdon, Y.T. Zhu, Applied stress controls the production of nano-twins in coarse-grained metals. Appl. Phys.Lett. 101 (2012) 231903.
[45] G. Laplanche, A. Kostka, O.M. Horst, G. Eggeler, E.P. George, Microstructure evolution and critical stress for twinning in the CrMnFeCoNi high-entropy alloy. Acta Mater. 118 (2016) 152-163.
[46] Y.S. Li, Y. Zhang, N.R. Tao, K. Lu, Effect of the Zener-Hollomon parameter on the microstructures and mechanical properties of Cu subjected to plastic deformation. Acta Mater. 57 (2009) 761-772.
[47] L.E. Murr, M.A. Meyers, C.S. Niou, Y.J. Chen, S. Pappu, C. Kennedy, Shock-induced deformation twinning in tantalum. Acta Mater. 45 (1997) 157-175.
[48] I.J. Beyerlein, L.S. Tóth, Texture evolution in equal-channel angular extrusion. Progr. Mater. Sci. 54 (2009) 427-510.
[49] M.F. Ashby, The deformation of plastically non-homogeneous materials. Phil. Mag. 21 (1970) 399-424.
[50] D.A. Hughes, N. Hansen, D.J. Bammann, Geometrically necessary boundaries, incidental dislocation boundaries and geometrically necessary dislocations. Scripta Mater. 48 (2003) 147-153.
[51] P. Li, S.X. Li, Z.G. Wang, Z.F. Zhang, Fundamental factors on formation mechanism of dislocation arrangements in cyclically deformed fcc single crystals. Progr. Mater. Sci. 56 (2011) 328-377.
[52] D. Kuhlmann-Wilsdorf, Theory of plastic deformation: properties of low energy dislocation structures. Mater. Sci. Eng, A 113 (1989) 1-41.
[53] X.H. An, Q.Y. Lin, S. Qu, G. Yang, S.D. Wu, Z.F. Zhang, Influence of stacking-fault energy on the accommodation of severe shear strain in Cu-Al alloys during equal-channel angular pressing. J. Mater. Res. 24 (2009) 3636-3646.
[54] A.A.S. Mohammed, E.A. El-Danaf, A.A.Radwan, A criterion for shear banding localization in polycrystalline FCC metals and alloys and critical working conditions for different microstructural variables. J. Mater. Process. Technol. 186 (2007) 14-21.
[55] P. Müllner, A.E. Romanov, Internal twinning in deformation twinning. Acta Mater. 48 (2000) 2323-37.
[56] J.W. Christian, S. Mahajan, Deformation twinning. Progr. Mater. Sci. 39 (1995) 1-157.
[57] R. Lapovok, F.H. Dalla Torre, J. Sandlin, C.H.J. Davies, E.V. Pereloma, P.F. Thomson, Y. Estrin, Gradient plasticity constitutive model reflecting the ultrafine micro-structure scale: the case of severely deformed copper, J. Mech. Phys. Solids 53 (2005) 729-747.
[58] Y. Estrin, A. Molotnikov, C.H.J. Davies, R. Lapovok, Strain gradient plasticity modelling of high-pressure torsion, J. Mech. Phys. Solids 56 (2008) 1186-1202.
[59] C. Saldana, A.H. King, S. Chandrasekar, Thermal stability and strength of deformation microstructures in pure copper, Acta Mater 60 (2012) 4107-4116.
[60] H.L. Wang, Z.B. Wang, K. Lu, Interfacial diffusion in a nanostructured Cu produced by means of dynamic plastic deformation, Acta Mater. 59 (2011) 1818-1828.
[61] N. Hansen, Hall–Petch relation and boundary strengthening, Scripta Mater. 51 (2004) 801-806.
[62] S. Nemat-Nasser, Y. Li, Flow stress of f.c.c. polycrystals with application to OFHC Cu, Acta Mater. 46 (1998) 565-577.
[63] M. Cabibbo, Microstructure strengthening mechanisms in an Al–Mg–Si–Sc–Zr equal channel angular pressed aluminium alloy, Appl. Surf. Sci. 281 (2013) 38-43.
[64] W. Han, S. Wu, C. Huang, S. Li, Z. Zhang, Orientation design for enhancing deformation twinning in Cu single crystal subjected to equal channel angular pressing, Adv. Eng. Mater. 10 (2008) 1110-1113.
[65] S.D. Antolovich, R.W. Armstrong, Plastic strain localization in metals: origins and consequences, Progr. Mater. Sci. 59 (2014) 1-160.

[66] F. Dalla Torre, R. Lapovok, J. Sandlin, P.F. Thomson, C.H.J. Davies, E.V. Pereloma, Microstructures and properties of copper processed by equal channel angular extrusion for 1–16 passes, Acta Mater. 52 (2004) 4819-4832.
[67] N. Hansen, X. Huang, G. Winther, Grain orientation, deformation microstructure and flow stress, Mater. Sci. Eng. A 494 (2008) 61-67.
[68] N. Hansen, X. Huang, Microstructure and flow stress of polycrystals and single crystals, Acta Mater. 46 (1998) 1827-1836.
[69] R.W. Armstrong, P.J. Worthington, in Metallurgical Effects at High Strain Rates, ed. R.W. Rohde, B.M. Butcher, J.R. Holland, C.H. Karnes. Plenum Press, New York, USA (1973) 401-414.
[70] R. Lapovok, F.H. Dalla Torre, J. Sandlin, C.H.J. Davies, E.V. Pereloma, P.F. Thomson, Y. Estrin, Gradient plasticity constitutive model reflecting the ultrafine micro-structure scale: the case of severely deformed copper, J. Mech. Phys. Solids 53 (2005) 729-747.
[71] H. Mughrabi, Dislocation wall and cell structures and long-range internal stresses in deformed metal crystals, Acta Metall. 31 (1983) 1367-1379.
[72] H. Mughrabi, A two-parameter description of heterogeneous dislocation distributions in deformed metal crystals, Mater. Sci. Eng. A 85 (1987) 15-31.
[73] F.R.N. Nabarro, Work hardening and dynamical recovery of F.C.C. metals in multiple glide, Acta Metall. 37 (1989) 1521-1546.
[74] T. Ungár, L.S. Tóth, J. Illy, I. Kovács, Dislocation structure and work hardening in polycrystalline ofhc copper rods deformed by torsion and tension, Acta Metall. 34 (1986) 1257-1267.
[75] A.S. Argon, P. Haasen, A new mechanism of work hardening in the late stages of large strain plastic flow in F.C.C. and diamond cubic crystals, Acta Metall. Mater. 11 (1993) 3289-3306.
[76] Y.Estrin, L.S. Tóth, A. Molinari, Y. Bréchet, A dislocation-based model for all hardening stages in large strain deformation, Acta Mater. 46 (1998) 5509-5522.
[77] X. Feaugas, P. Pilvin, A Polycrystalline Approach to the Cyclic Behaviour of f.c.c. Alloys – Intra- Granular Heterogeneity, Adv. Eng. Mater. 11 (2009) 703-709.
[78] M.E. Kassner, P. Geantil, L.E. Levine, Long range internal stresses in single-phase crystalline materials, Int. J. Plast. 45 (2013) 44-60.
[79] E. Nes, T. Pettersen, K. Marthinsen, On the mechanisms of work hardening and flow-stress saturation, Scripa Mater. 43 (2000) 55-62.
[80] J.R. Cahoon, W.H. Broughton, A.R. Kutzak, The determination of yield strength from hardness measurements, Mater. Trans. 2 (1971) 1979-1983.
[81] E. Broitman, Indentation Hardness Measurements at Macro-, Micro-, and Nanoscale: A Critical Overview, Tribol. Lett. 65 (2017) 23-41.
[82] M. Tiryakioğlu, On the relationship between Vickers hardness and yield stress in Al–Zn–Mg–Cu Alloys, Mater. Sci. Eng. A 633 (2015) 17-19.
[83] A.E. Tekkaya, An Improved Relationship between Vickers Hardness and Yield Stress for Cold Formed Materials and its Experimental Verification, Annals CIRP 49 (2000) 205-208.
[84] M. Song, C. Sun, Y. Chen, Z. Shang, J. Li, Z. Fan, X. Zhang, Grain refinement mechanisms and strength-hardness correlation of ultrafine grained grade 91 steel processed by equal channel angular extrusion, Int.l J. Press. Vess. Piping 172 (2019) 212-219.
[85] P. Zhang, S.X. Li, Z.F. Zhang, General relationship between strength and hardness, Mater. Sci. Eng. A 529 (2011) 62-73.
[86] X.-L. Gao, An expanding cavity model incorporating strain-hardening and indentation size eff ects, Int. J. Solids Struct. 43 (2006) 6615-6629.

Figures and Tables captions

Fig. 1. Microstructure of the as annealed OFHC Cu.

Fig. 2. To scale scheme of HPT showing the location of extraction of the TEM discs.

Fig. 3. Microstructure evolution with cumulative HPT shear strain, at ε_{eq} = 0.40, a); ε_{eq} = 0.91, b); ε_{eq} = 1.21, c); ε_{eq} = 1.81, d); ε_{eq} = 2.42, e); ε_{eq} = 3.63, f). In b) the dark-field (DF) micrograph shows the early formation of low-angle boundaries (cells) from tangled dislocations (GNDs). Inset in b) is the indexed SAEDP. DF g-vector was g = [02-2]. By selecting this crystallographic plane the existing tangled dislocations and cell boundaries within the grains were almost entirely visible as they mostly lying in the [022] planes and (022) directions.

Fig. 4. Twinning formation induced by the HPT strain, ε_{eq} = 0.91, a); ε_{eq} = 1.81, b); ε_{eq} = 3.63, c). Cu crystals were oriented along [011]-zone axis to properly reveal the twin boundaries and lines; related indexed SAEDP is reported in d).

Fig. 5. Nanoindentation load-displacement curves, *P*-*h*, using a load *P* = 10 mN, for HPT OFHC 99.99% purity Cu at ε_{eq} = 0.40, 0.91, 1.21, 181, 2.42, and 3.63. The annealed OFHC Cu nanoindentation curve, ε_{eq} = 0, is reported for comparison.

Fig. 6. Plot of hardness, *H*, and reduced elastic modulus, E_r, vs. cumulative HPT straining, ε_{eq} = 0.40 to 3.63. Error bars were determined by averaging the obtained values from the 64 individual nanoindentation measurements that were performed at each experimental condition.

Fig. 7. The ISE phenomenon. Hardness, *H*, vs. indentation depth, h_c, for ε_{eq} = 0.40-to-3.63; the as-annealed curve is reported for comparison to the HPT experimental conditions.

Fig. 8. Minimum nanoindentation load to initiate ISE vs. mean grain and cell size produced by HPT of the OFHC 99.9% purity Cu.

Fig. 9. Evolution of twin mean spacing, λ_{Twin}, for HPT strains $0.91 < \varepsilon_{eq} < 2.42$.

Fig. 10. Grain size, d_{grain}, cell size, d_{cell}, twin spacing, λ_{Twin}, and twinned grain volume fraction, $f_{twinned\ grains}$, evolution with HPT strains ε_{eq} = 0.40-to-3.63.

Fig. 11. BF-TEM at ε_{eq} = 2.42 showing dislocation walls (DW), tangled dislocations (TD), geometrically-necessary dislocations (GND), twin boundaries (TB), and grain boundaries (GB).

Table 1. Chemical composition of the OFHC 99.99% purity copper (wt.%x1000), as reported by the supplier (purity standard identified as DIN1706-NFA51050 / CuC1, source FRW^{TM}).

Table 2. Equivalent strain ε_{eq} obtained by the different HPT experimental parameters at *N* = 1/18 (lowest) to 1/2 turns (highest), at radial distances *r* = 2 mm (almost mid-radius) from disc thick-center.

Table 3. Mean grain, d_g, and cell size, d_{cell}, of OFHC CU subjected to HPT at ε_{eq} = 0.40 to 3.63. These mean values were determined out of 3 different areas of the TEM thin discs accounting of some 0.56-to-0.74 mm^2 per each experimental condition.

Table 4. Dislocation density and dislocation wall volume fraction, *f*, for ε_{eq} = 0.40-to-3.63.

Table 5. Yield stress as calculated by the model of Eq. (6), σ_y^{model}, and as derived from the nanoindentation Hardness measurements, $\sigma_y^{nanoind}$. In this latter case, two different approaches are here proposed, one according to [**21**] in which a factor of χ = 2.9 was considered as *H* to σ_y ratio; a second according to [**82**] in which the ratio χ = 3.5. Data refers to ε_{eq} = 0.40, 0.91, 1.21, 1.81, 2.42, and 3.63.

Table 6. Gao's model of Eq. (7) applied to the microstructure strengthening model of the present study at ε_{eq} = 0.40, 0.91, 1.21, 1.81, 2.42, and 3.63.

Nanoindentation twin-sensitive measurements and strengthening model of HPT OFHC 99.99% purity copper

Marcello Cabibbo

DIISM / Università Politecnica delle Marche, Via Brecce Bianche 12, 60131 – Ancona, Italy.

Keywords: OFHC pure copper; Twinning; HPT; Nanoindentation; ISE; TEM.

Abstract. Severe plastic deformation (SPD) techniques are among the most effective deformation modes of introducing a high rate and density of dislocations in metallic materials and alloys. The newly introduced dislocations have different characters. These were classified after Hansen and the Risœ group as statistically stored (SSD), also called incidental dislocations (ID), and geometrically necessary (GND) dislocations. As the strain cumulates some of these dislocations, namely the GNDs, are promoted to form very-low, low, and eventually high-angle boundaries. That is, new cell and grain structured are formed as the plastic deformation accumulate. Studies of the early stages of plastic deformation inducing microstructure modifications are properly carried out on pure metals as they strengthen only by the effect of dislocation, crystallite boundaries, and texturing of the metallic matrix. On this basis, the present work focuses on an electron microscopy study of the early plastic deformation stages induced in an OFHC 99.99% pure copper by high-pressure torsion (HPT). A threshold stress for the initiation of twinning formation within the Cu-grains was identified. Nanoindentation measurements were performed at different penetration depths. Thus, a correlation between the tip size-sensitive hardness evaluation (known as indentation size effect, ISE), occurring at the lower penetration depths, and the twinning formation during the early stages of HPT was found.

1. Introduction

Ultrafine-grained (UFG) metallic materials and alloys are known to possess superior mechanical properties compared to the conventional grained counterparts **[1]**. In the last two-three decades a number of grain refining methods were proposed and developed. These include top-down approaches, such as severe plastic deformation (SPD), and bottom-up approaches starting from powder metallurgy processes **[2-4]**. As for the top-down approach, different SPD techniques showed reliable, cost-effective, and promising means for obtaining thermally stable ultra-fine, and sometimes nanometric size, grain structures of metals and alloys. The most relevant such techniques are high-pressure torsion (HPT), equal-channel angular pressing (ECAP), accumulative roll-bonding (ARB), accumulative press-bonding (APB), twist extrusion (TE), friction stir processing (FSP), cyclic extrusion-compression (CEC), repetitive corrugation and straightening (RCS), accumulative back extrusion (ABE) and hydrostatic extrusion (HSE), high-pressure sliding (HPS) (**[5-13]** and references therein).

The exceptional mechanical properties achieved by the UFG metals are due to both the sub-micron cell, grain size and the mobile dislocations inside the UFGs. In addition, low stacking fault energy (SFE) materials, such as copper-alloys and pure copper, also strengthen by twinning formation within the grains. It is generally agreed that UFG processes proceed from newly introduced tangled dislocations (TD) and cell boundaries (both very-low, VLABs, and low-angle boundaries, LABs) [**5-8,11,14-19**]. These are continuously introduced in the material and eventually induced to rearrange and form cell structures by SPD. Cells are in turns induced to increase their

misorientation angle to eventually become grain boundaries (high-angle boundaries, HABs) **[14-19]**. More specifically, the dislocations generated during plastic deformation are typically classified into two categories that reflect the sliding mobility attitude and the special arrangement they tend to follow.

Thus, according to Huges *et al.* [**20**] one type of dislocations are called geometrically necessary dislocations (GNDs), and incidental dislocations (IDs), or statistically stored dislocations (SSDs). GNBs form between regions of different strain patterns to accommodate the strain induced lattice rotation. IDs (or SSDs) form by random trapping processes of dislocation during straining. These latter are stored within the already existing grains as a statistical necessary process of accommodating the local straining in the metallic material. Upon SPD different strain patterns can be activated in the material involving activation of different slip systems. This, in turns, generates differences in the partitioning of slip activity on the same slip systems of the newly introduced dislocations, and then differences in the level of equivalent strain acting in the deforming material. These differences in slip pattern ultimately promote dislocation interactions, namely between IDs, GNDs, and among IDs and GNDs, resulting in a significant energy reduction. That is, the evolution of IDs and GNDs to form cell and eventually grain boundaries is an energetic favoured process. The here described dislocation evolutionary process is in fact a statistically and thermodynamically most probable phenomenon which is activated and promoted in the metallic material by plastic and severe plastic deformation.

The dislocation strengthening mechanisms generate by the SPD are usually studied by using pure metals, such aluminum [**14,15,16,18,19,21,22**], nickel [**23-25**], copper [**11,26**], and the like [**27,28**]. In the present study a OFHC 99.99% pure copper was used to analyse the early stages of plastic deformation induced by HPT. The choice of using HPT was motivated by the almost continuous range of induced strains that it is able to induce simply by limiting the number and fraction of the metal rotations under pressure. In fact, HPT generates progressive plastic deformation levels for given number and fraction of turns, from the disc center, where it is minimum, to the disc periphery, where it is at its maximum. On the other hand, the level of induced strain strongly depends on the number of HPT rotations, *N*. In HPT the sample, in form of a thin disk, is placed between two large anvils and subjected to a high pressure and concurrent torsional straining. This way, the two meaningful parameters are the magnitude of the imposed pressure, *P*, and the number of revolutions applied to the sample, *N*. Since, the imposed strain chiefly depends on the distance from the center of the disc, the microstructure modifications imposed by HPT are greatly inhomogeneous, but continuous. For the present study, this latter aspect is considered as a key microstructure aspect to determine the minimum necessary strain level to form twinned grains in a fully annealed 99.99% pure copper.

In this sense, HPT is different from most of the other SPD processes where generally strain gradients are generated quite quickly, making almost impossible to determine the early stages of cell structure formation [**4-6,12,14,21**].

Strain gradients and strain hardening, as well as metal plastic properties, such yield stress, hardness, toughness, strongly depend on the dislocation density, ρ_{disl}. That is, when a material is plastically deformed the dislocation density increases, leading to strain gradients and metal strain hardening. The metallic material straining under plastic deformation is usually studied by electron microscopy techniques (electron back-scattered diffraction, EBSD, field-emission gun scanning electron microscopy, FEGSEM, transmission electron microscopy, TEM). Anyhow, this was also characterized by performing extremely small indentations (nanoindentations) in low defect density materials [**29,30**]. Moreover, whenever strain gradients are formed by indentations using either pyramidal or conical indenters, GNDs are generated into the material in order to accommodate the induced strain [**31,32**]. Since strain gradient increases by reducing the deformation scale (*i.e.*, small penetration depths) the density of GNDs and, consequently, the hardness of the material, increase when the size of the deformed region decreases. This quite important experimental factor that affect the process of indentation of metallic material is known as indentation size effect (ISE) [**32,33**].

With this regard, it was found that the ISE can be described by taking into account the two types of dislocations introduced during plastic deformation. That is, ISE can be described by taking into account the statistically stored dislocations (SSDs) and the geometrically necessary dislocations (GNDs) [**34**].

Following pioneering studies by Nix and Gao [**32**] nanoindentation hardness overestimation for lower tip penetration depths is directly related to underestimation of the plastic zone volume. In their model, Nix and Gao assumed plastic zones assumed to be hemispherical with a radius equal to the contact radius, a. This hemisphere volume, V, is calculated as: $V = 2\pi h^3/(3\tan^3\varphi)$, where φ represents the angle between the indenter surface and the sample surface. The nanoindentation hardness, H, is thus expressed as: $H = 3\cdot\sigma = 3^{1.5}\alpha Gb(\rho_{SSD} + \rho_{GND})^{0.5}$, being α a constant, G the material shear modulus, b its Burgers vector, and ρ_{SSD}, ρ_{GND} the densities of SSDs and GNDs, respectively. Since, H_0 can be defined as the material hardness with no GNDs, this can be expressed as $H_0 = 3^{1.5}\alpha Gb(\rho_{SSD})^{0.5}$, and thence $H = [1+(\rho_{GND}/\rho_{SSD})]^{0.5} = [1+(h_0/h)]^{0.5}$, where h_0 is the length scale factor of a given material under indentation, and h is the indentation penetration depth. This approach is based on a hemispheric volume limited to the next neighbouring of the tip radius and the lateral tip edges. This indeed can depends on the type of tip used, that is a pyramidal Berkovich, a spherical, or a cube-corner geometry [**34**].

Anyhow, GNDs is known to spread beyond the hemisphere, and thence the plastic zone volume needs to be corrected. This was addressed later on by Durst *et al.* [**35,36**], where the radius of the plastic zone is assumed to be $f\cdot a$, with f ranging from 1 to 3.5, and simulated by finite element means. In polycrystals, hardness always increases with decreasing grain size. This behaviour can be explained by the well-known Hall-Petch (H-P) relationship, which is based on the interaction between dislocations and grain boundaries in grain structured metallic materials. Anyhow, whenever the grains are wide and/or the indentation penetration depth is shallow, the generation of SSDs and GNDs is strongly related to one or few grains. This means, that the indentation plastic zone in these cases has a local character.

In this study the role of twinning formation within plastically deforming grains on the nanoindentation grain size sensitive hardness and reduced Young's modulus measurements is addressed. In particular, the minimum necessary strain by HPT to induce twinning formation was identified and the role of the twin formation on the nanoindentation depth sensitive measurements was addressed.

2. Experimental procedures and Method

2.1. The material

10 mm-wide rods of OFHC of 99.99% pure copper was fully annealed at 673 K/1 h. The chemical composition of the 99.99% purity Cu is reported in **Table 1**. Discs 1.0 mm-thick were cut from the annealed bars. As shown in **Fig. 1**, the annealed Cu showed a coarse grained structure with no significant present of free dislocations within the grains.

2.2. High-pressure torsion (HPT) process

The fully-annealed OFHC 99.99% pure Cu in form of a disc 10 mm-wide and 1.0 mm-thick was subjected to HPT under quasi-constrained conditions at room temperature, thus avoiding material outflow during straining. Different strain levels were induced into the metals as to get a discrete close range of strain levels, *i.e.*, from ε_{eq} = 0.40-to-3.63, by processing HPT at following rotation number fractions: N = 1/18, 1/8, 1/6, 1/4, 1/3, 1/2 turns.

Fig. 2 is a scheme of the HPT strain deformation imposed to a typical disc sample, where the incremental shear strain is given by $d\omega/\omega$, being ω the angular rotation around the disc center. The equivalent vön Mises strain imposed by HPT, ε_{eq}, is calculated according to **[5,11,21,37]**, Eq. (1a):

$$\varepsilon_{eq} = \frac{2}{\sqrt{3}} ln\left[\left(\frac{1+\gamma^2}{4}\right)^{0.5} + \frac{\gamma}{2}\right] \qquad \text{Eq. (1a)}$$

where $\gamma = (2\pi Nr)/t$ is the shear strain, r the distance from the disc center, that is from 0 to the disc radius, R, t is the disc thickness. From Eq.(1a) the distance to disc center-dependent equivalent strain, ε_{eq}, is:

$$\varepsilon_{eq} = \frac{2\pi Nr}{t\sqrt{3}} \qquad \text{Eq. (1b)}$$

HPT was carried out by depressing the vertical anvils to a depth of 0.05 mm. Torsion strain was exerted by rotating the upper anvil at a low rotation speed of 0.7 rpm (~4° sec^{-1}) under a pressure of 2.0 GPa.

TEM inspections and nanoindentation measurements were performed at the mid-section of the discs (that is, at a thickness $t \cong 0.5$ mm) and at mid-radius (5 mm) from the disc center. Thus, according to Eq. (1b), the resulting equivalent strain, ε_{eq}, is as listed in **Table 2**.

HPT was here used as it is able to generate low incremental strain levels, starting form a minimum level of equivalent strain as low as $\varepsilon_{eq} = 0.40$.

To avoid any possible artefact during sample preparation, the ~1 mm-thick HPT processed discs were prepared for TEM inspections by chemical and electro-chemical means only. They were first punched to 3 mm TEM discs from the above-mentioned HPT disc position and indicated in **Fig. 2**. The 3 mm-wide and ~1 mm-thick TEM discs were mechanically grinded and then electrochemically thinned and symmetrically polished to a ~200 μm thickness using a solution of 30% of phosphoric acid 20% ethylic alcohol in 50% distilled water at room temperature and a voltage of 12V. Prior final thinning to electron transparency by precision ion-milling (PIPS), the 200 μm-thick discs were fixed by a commercially pure 0.5 mm-thick copper ring with 3 mm external diameter. Then, this was thinned by Gatan™ PIPS with a low dual incident beam whose angle was fixed to 2° respect to the disc surface, to minimize the possible artefacts coming from the disc preparation (*i.e.*, to minimize the dislocations possibly introduced during the ion-milling process).

2.3. Sample preparation for TEM and method

TEM inspections were carried out in a Philips™ C-20® working at 200 keV with a double-tilt specimen holder equipped with a liquid-nitrogen cooling stage. Inspections were performed at the middle height of the HPT discs.

Two-beam excitation conditions were selected for most of the TEM observation and dislocation characterizations. Dislocation density, $\rho_{disl.}$, was quantitatively evaluated by stereological methods, such as the Ham's interception method [**38**]. Thence, $\rho_{disl.}$ was calculated through the count of interception points between the mesh and the existing dislocations, n_{disl}, in the TEM micrographs. This was evaluated by $\rho_{disl.} = 2n_{disl}/(l_{mesh}t_{TEM})$, were, l_{mesh} is the total length of the mesh, and t_{TEM} is the thickness of the TEM foil. Converged electron beam diffraction (CBED) was used to measuring the crystal thickness, t_{TEM}, by analysing the corresponding diffracted beam intensity variation under dual beam conditions. Linear interpolation of data points in a $S^2/n_{fringes}^2$ vs. $n_{fringes}^{-2}$ graph, where S is the fringes spacing, and $n_{fringes}$ the number of counted fringes, was used to determine t_{TEM}. The statistical number of possible invisible dislocations (i.e., the ones oriented as to have $b \cdot g = 0$, where b is the Burgers vector and g refers to the dislocation lying crystallographic plane) can be

considered well within the experimental error of the foil thickness evaluation. Cell (LAB) and grain boundary (HAB) misorientation were measured by Kikuchi band patterns. Kikuchi pattern method was used for determining the misorientation across the boundaries (LABs and HABs), this procedure is fully described elsewhere in previous published works by this author [**14-16**]. TEM inspections were carried out by orienting the Cu-matrix as to have [001], [011]-crystallographic planes || I_{beam} (electron beam direction).

2.4. Nanoindentation measurements

Nanoindentation measurements were performed at same HPT disc height as the one set for TEM inspections. Samples were prepared by polishing the surfaces using the same chemical polishing solution used to prepare the TEM discs. A Hysitron™ Triboscope UBI-1® was used. Calibration procedures were followed according to [**39**]. A trapezoidal load function of 5 s loading, 15 s at the set load, and 5 s unloading was used, with a set load, P_{Max} = 10 mN, and at a constant loading rate of 0.25 mN/s. The reported data were averaged over a series of 4 [8x8]-matrix of individual measurements spaced 250 μm apart. Data analysis was performed according to the Oliver-Pharr model [**40**]. Thus, the hardness, H, was evaluated as $H = P_{Max}/A$, with $A = K_{ind}h_c^2$ being the contact area, K_{ind} an indenter tip dependent coefficient (24.56 for Berkovich tip [**41**]), h_c the contact depth related to the maximum penetration depth, h_m, which is $h_c = h_m - \chi P_{Max}/S$, χ = 0.75 for Berkovich tip [**40**] and S the material stiffness. This latter, according to the Oliver-Pharr approach [**40,41**] is measured as unloading slope at the maximum penetration depth, h_m, and it is $S = Bm(h_m - h_r)^{m-1}$, where B is the unloading curve intercept at $P = 0$, m is the unloading slope, and h_r is the residual depth (the permanent plastic penetration depth on unloading). Moreover, following the Oliver-Pharr method, the reduced elastic modulus can be derived as $E_r = [(\pi/4)^{0.5}/\beta]\cdot[S/(A)^{0.5}]$, where β = 1.034 for Berkovich tips [**40**]. Thence, in the present case, $H = 0.041\cdot P_{Max}/h_c^2$ and $E_r = 0.173\cdot S/h_c$.

3. Experimental Results

3.1. Microstructure

Fig. 3 shows representative TEM micrographs of the microstructure evolution driven by the HPT shear deformation, from ε_{eq} = 0.40 to 3.63.

It resulted that twinning formation within the Cu-grains started to occur from a HPT strain level of ε_{eq} = 0.91. Starting from this shear deformation level, the pure Cu microstructure deformed plastically to produce refined grains and by cumulative twin generation within the refining grains. That is, the deformation process did change microstructure mechanism as it proceeded only by SSD and GND formation at the earliest strain levels, ε_{eq} = 0.40 (**Fig. 3(a)**), to eventually form the first low-angle boundaries (cell boundaries) and new high-angle boundaries (grain boundaries), starting from ε_{eq} = 0.91 (**Fig. 3(b)**). At this latter strain level twinning started to form, and thus this further strengthening mechanism started to operate within the pure Cu microstructure. Thence, the strain level ε_{eq} = 0.91 can be considered a threshold-like, or a cut-off lower strain limit, to initiate a microstructure twin strengthening. At strain levels above it, ε_{eq} > 1.21, the pure copper plastically deformed under HPT straining by further generation of GNDs, that eventually form grain boundaries, and by the combining strengthening effect of grain refinement and twinning-induced generation (**Fig. 3(c)-to-(f)**). With this respect, **Fig. 4** shows the evolution of the twinning induced to form and cumulate by the HPT shear deformation, from ε_{eq} = 0.91 to 3.63.

Moreover, the OFHC Cu microstructure evolved rapidly already in the early stages of straining (**Fig. 4(a),(b)**). It resulted that at strain level within ε_{eq} < 1, the microstructure undergoes typical strain hardening associated with a significant generation of LABs and cell boundaries, as showed by

Fig. 4(b). The formation of LABs, and eventually some HABs, is accompanied by the concurrent formation of twin boundaries. Both these microstructure features contribute to generate arrays of ultrafine grains at the higher strain levels.

In **Fig. 3(c)** dislocation pile-up process is showed; in particular, this piling-up generated lattice distortion on both sides of the cell wall and evolves with the presence of the early formation of twinning. These twins nucleated at grain boundaries (GBs) to extend within the grain. The formation of these twins is responsible for the development of sharp grain boundaries, which in turns implies a substantial stress relief in the boundary surrounding areas.

As for the mean grain and cell size evolution with cumulative HPT straining, the statistical evaluation carried out by TEM inspections showed a continuous grain, and especially cell size reduction from ε_{eq} = 0.91 to 3.63 (**Table 3**). That is, the mean grin size, which in the annealed initial condition was d_g = 28 μm, reduced to 19 μm at ε_{eq} = 0.40, and down to 3.2 μm, at the maximum strain of ε_{eq} = 3.63. As for the cell size, these reduced from an initial mean value d_{cell} = 1100 nm, down to 360 nm, at ε_{eq} = 3.63.

It resulted that cell size reduction process induced by HPT appeared to slow down at $\varepsilon_{eq} \geq 1.21$, when twinning formation started to characterized the grain interior and start to act as further barrier against dislocations (actually both SSDs and GNDs) sliding motion.

3.2. Nanoindentation Hardness, H, and elastic modulus, E_r

Fig. 5 reports representative nanoindentation load-displacement curves, *P-h*, for a load *P* = 10 mN, of OFHC Cu subjected to HPT at ε_{eq} = 0.40, 0.91, 1.21, and 3.63. As expected the penetration depth, h_c, reduced with cumulative straining. Yet, the unloading slope of the *P-h* slightly increased from the minimum detected strain of ε_{eq} = 0.40 to ε_{eq} = 0.91. This did not changed as the strain rose up to the maximum tested strain of ε_{eq} = 3.63. Since the unloading slope is related to the material reduced Young's modulus, E_r, the observed slope increment means that the elastic modulus of the OFHC Cu slightly increased at ε_{eq} = 0.91. This in turns implies that the occurrence of twinning formation within the grains is somehow responsible for the material changes of elastic response.
Hardness, *H*, and reduced elastic modulus, E_r, were measured according to the Oliver-Pharr approach [**40,41**], and results were plotted in **Fig. 6** as a function of the HPT shear deformation. Accordingly, the metal *H* steadily increased from the minimum, ε_{eq} = 0.40, to the top strain level, ε_{eq} = 3.63, although at ε_{eq} = 2.42, a plateau-like value of H ≅ 1.15 GPa was reached. The reduced elastic modulus, E_r, appeared to follow quite closely the hardness incremental trend with cumulative straining. Moreover, a similar plateau-like was reached at ε_{eq} = 2.42, with values E_r ≅ 170 GPa. These results are in good agreement with some previously reported study on commercially pure and quite similar OFHC pure Cu [**11**].

4. Discussion

4.1.Microstructure evolution and twinning formation induced by HPT

Dislocation formation (SSDs and GNDs) and twin formation with cumulative straining are two key mechanisms of microstructure strengthening especially for pure metals, such as the here studied OFHC 99.99% purity Cu. In fact, it is known that whenever a metallic material is subjected to plastic deformation, the newly introduced dislocations are induced to slide, in addition deformation twinning is activated, and thence both accommodate the imposed plastic strain [**42**]. The mean factors governing these microstructure induced modifications include the material SFE, the grain size and crystallographic orientation [**43-45**]. Also the external loading conditions such as stress [**46**], strain [**47**], strain rate [**48,49**], and temperature [**48**] play a crucial role. Compared to

conventional materials processing, SPD techniques impose severe shear strains producing unusual and quite high mechanical properties that are ultimately driven by the unique microstructure modifications and evolution [**50,51**]. In the present case, understanding the competitive relationship between SSDs, GNDs, the cell and grain boundary formation and the deformation twinning induced by the HT shear deformation was considered as a key factor for the description of the early stages of deformation occurring in pure bcc low SFE metals, such as copper.

In materials with medium to high SFE, GNDs and SSDs develop since the early stages of plastic deformation [**52,53**]. The role of GNDs is to accommodate the shear strain gradients throughout the microstructure. SSDs are formed by tangled dislocation random trapped under uniform localized deformation. These newly introduced dislocations easily slide by cross slip by which the formation of dislocation boundaries (both low- and high-angle) is favoured with cumulative strain. The mechanism of boundary formation out of chiefly GNDs is driven by a mutual trapping, rearrangement, and annihilation process [**53,54**]. In fact, it is known that the dislocation types that do contribute to the crystal lattice rotation are the GNDs [**54**].

On the other hand, for lower SFE metals, such as copper, the formation of initially few, and then more and more volume fraction of stacking faults and twinning is favoured with cumulative straining [**55**]. Under severe plastic deformation regimes, the twinned grains contribute to accommodate the plastic deformation as well as the refining grains do. Moreover, when twinned grains have a proper crystallographic orientation respect to the external load, multiple twinning systems are activated, leading to twin-twin intersection phenomena. These, in turns, become a further strengthening mechanism for the twinned metallic material [**55,56**].

Thence, in low SFE metals the reduced dislocation mobility make the twinning deformation a necessary-like mechanism for the material to rearrange the microstructure, by strengthening it, under the applied external load. In the present study this necessary-like microstructure mechanism of twinning formation under HPT was found to occur for a strain level as low as ε_{eq} = 0.91. No traces of twinning formation was found for lower equivalent strains, where the microstructure strengthening proceeded only by formation and evolution of SSDs, GNDs, cell walls and eventually of some GB. The role of the SSDs and GNDs referring to the continuous process of cell and grain refinement induced by the HPT deformation was twofold. On one side, it was that of a microstructure source of active line defects able to thickening the newly generated boundaries, either cell or grain; on another side, it was that of contributing to rise the boundary misorientation angle as they continuously formed by the HPT action. As soon as the twins started to be generated, they behaved as a further microstructure strengthening term that did not affected the grain refining process driven by the HPT cumulative deformation.

4.2.Indentation size effect (ISE)

In nanoindentation measurements, as the indentation depths get shallow, by reducing the applied load, the obtained hardness is known to increase accordingly. This indentation size effect (ISE) was observed in metallic materials [**32-36**]. Nix and Gao proposed a model, also known as NG-model, that relates this ISE to the generation of GNDs, whose density is proportional to the inverse indentation depth [**32**]. The additional hardening due to the GNDs is a mere effect of an indentation tip-to-the beneath indentation plastically deformed volume interaction phenomenon. Thus, ISE is particularly evident and pronounced in soft annealed metallic materials, such as the present case of annealed OFHC 99.99 purity Cu. On the contrary, ISE is typically of minimal significance in hardened metallic materials. This behaviour is directly correlated to the inner length scale of the material due to the induced increased dislocation density driven by the cumulative flow stress.

The ISE phenomenon is known to be generated by additional hardening given by the GNDs. This penetration depth sensitivity of the nanoindentation measurements is mainly based on two factors. One, is a microstructure-based factor, which is constituted by the total line length of dislocations necessary to form the permanent indented profile; the second, is geometrical-based and

is related to the overall extension of the material volume in which the dislocations are stored. Indeed, both factors are strongly related to the generation of stored and necessary dislocations, *i.e.* SSDs and GNDs. A study of the ISE occurring on the early stages of HPT is here presented. To do that, nanoindentation load was almost continuously reduced from 10 mN to loads as low as ~100 μN. The obtained hardness, *H*, increment due to the ISE, as a function of lowering penetration depths down to few hundreds of nanometer, for strain levels of ε_{eq} = 0.40-to-3.63 is reported in **Fig. 7**. It is worth to note that the measured *H* variation with lowering penetration depths followed different slopes depending on the strain level to which the pure copper was subjected. It appeared that from HPT strains ε_{eq} < 0.40 / 0.91. *H* followed an almost continuous incremental rate as the load and penetration depth lowered. Starting from ε_{eq} = 0.91 and up to ε_{eq} = 3.63, *H* increment by lowering the penetration depth followed an initial almost linear trend, to drastically rise for penetration depths lower than 900-800 nm. This different ISE trend is believed to be somehow determined by the reducing grain size and the concurrent formation of twinned grains.

4.3. Twinning formation role in ISE

Results reported **Fig. 7** showed an ISE-driven hardness increment of ~10% at indentation depths ranging 1.8-to-0.9 μm, from as-annealed to HPT strain ε_{eq} = 3.63. This increment can be identified as the minimal deviation from the actual *H* evaluation due to the ISE phenomenon and is reported in **Fig. 8**. Thus, the measured depth range to reach a *H* variation by 10% from the asymptotical and actual value, obtained at higher penetration depth ranges, strongly depended on the strain level and, ultimately, on the induced grain/cell size reduction. The corresponding penetration depth value is also called length scale, h^*. That is, as reported in the plot of **Fig. 8**, a direct correlation exists between the occurrence of a significant ISE and the mean grain (and cell) size of the testing metallic material. Present result appears to be in good agreement to data reported by Nix and Gao in [**32**] derived by a linear fitting of $(H/H_0)^2$ vs. h_c^{-1} in pure Cu, where a value of length scale of ISE h^* = 1.60 μm was reported. Thence, the here obtained results showed the length scale, h^*, to rise with grain, cell size reduction, and with occurrence of twinned grains. That is, the ISE appeared to anticipate by refining the grained structure of pure Cu by cumulative HPT straining. To some extent, this issue was addressed and discussed by Yang and Vehoff [**34**] who studied ISE occurring in high-purity nanocrystalline Ni with different mean grain size obtained by plastic deformation techniques. Similarly, Lapovok *et al.* [**57**] reported a certain degree of ISE initiation dependency to the level of ECAP shear straining in pure Cu. They show ISE occurring with lower penetration depth as the ECAP shear straining cumulate and thus as the resulting mean grain refined. Similar trends for commercially pure Cu were reported in [**58**] by HPT, and in [**36**] by ECAP.

Fig. 8 shows *H* rising trend slopes for the two strain levels above mentioned, that is, for ε_{eq} < 0.91, and for 0.91 < ε_{eq} < 2.42. It thus resulted that the *H* increment was slow (0.93 GPaμm^{-1}) at the earliest stages of deformation, to double (1.84 GPaμm^{-1}) for strain levels by which grain started to refine and twins started to form within the grains. This would ultimately means that a direct correlation between the rate and amplitude of ISE and the grained structure of pure copper exists. To better understand this ISE microstructure dependency, twin spacing, λ_{Twin}, was measured for strains 0.91 < ε_{eq} < 2.42, that is for the strain levels where twins started to form (ε_{eq} = 0.91) and then filled the grained structures (ε_{eq} = 2.42). The statistical evaluation of twin spacing, carried out for strain levels ε_{eq} = 0.91-to-2.42 is reported in **Fig. 9**.

The twin spacing appeared not to evolve significantly with cumulative HPT strain. Mean twin spacing was $\lambda_{Twin} \cong 32 \pm 2$ nm irrespective of the strain level throughout the range 0.91 < ε_{eq} < 2.42. The only clear aspect that differentiated the λ_{Twin} size distribution with HPT strain was the maximum twin spacing sizes that appeared to reduced form 80 nm, at ε_{eq} = 0.91, down to 60 nm, at ε_{eq} =2.42.

Quite similar twin spacing sizes were also reported by Yang and Vahoff [**34**] in SPD high-purity nickel and by Saldana *et al.* [**59**] in SPD same OFHC 99.99 purity copper. In particular, Saldana *et al.* accounted on thermomechanical stability in ultra-fine grained copper with high density of twin boundaries. Nanoscale network of twins within the grains are generally induced to form by SPD processes. In this sense, the here reported formation and evolution of twins induced by the HPT cumulative strain was actually expected mostly on the basis of the relative low OFHC Cu SFE. Moreover, twin boundary formation promoted by SPD (HPT in the present case) are strongly affected by the generation and evolution with strain of SSDs and GNDs. In particular, the twins formed during SPD means can have a significant high aspect ratio, that is a high length to spacing ratio). This microstructure feature was widely observed in the present study and the corresponding morphological twin evolution with SPD strain was also reported by Wang *et al.* in a nanostructured pre Cu [**60**].

Fig. 10 shows a direct comparison between the twin spacing and grain/cell evolution with cumulative HPT straining. The general refining trend of both cells and grains was accompanied by a non-significant twin spacing variation, although twin volume fraction increased to a great extent in the strain range ε_{eq} = 1.21-to-2.42.

4.4. Strengthening model

It is well known how strength of a metallic material can be directly related to the microstructural features, such dislocations, cell and grain boundaries (and related mean size), and, limited to the low-to-medium SFE metals, to the twin boundaries (TB). The flow stress, namely the material yield stress, can be derived as contributions aggregate of the above-mentioned strengthening terms [**61,62**]. Apart from the grain boundary strengthening which is modelled by the Hall-Petch relationship, a number of models accounted on the strength contribution coming from cell boundaries. These can actually have a low-angle, but also a very low-angle character [**14**]. The first ones are typically boundaries with misorientation angle within ~4-14°, the second ones have typical misorientation of ~2-4° and always show Moiré fringes on TEM. For the first case, the strength contribution can be modelled as to be proportional to the square root of the density of dislocation stored inside the boundaries (essentially SSDs) [**61**]. The second case corresponds to the existing tangled dislocations (TDs) [**14,62,63**]. On the other hand, the occurrence of TB from strain levels of ε_{eq} > 0.40, makes necessary considering this further microstructure strengthening contribution [**64,65**]. Thence, the following relationship was proposed for modelling the OFHC Cu yield stress as determined by the nanoindentation hardness measurements, Eq. (1):

$$\sigma_y = \sigma_0 + \sigma_{disl.} + \sigma_{HP} + \sigma_{TB} \qquad \text{Eq. (1)}$$

where σ_0, $\sigma_{disl.}$ is the stress due to SSDs and GNDs, σ_{HP} is the stress given by the grained structure (calculated through the Hall-Petch relationship), σ_{TB} is the stress due to the twins (twin boundaries, TB).

The dislocation contribution is the linear combination of the SSDs and of the GNDs strengthening, and they are both directly dependent on the related densities. In particular, SSDs do form very low-angle and low-angle boundaries under plastic deformation, and thus their density is expressed as, Eq. (2):

$$\rho_{SSD} = f\rho_{wall} + (1-f)\rho_{TD} \qquad \text{Eq. (2)}$$

W here f is the fraction of the SSDs that do contribute to the wall (boundary) formation, ρ_{wall} is the density of the formed walls, and ρ_{TD} represents the density of the dislocations existing in the cell and grain interiors that did not form boundaries and that are generally referred as to tangled

dislocations (TD). According to [**57**] the value of f can be determined as $f = 1-(1-\lambda_{wall}/d_{cell})^3$, λ_{wall} and d_{cell} being the mean wall (cell boundary) thickness and cell size, respectively.
Thence, the dislocation strengthening contribution, $\sigma_{disl.}$, can be calculated as, Eq. (3):

$$\sigma_{disl.} = M\alpha Gb[f\rho_{wall} + (1-f)\rho_{TD} + \rho_{GND}]^{0.5} \qquad \text{Eq. (3)}$$

where $M = 3.06$ is the Taylor factor [**66**], $\alpha = 0.33$ [**66**], $G = 48.2$ GPa is the shear modulus of pure copper [**66**], $b = 0.256$ nm is the copper Burgers vector [**61,65**].

Here the walls are actually considered as the continuously generated very-low and low-angle boundaries, *i.e.* the cell boundaries.

Onset of twinning occurs whenever the slip stress reaches the minimum necessary strain to activate the twinning. The present results showed that the minimum necessary strain level to initiate the twin formation was $\varepsilon_{eq} = 0.91$. Thence, whenever formed, the twins yield a further strengthening contribution given by their boundaries (twin boundary, TB), σ_{TB}. This strengthening contribution is modelled similarly to an Hall-Petch relationship but with a constant, K_{TB}, significantly higher than that pertaining the grain boundary strengthening, K_{HP}. Thus, according to Hansen [**61,67,68**], Armstrong and Worthington [**69**] and Meyers *et al.* [**42**], $K_{TB} = 0.28$ MPa·m$^{1/2}$, compared to $K_{HP} = 0.14$ MPa·m$^{1/2}$, and the corresponding strengthening contribution can be modelled as, Eq. (4):

$$\sigma_{TB} = K_{TB} \cdot d_g^{-1/2} \qquad \text{Eq. (4)}$$

By taking into account the actual fraction of twinned grains, f_{twin}, rising with cumulative HPT straining, the following strengthening model was here proposed, Eq. (5):

$$\sigma_y = \sigma_0 + M\alpha Gb\{[f\rho_{wall} + (1-f)\rho_{TD} + \rho_{GND}]^{1/2} + [(f_{twin} \cdot K_{TB} + (1- f_{twin}) \cdot K_{HP}]d_g^{-1/2}\} \qquad \text{Eq. (5)}$$

The calculated values of f_{twin} are also reported in the plot of **Fig. 10**. Referring to Eq. (5), **Fig. 11** shows a representative TEM micrograph of the microstructure at $\varepsilon_{eq} = 2.42$ in which all the strengthening features are present, *i.e.* dislocation walls, tangled dislocations, geometrically-necessary dislocations, twin boundaries, and grain boundaries.

Dislocation density, namely ρ_{wall}, ρ_{TD}, ρ_{GND}, and fraction of wall boundaries, f, were determined by TEM stereology analyses (ASM EN-112). The mean data for each experimental condition, $\varepsilon_{eq} =$ 0.40-to-3.63, are reported in the following **Table 4**.

The dislocation density data obtained in the present study well agree to previously published results on severely plastic deformed pure copper by ECAP up to 16 passes [**70**]. On the other hand, Lapovok *et al.* [**70**] reported dislocation wall spacing four times lower than the cell size at the early stages of ECAP deformation. In the present case a typical spacing of the dislocation walls of almost one-order of magnitude lower than the cell spacing was found.

On the basis of the data reported in **Table 3**, for grain sizes, and **Table 4**, for dislocation densities and fraction of the dislocation walls, Eq. (5) gives a microstructure-based quantitative evaluation of the OFHC 99.99 purity Cu yield stress, as reported in **Table 5**.

The present approach founds a number of scientific support given by previously published works and models proposed for different pure metals and alloys. These include the early studies on the impact of heterogeneous nature and distribution of dislocations on the metal and alloy shear stress, which were evaluated by Mughrabi using a composite-like model [**71,72**]. Following the pioneering works by Mughrabi, several other authors applied and adapted the Mughrabi composite-like model to different metals, alloys, and plastic deformation techniques [**73-78**]. These previous works report and apply strengthening models essentially same as the one here presented and applied to the OFHC 99.99 purity Cu. Moreover, the present approach is also able to describe metals and

alloys work hardening mechanisms up to flow-stress saturation, as exhaustively reported by Nes and co-workers in [**79**].

Table 5 also reports a direct comparison between the yield stress as obtained through Eq. (5), and the one derived from the nanoindentation hardness measurements, $\sigma_y^{nanoind}$. With this respect, a linear relationship is known to hold between hardness, H, and yield stress, given by $H = (\sigma_y/3)\cdot(0.1)^{m-2}$, where m is the Meyer's hardness coefficient [**80**]. With this respect several published works on different metallic materials and alloys reported a hardness-to-yield stress relationship with a narrow ratio interval of $\chi = H_V/\sigma_y$ = 2.7-3.1 [**81-83**]. In the cold-rolled metallurgical status this relationship was reported to essentially have the same ratio range of 2.8-3.1 [**80,81**]. A Meyer's hardness similar approach was recently used and applied to aluminum alloys by Tiryakioğlu in [**82**]. In this case a $\sigma_y = A\cdot H_V + B$ type relationship was used starting from a Meyer's hardness approach as: $\sigma_y = H_V /0.947\cdot C - \Delta\sigma_y$. This type of approach to determining yield stress from hardness measurements, namely nanoindentation measurements, was also used by the present author for a 6N-Al subjected to low strains by HPT [**21]**. On the other hand, Tekkaya [**83**] for cold-worked Cu-based alloys introduced a step-like variation of the yield stress-to-hardness ratio depending on the yield offset that can be taken into account. For yield offset of within 0.112% the following relationship was proposed and experimentally validated: $H_V = 2.475\cdot\sigma_y$, where H_V is the Vickers hardness number. This relationship was generalized in a form of $\sigma_y = 9.81\cdot H_V/2.475$ for yield offsets up to 0.2%. In any case, by converting the Vickers number to MPa, the two previously reported approaches (Tiryakioğlu's and Tekkaya's) can be expressed as $\sigma_y = 0.375\cdot H^{nanoind}$, that is $\chi = H_V/\sigma_y = 2.7$. Very recently, Song *et al.* [**84**] reported a rather wider variation for $\chi = H_V/\sigma_y$ = 3-4.5, this reduces down to $\chi \cong 3.24$ whenever the ultimate stress is considered instead of the yield stress. Other studies, such as the work by Zhang *et al.* [**85**] indicated values ranging 3.26-3.70 (with a mean value of χ = 3.5) in pure copper subject to ECAP. In his work, Zhang *et al.* reported an overview of the factor influencing the χ ratio between H_V and σ_y for different copper alloys.

Thence, in the present study both values of χ = 2.9 and χ = 3.5 were taken into consideration for the identification of the more appropriate value able to meet the yield stress determined by the microstructure based model here described. It is worth to underline here that the χ = 2.9-2.8 was found to be an appropriate ratio between H_V and σ_y in metallic alloys, as well as pure metals, such aluminum ([**21,80-82**] and references therein).

The direct comparison of yield stress obtained by using both $\chi = H^{nanoind}/\sigma_y$ = 2.9 and 3.5,showed a quite better agreement to the yield stress given by applying Eq. (5) with χ = 3.5 rather than by using χ = 2.9. Present results seem to indicate that a slight difference of the H/σ_y does exist whenever low-SFE metals (namely pure metals) or high-SFE metals subjected to SPD are considered.

To better understand this fitting ratio between the two yield stress values obtained by microstructure inspections and by indirect hardness measurements the Gao's approach was here reported and discussed. Gao's relationship between hardness and yield stress also includes the material elastic modulus, E, Eq. (6):

$$H^{nanoind} = \frac{2}{3}\sigma_y\left\{1 + \frac{3}{4}\left(\frac{1}{3}\frac{E_r}{\sigma_y}\cot(\alpha)\right)^n + \frac{1}{n}\left[\left(\frac{1}{3}\frac{E_r}{\sigma_y}\cot(\alpha)\right)^n - 1\right]\right\} \qquad \text{Eq. (6)}$$

where α is the semi-angle of the indentation tip, and n is the work-hardening coefficient. This approach and equation was applied to the present case, where the reduced (local) elastic modulus was determined by the nanoindentation measurements and the semi-angle α = 65°, for a Berkovich tip. The work-hardening coefficient n can be set equals to the true strain at necking and it can be derived from nanoindentation assuming a 8-to-10% plastic strain acting during the indentation process ([**85,86**] and references therein). That is, the value of work-hardening in stress-strain curves for annealed copper was is used, n = 0.54. By putting the constant values of Eq. (6) and the obtained

reduced elastic modulus values as obtained different experimental conditions here tested, the data reported in **Table 6** were obtained. **Table 6** shows a reasonably good agreement between the Gao's model data and the microstructure strengthening model for strain levels $\varepsilon_{eq} > 1.21$,while for lower strain levels the agreement was less evident. On the other hand, this approach seemed not to show a better result alignment to the data obtained by the strengthening model compared to simply considering the ratio $\chi = H_V/\sigma_y = 3.5$.

5. Conclusions

In this study early stages of plastic deformation by HPT were characterized by electron microscopy inspections. A OFHC 99.99 pure copper was subjected to strain levels as low as ε_{eq} = 0.40-to-3.63. Mechanical properties were tested by nanoindentation and the indentation size effect phenomenon was correlated to the microstructure evolution induced by the cumulative straining.

The following major findings can be outlined.

1. A minimum necessary strain level to induce the formation of twins was found and it resulted to be $\varepsilon_{eq} = 0.91$;
2. The occurrence of twinning within the refining grains influenced the ISE as it contributed to change the hardness-to-penetration depth curves. That is, the ISE depended to some extent to the formation of twins in pure Cu. With this respect, the hardness rise due to the ISE accelerated with reducing cell and grain size and with occurrence of twins. At the same time, the penetration depth by which ISE started to occur reduced with twin formation and progressive generation within the refining grains;
3. A microstructure based strengthening model was proposed and all the meaningful strengthening contributions were taken into account. In particular, SSDs, dislocation walls, GNDs, grain boundaries and twin boundaries strengthening contributions were modelled. OFHC pure Cu yield stress given by the microstructure based model was directly compared to the yield stress as derived from the nanoindentation hardness.
4. Discussion on the different models of relationship between hardness and yield stress seemed to indicate that $\chi = H_V/\sigma_y = 3.5$ was the more appropriate coefficient to be considered.

Declaration of Competing Interest

None.

Acknowledgements.

The author wish to thank Mr. M. Pieralisi for his assistance in performing the HPT tests.

References

[1] X.X. Huang, N. Hansen, N. Tsuji, Hardening by annealing and softening by deformation in nanostructured metals, Science 312 (2006) 249-251.

[2] I.A. Ovid'ko, R.Z. Valiev, Y.T. Zhu, Review on superior strength and enhanced ductility of metallic nanomaterials, Prog. Mater. Sci. 94 (2018) 462-540.

[3] M. Cabibbo, Nanostructured Cobalt Obtained by Combining Bottom-Up and Top-Down Approach, Metals 8(11) (2018) 962-971.

[4] I. Sabirova, M.Yu. Murashkin, R.Z. Valiev, Nanostructured aluminium alloys produced by severe plastic deformation: New horizons in development Mater. Sci. Eng. A 560 (2013) 1-24.
[5] A.P. Zhilyaev, T.G. Langdon, Using high-pressure torsion for metal processing: Fundamentals and applications, Progr. Mater. Sci. 53 (2008) 893-979.
[6] R.Z. Valiev, T.G. Langdon, Principles of equal-channel angular pressing as a processing tool for grain refinement, Progr. Mater. Sci., 51 (2006) 881-981.
[7] A. Vinogradov, Y. Estrin, Analytical and numerical approaches to modelling severe plastic deformation, Progr. Mater. Sci. 95 (2018) 172-242.
[8] Y. Cao, S. Ni, X. Liao, M. Song, Y. Zhu, Structural evolutions of metallic materials processed by severe plastic deformation, Mater. Sci. Eng. R 133 (2018) 1-59.
[9] B.L. Li, N. Tsuji, N. Kamikawa, Microstructure homogeneity in various metallic materials heavily deformed by accumulative roll-bonding, Mater. Sci. Eng. A 423 (2006) 331-342.
[10] Y. Xun, F.A. Mohamed, Refining efficiency and capability of top-down synthesis of nanocrystalline materials, Mater. Sci. Eng. A 528 (2011) 5446-5452.
[11] A.I. Almazrouee, K.J. Al-Fadhalah, S.N. Alhajeri, T.G. Langdon, Microstructure and microhardness of OFHC copper processed by high-pressure torsion, Mater. Sci. Eng. A 641 (2015) 21-28.
[12] M. Ebrahimi, C. Gode, Severely deformed copper by equal channel angular pressing, Progr. Nat. Sci.: Mater. Int.l 27 (2017) 244-250.
[13] N.Q. Chinh, T. Csanádi, J. Gubicza, T.G. Langdon, Plastic behavior of face-centered-cubic metals over a wide range of strain, Acta Mater. 58 (2010) 5015-5021.
[14] M. Cabibbo, Microstructure strengthening mechanisms in different equal channel angular pressed aluminum alloys, Mater. Sci. Eng. A560 (2013) 413-432.
[15] M. Cabibbo, A TEM Kikuchi pattern study of ECAP AA1200 via routes A, C, B_C, Mater. Character. 61 (2010) 613-625.
[16] M. Cabibbo, W. Blum, E. Evangelista, M.E. Kassner, M.A. Meyers, Transmission electron microscopy study of strain induced low- and high-angle boundary development in equal-channel angular-pressed commercially pure aluminum, Metall. Mater. Trans. A39 (2008) 181-192.
[17] C. Xu, Z. Horita, T.G. Langdon, The evolution of homogeneity in processing by high-pressure torsion, Acta Mater. 55 (2007) 203-212.
[18] G. Sakai, Z. Horita, T.G. Langdon, Grain refinement and superplasticity in an aluminum alloy processed by high-pressure torsion, Mater. Sci. Eng. A 393 (2005) 344-351.
[19] Y. Ito, K. Edalati, Z. Horita, High-pressure torsion of aluminum with ultrahigh purity (99.9999%) and occurrence of inverse Hall-Petch relationship, Mater. Sci. Eng. A 679 (2017) 428-434.
[20] D.A. Hughes, N. Hansen, D.J. Bammann, Geometrically necessary boundaries, incidental dislocation boundaries and geometrically necessary dislocations, Scripta Mater. 48 (2003) 147-153.
[21] M. Cabibbo, Minimum necessary strain to induce tangled dislocation to form cell and grain boundaries in a 6N–Al, Mater. Sci. Eng. A 77 (2020) 138420.
[22] I. Sabirov, M.Yu. Murashkin, R.Z. Valiev, Nanostructured aluminium alloys produced by severe plastic deformation: New horizons in development, Mater. Sci. Eng. A 560 (2013) 1-24.
[23] A. P. Zhilyaev, B.-K. Kim, J.A. Szpunar, M.D. Baró, T.G. Langdon, The microstructural characteristics of ultrafine-grained nickel, Mate. Sci. Eng. A 391 (2005) 377-389.
[24] G.B. Rathmayr, A. Hohenwarter, R. Pippan, Influence of grain shape and orientation on the mechanical properties of high pressure torsion deformed nickel, Mater. Sci. Eng. A 560 (2013) 224-231.
[25] K.S. Raju, M.G. Krishna, K.A. Padmanabhan, K. Muraleedharan, N.P. Gurao, G. Wilde, Grain size and grain boundary character distribution in ultra-fine grained (ECAP) nickel, Mater. Sci. Eng. A 491 (2008) 1–7.
[26] Q. Xue, I.J. Beyerlein, D.J. Alexander, G.T. Gray III, Mechanisms for initial grain refinement in OFHC copper during equal channel angular pressing, Acta Mater. 55 (2007) 655-668.

[27] A. Azushima, R. Kopp, A. Korhonen, D.Y. Yang, A. Yanagida, Severe plastic deformation (SPD) processes for metals, CIRP Annals 57 (2008) 716-735.
[28] R.Z. Valiev, Producing bulk nanostructured metals and alloys by severe plastic deformation (SPD), Nanostruct. Metals All. Chapter 1 (2011) 3-39.
[29] D. Lorenz, A. Zeckzer, U. Hilpert, P. Grau, H. Johansen, H.S. Leipner , Pop-in effect as homogeneous nucleation of dislocations during nanoindentation, Phys. Rev. B 67 (2003) 172101 1-4.
[30] A. Asenjo, M. Jaafar, E. Carrasco, J.M. Rojo, Dislocation mechanisms in the first stage of plasticity of nanoindented Au(111) surfaces, Phys. Rev. B 73 (2006) 075431 1-7.
[31] N.A. Fleck, G.M. Muller, M.F. Ashby, J.W. Hutchinson, Strain gradient plasticity: Theory and experiment, Acta Metall. Mater. 42 (1994) 475-487.
[32] W.D. Nix, H.J. Gao, Indentation size effects in crystalline materials: A law for strain gradient plasticity, Mech. Phys. Solids 46 (1998) 411-425.
[33] W. Liu, L. Chen, Y. Cheng, L. Yu, X. Yi, H. Gao, H. Duan, Model of nanoindentation size effect incorporating the role of elastic deformation, J. Mech. Phys. Solids 126 (2019) 245-255.
[34] B. Yang, H. Vehoff, Dependence of nanohardness upon indentation size and grain size – A local examination of the interaction between dislocations and grain boundaries, Acta Mater. 55 (2007) 849-856.
[35] K. Durst, M. Göken, G.M. Pharr, Indentation size effect in spherical and pyramidal indentations, J. phys. D: Appl. Phys. 41 (2008) 074005.
[36] K. Durst, B. Backes, M. Göken, Indentation size effect in metallic materials: Correcting for the size of the plastic zone, Scripta Mater. 52 (2005) 1093-1097.
[37] N.H. Polakowski, E.J. Ripling, Strength and Structure of Engineering Materials, Prentice-Hall, Englewood Cliffs, NJ, 1966.
[38] J. C. Russ, R., T. Dehoff, Practical Stereology, 2nd Ed. Springer Science & Business Media LLC New York, 2000.
[39] M. Cabibbo, P. Ricci, R. Cecchini, Z. Rymuza, J. Sullivan, S. Dub, S. Cohen, An international round-robin calibration protocol for nanoindentation measurements, Micron 43 (2012) 215-222.
[40] W.C. Oliver, G.M. Pharr, Measurement of hardness and elastic modulus by instrumented indentation: Advances in understanding and refinements to methodology, J. Mater. Res. 19 (2004) 3-20.
[41] J.H. Gong, H.Z. Miao, Z.J. Peng, Analysis of the nanoindentation data measured with a Berkovich indenter for brittle materials: effect of the residual contact stress, Acta Mater. 52 (2004) 785-793.
[42] M.A. Meyers, O. Vöhringer, V.A. Lubarda, The onset of twinning in metals: a constitutive description. Acta Mater. 49 (2001) 4025-4039.
[43] W.Z. Han, Z.F. Zhang, S.D. Wu, S.X. Li, Combined effects of crystallographic orientation, stacking fault energy and grain size on deformation twinning in fcc crystals, Phil. Mag. 88 (2008) 3011-3029.
[44] Y. Cao, Y.B. Wang, X.Z. Liao, M. Kawasaki, S.P. Ringer, T.G. Langdon, Y.T. Zhu, Applied stress controls the production of nano-twins in coarse-grained metals. Appl. Phys.Lett. 101 (2012) 231903.
[45] G. Laplanche, A. Kostka, O.M. Horst, G. Eggeler, E.P. George, Microstructure evolution and critical stress for twinning in the CrMnFeCoNi high-entropy alloy. Acta Mater. 118 (2016) 152-163.
[46] Y.S. Li, Y. Zhang, N.R. Tao, K. Lu, Effect of the Zener-Hollomon parameter on the microstructures and mechanical properties of Cu subjected to plastic deformation. Acta Mater. 57 (2009) 761-772.
[47] L.E. Murr, M.A. Meyers, C.S. Niou, Y.J. Chen, S. Pappu, C. Kennedy, Shock-induced deformation twinning in tantalum. Acta Mater. 45 (1997) 157-175.

[48] I.J. Beyerlein, L.S. Tóth, Texture evolution in equal-channel angular extrusion. Progr. Mater. Sci. 54 (2009) 427-510.
[49] M.F. Ashby, The deformation of plastically non-homogeneous materials. Phil. Mag. 21 (1970) 399-424.
[50] D.A. Hughes, N. Hansen, D.J. Bammann, Geometrically necessary boundaries, incidental dislocation boundaries and geometrically necessary dislocations. Scripta Mater. 48 (2003) 147-153.
[51] P. Li, S.X. Li, Z.G. Wang, Z.F. Zhang, Fundamental factors on formation mechanism of dislocation arrangements in cyclically deformed fcc single crystals. Progr. Mater. Sci. 56 (2011) 328-377.
[52] D. Kuhlmann-Wilsdorf, Theory of plastic deformation: properties of low energy dislocation structures. Mater. Sci. Eng, A 113 (1989) 1-41.
[53] X.H. An, Q.Y. Lin, S. Qu, G. Yang, S.D. Wu, Z.F. Zhang, Influence of stacking-fault energy on the accommodation of severe shear strain in Cu-Al alloys during equal-channel angular pressing. J. Mater. Res. 24 (2009) 3636-3646.
[54] A.A.S. Mohammed, E.A. El-Danaf, A.A.Radwan, A criterion for shear banding localization in polycrystalline FCC metals and alloys and critical working conditions for different microstructural variables. J. Mater. Process. Technol. 186 (2007) 14-21.
[55] P. Müllner, A.E. Romanov, Internal twinning in deformation twinning. Acta Mater. 48 (2000) 2323-37.
[56] J.W. Christian, S. Mahajan, Deformation twinning. Progr. Mater. Sci. 39 (1995) 1-157.
[57] R. Lapovok, F.H. Dalla Torre, J. Sandlin, C.H.J. Davies, E.V. Pereloma, P.F. Thomson, Y. Estrin, Gradient plasticity constitutive model reflecting the ultrafine micro-structure scale: the case of severely deformed copper, J. Mech. Phys. Solids 53 (2005) 729-747.
[58] Y. Estrin, A. Molotnikov, C.H.J. Davies, R. Lapovok, Strain gradient plasticity modelling of high-pressure torsion, J. Mech. Phys. Solids 56 (2008) 1186-1202.
[59] C. Saldana, A.H. King, S. Chandrasekar, Thermal stability and strength of deformation microstructures in pure copper, Acta Mater 60 (2012) 4107-4116.
[60] H.L. Wang, Z.B. Wang, K. Lu, Interfacial diffusion in a nanostructured Cu produced by means of dynamic plastic deformation, Acta Mater. 59 (2011) 1818-1828.
[61] N. Hansen, Hall–Petch relation and boundary strengthening, Scripta Mater. 51 (2004) 801-806.
[62] S. Nemat-Nasser, Y. Li, Flow stress of f.c.c. polycrystals with application to OFHC Cu, Acta Mater. 46 (1998) 565-577.
[63] M. Cabibbo, Microstructure strengthening mechanisms in an Al–Mg–Si–Sc–Zr equal channel angular pressed aluminium alloy, Appl. Surf. Sci. 281 (2013) 38-43.
[64] W. Han, S. Wu, C. Huang, S. Li, Z. Zhang, Orientation design for enhancing deformation twinning in Cu single crystal subjected to equal channel angular pressing, Adv. Eng. Mater. 10 (2008) 1110-1113.
[65] S.D. Antolovich, R.W. Armstrong, Plastic strain localization in metals: origins and consequences, Progr. Mater. Sci. 59 (2014) 1-160.
[66] F. Dalla Torre, R. Lapovok, J. Sandlin, P.F. Thomson, C.H.J. Davies, E.V. Pereloma, Microstructures and properties of copper processed by equal channel angular extrusion for 1–16 passes, Acta Mater. 52 (2004) 4819-4832.
[67] N. Hansen, X. Huang, G. Winther, Grain orientation, deformation microstructure and flow stress, Mater. Sci. Eng. A 494 (2008) 61-67.
[68] N. Hansen, X. Huang, Microstructure and flow stress of polycrystals and single crystals, Acta Mater. 46 (1998) 1827-1836.
[69] R.W. Armstrong, P.J. Worthington, in Metallurgical Effects at High Strain Rates, ed. R.W. Rohde, B.M. Butcher, J.R. Holland, C.H. Karnes. Plenum Press, New York, USA (1973) 401-414.
[70] R. Lapovok, F.H. Dalla Torre, J. Sandlin, C.H.J. Davies, E.V. Pereloma, P.F. Thomson, Y. Estrin, Gradient plasticity constitutive model reflecting the ultrafine micro-structure scale: the case of severely deformed copper, J. Mech. Phys. Solids 53 (2005) 729-747.

[71] H. Mughrabi, Dislocation wall and cell structures and long-range internal stresses in deformed metal crystals, Acta Metall. 31 (1983) 1367-1379.
[72] H. Mughrabi, A two-parameter description of heterogeneous dislocation distributions in deformed metal crystals, Mater. Sci. Eng. A 85 (1987) 15-31.
[73] F.R.N. Nabarro, Work hardening and dynamical recovery of F.C.C. metals in multiple glide, Acta Metall. 37 (1989) 1521-1546.
[74] T. Ungár, L.S. Tóth, J. Illy, I. Kovács, Dislocation structure and work hardening in polycrystalline ofhc copper rods deformed by torsion and tension, Acta Metall. 34 (1986) 1257-1267.
[75] A.S. Argon, P. Haasen, A new mechanism of work hardening in the late stages of large strain plastic flow in F.C.C. and diamond cubic crystals, Acta Metall. Mater. 11 (1993) 3289-3306.
[76] Y.Estrin, L.S. Tóth, A. Molinari, Y. Bréchet, A dislocation-based model for all hardening stages in large strain deformation, Acta Mater. 46 (1998) 5509-5522.
[77] X. Feaugas, P. Pilvin, A Polycrystalline Approach to the Cyclic Behaviour of f.c.c. Alloys – Intra- Granular Heterogeneity, Adv. Eng. Mater. 11 (2009) 703-709.
[78] M.E. Kassner, P. Geantil, L.E. Levine, Long range internal stresses in single-phase crystalline materials, Int. J. Plast. 45 (2013) 44-60.
[79] E. Nes, T. Pettersen, K. Marthinsen, On the mechanisms of work hardening and flow-stress saturation, Scripa Mater. 43 (2000) 55-62.
[80] J.R. Cahoon, W.H. Broughton, A.R. Kutzak, The determination of yield strength from hardness measurements, Mater. Trans. 2 (1971) 1979-1983.
[81] E. Broitman, Indentation Hardness Measurements at Macro-, Micro-, and Nanoscale: A Critical Overview, Tribol. Lett. 65 (2017) 23-41.
[82] M. Tiryakioğlu, On the relationship between Vickers hardness and yield stress in Al–Zn–Mg–Cu Alloys, Mater. Sci. Eng. A 633 (2015) 17-19.
[83] A.E. Tekkaya, An Improved Relationship between Vickers Hardness and Yield Stress for Cold Formed Materials and its Experimental Verification, Annals CIRP 49 (2000) 205-208.
[84] M. Song, C. Sun, Y. Chen, Z. Shang, J. Li, Z. Fan, X. Zhang, Grain refinement mechanisms and strength-hardness correlation of ultrafine grained grade 91 steel processed by equal channel angular extrusion, Int.l J. Press. Vess. Piping 172 (2019) 212-219.
[85] P. Zhang, S.X. Li, Z.F. Zhang, General relationship between strength and hardness, Mater. Sci. Eng. A 529 (2011) 62-73.
[86] X.-L. Gao, An expanding cavity model incorporating strain-hardening and indentation size eff ects, Int. J. Solids Struct. 43 (2006) 6615-6629.

Figures and Tables captions

Fig. 1. Microstructure of the as annealed OFHC Cu.

Fig. 2. Scheme of HPT showing the location of extraction of the TEM discs.

Fig. 3. Microstructure evolution with cumulative HPT shear strain, at ε_{eq} = 0.40, a); ε_{eq} = 0.91, b); ε_{eq} = 1.21, c); ε_{eq} = 1.81, d); ε_{eq} = 2.42, e); ε_{eq} = 3.63, f). In b) the dark-field (DF) micrograph shows the early formation of low-angle boundaries (cells) from tangled dislocations (GNDs), SAEDP with crystallographic spot selected is reported in the inset. The DF *g*-vector was *g* = [02-2] allow to show the dislocations and cell/grain boundary lines.

Fig. 4. Twinning formation induced by the HPT strain, ε_{eq} = 0.91, a); ε_{eq} = 1.81, b); ε_{eq} = 3.63, c). Cu crystals oriented as [011] allow to reveal the twin boundaries and lines.

Fig. 5. Nanoindentation load-displacement curves, *P-h*, using a load *P* = 10 mN, for HPT OFHC 99.99% purity Cu at ε_{eq} = 0.40, 0.91, 1.21, 181, 2.42, and 3.63. The annealed OFHC Cu nanoindentation curve, ε_{eq} = 0, is reported for comparison.

Fig. 6. Plot of hardness, *H*, and reduced elastic modulus, E_r, vs. cumulative HPT straining, ε_{eq} = 0.40 to 3.63.

Fig. 7. The ISE phenomenon. Hardness, *H*, vs. indentation depth, h_c, for ε_{eq} = 0.40-to-3.63; the as-annealed curve is reported for comparison to the HPT experimental conditions.

Fig. 8. Minimum nanoindentation load to initiate ISE vs. mean grain and cell size produced by HPT of the OFHC 99.9% purity Cu.

Fig. 9. Evolution of twin mean spacing, λ_{Twin}, for HPT strains 0.91 < ε_{eq} < 2.42.

Fig. 10. Grain size, d_{grain}, cell size, d_{cell}, twin spacing, λ_{Twin}, and twinned grain volume fraction, $f_{twinned\ grains}$, evolution with HPT strains ε_{eq} = 0.40-to-3.63.

Fig. 11. BF-TEM at ε_{eq} = 2.42 showing dislocation walls (DW), tangled dislocations (TD), geometrically-necessary dislocations (GND), twin boundaries (TB), and grain boundaries (GB).

Table 1. Chemical composition of the OFHC 99.99% purity copper (wt.%x1000).

Table 2. Equivalent strain ε_{eq} obtained by the different HPT experimental parameters at *N* = 1/18 (lowest) to 1/2 turns (highest), at radial distances *r* = 5 mm (mid-radius) from disc thick-center.

Table 3. Mean grain, d_g, and cell size, d_{cell}, of OFHC CU subjected to HPT at ε_{eq} = 0.40 to 3.63.

Table 4. Dislocation density and dislocation wall volume fraction, *f*, for ε_{eq} = 0.40-to-3.63.

Table 5. Yield stress as calculated by the model of Eq. (5), σ_y^{model}, and as derived from the nanoindentation Hardness measurements, $\sigma_y^{nanoind}$. In this latter case, two different approaches are here proposed, one according to [**21**] in which a factor of χ = 2.9 was considered as *H* to σ_y ratio; a second according to [**82**] in which the ratio χ = 3.5. Data refers to ε_{eq} = 0.40, 0.91, 1.21, 1.81, 2.42, and 3.63.

Table 6. Gao's model of Eq. (6) applied to the microstructure strengthening model of the present study at ε_{eq} = 0.40, 0.91, 1.21, 1.81, 2.42, and 3.63.

Nanoindentation twin-sensitive measurements and strengthening model of HPT OFHC 99.99% purity copper

Marcello Cabibbo

DIISM / Università Politecnica delle Marche, Via Brecce Bianche 12, 60131 – Ancona, Italy.

Keywords: OFHC pure copper; Twinning; HPT; Nanoindentation; ISE; TEM.

Abstract. Severe plastic deformation (SPD) techniques are among the most effective deformation modes of introducing a high rate and density of dislocations in metallic materials and alloys. The newly introduced dislocations have different characters. These were classified after Hansen and the Risœ group as statistically stored (SSD), also called incidental dislocations (ID), and geometrically necessary (GND) dislocations. As the strain cumulates some of these dislocations, namely the GNDs, are promoted to form very-low, low, and eventually high-angle boundaries. That is, new cell and grain structured are formed as the plastic deformation accumulate. Studies of the early stages of plastic deformation inducing microstructure modifications are properly carried out on pure metals as they strengthen only by the effect of dislocation, crystallite boundaries, and texturing of the metallic matrix. On this basis, the present work focuses on an electron microscopy study of the early plastic deformation stages induced in an OFHC 99.99% pure copper by high-pressure torsion (HPT). A threshold stress for the initiation of twinning formation within the Cu-grains was identified. Nanoindentation measurements were performed at different penetration depths. Thus, a correlation between the tip size-sensitive hardness evaluation (known as indentation size effect, ISE), occurring at the lower penetration depths, and the twinning formation during the early stages of HPT was found.

1. Introduction

Ultrafine-grained (UFG) metallic materials and alloys are known to possess superior mechanical properties compared to the conventional grained counterparts **[1]**. In the last two-three decades a number of grain refining methods were proposed and developed. These include top-down approaches, such as severe plastic deformation (SPD), and bottom-up approaches starting from powder metallurgy processes **[2-4]**. As for the top-down approach, different SPD techniques showed reliable, cost-effective, and promising means for obtaining thermally stable ultra-fine, and sometimes nanometric size, grain structures of metals and alloys. The most relevant such techniques are high-pressure torsion (HPT), equal-channel angular pressing (ECAP), accumulative roll-bonding (ARB), accumulative press-bonding (APB), twist extrusion (TE), friction stir processing (FSP), cyclic extrusion-compression (CEC), repetitive corrugation and straightening (RCS), accumulative back extrusion (ABE) and hydrostatic extrusion (HSE), high-pressure sliding (HPS) (**[5-13]** and references therein).

The exceptional mechanical properties achieved by the UFG metals are due to both the sub-micron cell, grain size and the mobile dislocations inside the UFGs. In addition, low stacking fault energy (SFE) materials, such as copper-alloys and pure copper, also strengthen by twinning formation within the grains. It is generally agreed that UFG processes proceed from newly introduced tangled dislocations (TD) and cell boundaries (both very-low, VLABs, and low-angle boundaries, LABs) [**5-8,11,14-19**]. These are continuously introduced in the material and eventually induced to rearrange and form cell structures by SPD. Cells are in turns induced to increase their

misorientation angle to eventually become grain boundaries (high-angle boundaries, HABs) **[14-19]**. More specifically, the dislocations generated during plastic deformation are typically classified into two categories that reflect the sliding mobility attitude and the special arrangement they tend to follow. Thus, according to Huges *et al.* [**20**] one type of dislocations are called geometrically necessary dislocations (GNDs), and incidental dislocations (IDs), or statistically stored dislocations (SSDs). GNBs form between regions of different strain patterns to accommodate the strain induced lattice rotation. IDs (or SSDs) form by random trapping processes of dislocation during straining. These latter are stored within the already existing grains as a statistical necessary process of accommodating the local straining in the metallic material. Upon SPD different strain patterns can be activated in the material involving activation of different slip systems. This, in turns, generates differences in the partitioning of slip activity on the same slip systems of the newly introduced dislocations, and then differences in the level of equivalent strain acting in the deforming material. These differences in slip pattern ultimately promote dislocation interactions, namely between IDs, GNDs, and among IDs and GNDs, resulting in a significant energy reduction. That is, the evolution of IDs and GNDs to form cell and eventually grain boundaries is an energetic favoured process. The here described dislocation evolutionary process is in fact a statistically and thermodynamically most probable phenomenon which is activated and promoted in the metallic material by plastic and severe plastic deformation.

The dislocation strengthening mechanisms generate by the SPD are usually studied by using pure metals, such aluminum [**14,15,16,18,19,21,22**], nickel [**23-25**], copper [**11,26**], and the like [**27,28**]. In the present study a OFHC 99.99% pure copper was used to analyse the early stages of plastic deformation induced by HPT. The choice of using HPT was motivated by the almost continuous range of induced strains that it is able to induce simply by limiting the number and fraction of the metal rotations under pressure. In fact, HPT generates progressive plastic deformation levels for given number and fraction of turns, from the disc center, where it is minimum, to the disc periphery, where it is at its maximum. On the other hand, the level of induced strain strongly depends on the number of HPT rotations, *N*. In HPT the sample, in form of a thin disk, is placed between two large anvils and subjected to a high pressure and concurrent torsional straining. This way, the two meaningful parameters are the magnitude of the imposed pressure, *P*, and the number of revolutions applied to the sample, *N*. Since, the imposed strain chiefly depends on the distance from the center of the disc, the microstructure modifications imposed by HPT are greatly inhomogeneous, but continuous. For the present study, this latter aspect is considered as a key microstructure aspect to determine the minimum necessary strain level to form twinned grains in a fully annealed 99.99% pure copper.

In this sense, HPT is different from most of the other SPD processes where generally strain gradients are generated quite quickly, making almost impossible to determine the early stages of cell structure formation [**4-6,12,14,21**].

Strain gradients and strain hardening, as well as metal plastic properties, such yield stress, hardness, toughness, strongly depend on the dislocation density, ρ_{disl}. That is, when a material is plastically deformed the dislocation density increases, leading to strain gradients and metal strain hardening. The metallic material straining under plastic deformation is usually studied by electron microscopy techniques (electron back-scattered diffraction, EBSD, field-emission gun scanning electron microscopy, FEGSEM, transmission electron microscopy, TEM). Anyhow, this was also characterized by performing extremely small indentations (nanoindentations) in low defect density materials [**29,30**]. Moreover, whenever strain gradients are formed by indentations using either pyramidal or conical indenters, GNDs are generated into the material in order to accommodate the induced strain [**31,32**]. Since strain gradient increases by reducing the deformation scale (*i.e.*, small penetration depths) the density of GNDs and, consequently, the hardness of the material, increase when the size of the deformed region decreases. This quite important experimental factor that affect the process of indentation of metallic material is known as indentation size effect (ISE) [**32,33**]. With this regard, it was found that the ISE can be described by taking into account the two types of

dislocations introduced during plastic deformation. That is, ISE can be described by taking into account the statistically stored dislocations (SSDs) and the geometrically necessary dislocations (GNDs) [**34**].

Following pioneering studies by Nix and Gao [**32**] nanoindentation hardness overestimation for lower tip penetration depths is directly related to underestimation of the plastic zone volume. In their model, Nix and Gao assumed plastic zones assumed to be hemispherical with a radius equal to the contact radius, a. This hemisphere volume, V, is calculated as: $V = 2\pi h^3/(3\tan^3\varphi)$, where φ represents the angle between the indenter surface and the sample surface. The nanoindentation hardness, H, is thus expressed as: $H = 3\cdot\sigma = 3^{1.5}\alpha Gb(\rho_{SSD} + \rho_{GND})^{0.5}$, being α a constant, G the material shear modulus, b its Burgers vector, and ρ_{SSD}, ρ_{GND} the densities of SSDs and GNDs, respectively. Since, H_0 can be defined as the material hardness with no GNDs, this can be expressed as $H_0 = 3^{1.5}\alpha Gb(\rho_{SSD})^{0.5}$, and thence $H = [1+(\rho_{GND}/\rho_{SSD})]^{0.5} = [1+(h_0/h)]^{0.5}$, where h_0 is the length scale factor of a given material under indentation, and h is the indentation penetration depth. This approach is based on a hemispheric volume limited to the next neighbouring of the tip radius and the lateral tip edges. This indeed can depends on the type of tip used, that is a pyramidal Berkovich, a spherical, or a cube-corner geometry [**34**].

Anyhow, GNDs is known to spread beyond the hemisphere, and thence the plastic zone volume needs to be corrected. This was addressed later on by Durst *et al.* [**35,36**], where the radius of the plastic zone is assumed to be $f\cdot a$, with f ranging from 1 to 3.5, and simulated by finite element means. In polycrystals, hardness always increases with decreasing grain size. This behaviour can be explained by the well-known Hall-Petch (H-P) relationship, which is based on the interaction between dislocations and grain boundaries in grain structured metallic materials. Anyhow, whenever the grains are wide and/or the indentation penetration depth is shallow, the generation of SSDs and GNDs is strongly related to one or few grains. This means, that the indentation plastic zone in these cases has a local character.

In this study the role of twinning formation within plastically deforming grains on the nanoindentation grain size sensitive hardness and reduced Young's modulus measurements is addressed. In particular, the minimum necessary strain by HPT to induce twinning formation was identified and the role of the twin formation on the nanoindentation depth sensitive measurements was addressed.

2. Experimental procedures and Method

2.1. The material

Rods of OFHC 99.99% pure copper had a 10 mm diameter and they were subjected to a fully annealing treatment. This consisted to baking the rods at 673 K for 1 h, followed by cooling in the turned off furnace, corresponding to a cooling to room temperature of 8 h. The chemical composition of the 99.99% purity Cu is reported in **Table 1**. Discs 1.0 mm-thick were cut from the annealed bars. As shown in **Fig. 1**, the annealed Cu showed a coarse grained structure with rare presence of few dislocations within the grains whose volume fraction was so low to do not form any sort of entanglement.

2.2. High-pressure torsion (HPT) process

The fully-annealed OFHC 99.99% pure Cu in form of a disc of 10 mm-diameter and 1.0 mm-thick was subjected to HPT under quasi-constrained conditions at room temperature, thus avoiding material outflow during straining. Different strain levels were induced into the metals as to get a discrete close range of strain levels, *i.e.*, from ε_{eq} = 0.40-to-3.63, by processing HPT at following rotation number fractions: N = 1/18, 1/8, 1/6, 1/4, 1/3, 1/2 turns.

Fig. 2 is a scheme of the HPT strain deformation imposed to a typical disc sample, where the incremental shear strain is given by $d\omega/\omega$, being ω the angular rotation around the disc center.
Since in the present case the disc thickness does not dependent on the rotation angle $\omega = 2\pi N$, the resulting HPT shear strain, γ, can be calculated as **[5]**, Eq. (1a):

$$\gamma = 2\pi Nr/t \qquad \text{Eq. (1a)}$$

where r is the distance from the disc center, ranging from 0 to the disc radius, R, t is the disc thickness. For large HPT strains, typically $\gamma > 0.8$, the resulting equivalent vön Mises strain can be written as **[5,37]**, Eq. (1b):

$$\varepsilon_{eq} = \frac{2}{\sqrt{3}} ln\left[\left(\frac{1+\gamma^2}{4}\right)^{0.5} + \frac{\gamma}{2}\right] \qquad \text{Eq. (1b)}$$

On the other hand, for low HPT shear strain, γ, the resulting vön Mises strain can be expressed as **[5,37]**, Eq. (1c):

$$\varepsilon_{eq} = \frac{\gamma}{\sqrt{3}} = \frac{2\pi Nr}{t\sqrt{3}} \qquad \text{Eq. (1c)}$$

Thence, in the present study, Eq. (1c) was the one used to model the shear deformation induced in the OFHC pure Cu.
HPT was carried out by depressing the vertical anvils to a depth of 0.05 mm into the 1 mm-thick HPT discs. Torsion strain was exerted by rotating the upper anvil at a low rotation speed of 0.7 rpm (~4° sec^{-1}) under a pressure of 2.0 GPa.
TEM inspections and nanoindentation measurements were performed at the mid-section of the discs (that is, at a thickness $t \cong 0.5$ mm) and at mid-radius (5 mm) from the disc center. Thus, according to Eq. (1b), the resulting equivalent strain, ε_{eq}, is as listed in **Table 2**.
The reason to use HPT to perform the present study is based on the possibility to generate low incremental strain levels, starting form a minimum level of equivalent strain as low as $\varepsilon_{eq} = 0.40$.
To avoid any possible artefact during sample preparation, the ~1 mm-thick HPT processed discs were prepared for TEM inspections by chemical and electro-chemical means only. They were first punched to 3 mm TEM discs from the above-mentioned HPT disc position and indicated in **Fig. 2**. The 3 mm TEM discs were ~1 mm-thick, this initial thickness was mechanically grinded and then electrochemically thinned and symmetrically polished to a ~200 μm thickness using a solution of 30% of phosphoric acid 20% ethylic alcohol in 50% distilled water at room temperature and a voltage of 12V. Prior final thinning to electron transparency by precision ion-milling (PIPS), the 200 μm-thick discs were fixed by a commercially pure 0.5 mm-thick copper ring with 3 mm external diameter. Then, this was thinned by Gatan™ PIPS with a low dual incident beam whose angle was fixed to 2° respect to the disc surface, to minimize the possible artefacts coming from the disc preparation (*i.e.*, to minimize the dislocations possibly introduced during the ion-milling process).

2.3. Sample preparation for TEM and method

TEM inspections were carried out in a Philips™ C-20® working at 200 keV with a double-tilt specimen holder equipped with a liquid-nitrogen cooling stage. Inspections were performed at the middle height of the HPT discs.
Two-beam excitation conditions were selected for most of the TEM observation and dislocation characterizations. Dislocation density, $\rho_{disl.}$, was quantitatively evaluated by stereological methods, such as the Ham's interception method [**38**]. Thence, $\rho_{disl.}$ was calculated through the count of

interception points between the mesh and the existing dislocations, n_{disl}, in the TEM micrographs. This was evaluated by $\rho_{disl.} = 2n_{disl}/(l_{mesh}t_{TEM})$, were, l_{mesh} is the total length of the mesh, and t_{TEM} is the thickness of the TEM foil. Crystal thickness, t_{TEM}, was determined through the diffracted beam intensity variation under dual beam conditions, using converged electron beam diffraction (CBED) patterns. This way, by plotting the linear interpolation of data points in a $S^2/n_{fringes}^2$ vs. $n_{fringes}^{-2}$ graph, where S is the fringes spacing, and $n_{fringes}$ the number of counted fringes, t_{TEM}^{-2} was determined at y-axis line intercept. The error due to the invisible dislocations (i.e., the ones oriented as to have $b \cdot g = 0$, where b is the Burgers vector and g refers to the dislocation lying crystallographic plane) is within the experimental error of the foil thickness evaluation. Cell (LAB) and grain boundary (HAB) misorientation were measured by Kikuchi band patterns. The misorientation angle measurement procedure by Kikuchi pattern on TEM is fully described elsewhere in previous published works by this author [**14-16**]. TEM inspections were carried out by orienting the Cu-matrix as to have [001], [011]-crystallographic planes || I_{beam} (electron beam direction).

2.4. Nanoindentation measurements

Nanoindentation measurements were performed at same HPT disc height as the one set for TEM inspections. For the nanoindentation measurements, samples were prepared by the same chemical polishing methods used for the TEM disc preparation. A Hysitron™ Triboscope UBI-1® was used. Calibration procedures were followed according to [**39**]. A trapezoidal load function of 5 s loading, 15 s at the set load, and 5 s unloading was used, with a set load, P_{Max} = 10 mN, and at a constant loading rate of 0.25 mN/s. Nanoindentations were performed for each experimental conditions, that is for strain levels ε_{eq} = 0.40-to-3.63. Each reported experimental datum is the average value obtained out of series of [8x8]-matrix of individual measurements spaced 250 μm apart, giving a total of 64 individual measurements per experimental condition.
Data analysis was performed according to the Oliver-Pharr model [**40**]. Thus, the hardness, H, was evaluated as $H = P_{Max}/A$, with $A = K_{ind}h_c^2$ being the contact area, K_{ind} an indenter tip dependent coefficient (24.56 for Berkovich tip [**41**]), h_c the contact depth related to the maximum penetration depth, h_m, which is $h_c = h_m - \chi P_{Max}/S$, χ = 0.75 for Berkovich tip [**40**] and S the material stiffness. This latter, according to the Oliver-Pharr approach [**40,41**] is measured as unloading slope at the maximum penetration depth, h_m, and it is $S = Bm(h_m - h_r)^{m-1}$, where B is the unloading curve intercept at $P = 0$, m is the unloading slope, and h_r is the residual depth (the permanent plastic penetration depth on unloading). Moreover, following the Oliver-Pharr method, the reduced elastic modulus can be derived as $E_r = [(\pi/4)^{0.5}/\beta] \cdot [S/(A)^{0.5}]$, where β = 1.034 for Berkovich tips [**40**]. Thence, in the present case, $H = 0.041 \cdot P_{Max}/h_c^2$ and $E_r = 0.173 \cdot S/h_c$.

3. Experimental Results

3.1. Microstructure

Fig. 3 shows representative TEM micrographs of the microstructure evolution driven by the HPT shear deformation, from ε_{eq} = 0.40 to 3.63.
The initial generation of twinning, lying within the Cu-grains, started from a HPT strain level of ε_{eq} = 0.91. From this strain level of HPT plastic deformation the OFHC Cu started to refine its grain structure. At the same time, twins started to cumulate within the refining grains. That is, the deformation process did change microstructure mechanism as it proceeded only by SSD and GND formation at the earliest strain levels ε_{eq} = 0.40 (**Fig. 3(a)**). From a strain ε_{eq} = 0.91 both SSD and GND eventually were promoted to form the first low-angle boundaries (cell boundaries) and new high-angle grain boundaries (**Fig. 3(b)**). At this latter strain level twinning started to form, and thus

this further strengthening mechanism started to operate within the pure Cu microstructure. Thence, the strain level ε_{eq} = 0.91 can be considered a threshold-like, or a cut-off lower strain limit, to initiate a microstructure twin strengthening. At strain levels above it, ε_{eq} > 1.21, the pure copper plastically deformed under HPT straining by further generation of GNDs, that eventually form grain boundaries, and by the combining strengthening effect of grain refinement and twinning-induced generation (**Fig. 3(c)-to-(f)**). With this respect, **Fig. 4** shows the evolution of the twinning induced to form and cumulate by the HPT shear deformation, from ε_{eq} = 0.91 to 3.63.

Moreover, the OFHC Cu microstructure evolved rapidly already in the early stages of straining (**Fig. 4(a),(b)**). It resulted that at strain level within ε_{eq} < 1, the microstructure undergoes typical strain hardening associated with a significant generation of LABs and cell boundaries, as showed by **Fig. 4(b)**. The formation of LABs, and eventually some HABs, is accompanied by the concurrent formation of twin boundaries. Both these microstructure features contribute to generate arrays of ultrafine grains at the higher strain levels.

In **Fig. 3(c)** dislocation pile-up process is showed; in particular, this piling-up generated lattice distortion on both sides of the cell wall and evolves with the presence of the early formation of twinning. These twins nucleated at grain boundaries (GBs) to extend within the grain. The formation of these twins is responsible for the development of sharp grain boundaries, which in turns implies a substantial stress relief in the boundary surrounding areas.

As for the mean grain and cell size evolution with cumulative HPT straining, the statistical evaluation carried out by TEM inspections showed a continuous grain, and especially cell size reduction from ε_{eq} = 0.91 to 3.63 (**Table 3**). That is, the mean grin size, which in the annealed initial condition was d_g = 28 μm, reduced to 19 μm at ε_{eq} = 0.40, and down to 3.2 μm, at the maximum strain of ε_{eq} = 3.63. As for the cell size, these reduced from an initial mean value d_{cell} = 1100 nm, down to 360 nm, at ε_{eq} = 3.63.

It resulted that cell size reduction process induced by HPT appeared to slow down at $\varepsilon_{eq} \geq 1.21$, when twinning formation started to characterized the grain interior and start to act as further barrier against dislocations (actually both SSDs and GNDs) sliding motion.

3.2. Nanoindentation Hardness, H, and elastic modulus, E_r

Fig. 5 reports representative nanoindentation load-displacement curves, *P-h*, for a load *P* = 10 mN, of OFHC Cu subjected to HPT at ε_{eq} = 0.40, 0.91, 1.21, and 3.63. As expected the penetration depth, h_c, reduced with cumulative straining. Yet, the unloading slope of the *P-h* slightly increased from the minimum detected strain of ε_{eq} = 0.40 to ε_{eq} = 0.91. This did not changed as the strain rose up to the maximum tested strain of ε_{eq} = 3.63. Since the unloading slope is related to the material reduced Young's modulus, E_r, the observed slope increment means that the elastic modulus of the OFHC Cu slightly increased at ε_{eq} = 0.91. This in turns implies that the occurrence of twinning formation within the grains is somehow responsible for the material changes of elastic response.

Hardness, *H*, and reduced elastic modulus, E_r, were measured according to the Oliver-Pharr approach [**40,41**], and results were plotted in **Fig. 6** as a function of the HPT shear deformation. Accordingly, the metal *H* steadily increased from the minimum, ε_{eq} = 0.40, to the top strain level, ε_{eq} = 3.63, although at ε_{eq} = 2.42, a plateau-like value of H ≅ 1.15 GPa was reached. The reduced elastic modulus, E_r, appeared to follow quite closely the hardness incremental trend with cumulative straining. Moreover, a similar plateau-like was reached at ε_{eq} = 2.42, with values E_r ≅ 170 GPa. These results are in good agreement with some previously reported study on commercially pure and quite similar OFHC pure Cu [**11**].

4. Discussion

4.1.Microstructure evolution and twinning formation induced by HPT

Dislocation formation (SSDs and GNDs) and twin formation with cumulative straining are two key mechanisms of microstructure strengthening especially for pure metals, such as the here studied OFHC 99.99% purity Cu. In fact, it is known that whenever a metallic material is subjected to plastic deformation, the newly introduced dislocations are induced to slide, in addition deformation twinning is activated, and thence both accommodate the imposed plastic strain [**42**]. The mean factors governing these microstructure induced modifications include the material SFE, the grain size and crystallographic orientation [**43-45**]. Also the external loading conditions such as stress [**46**], strain [**47**], strain rate [**48,49**], and temperature [**48**] play a crucial role. Compared to conventional materials processing, SPD techniques impose severe shear strains producing unusual and quite high mechanical properties that are ultimately driven by the unique microstructure modifications and evolution [**50,51**]. In the present case, understanding the competitive relationship between SSDs, GNDs, the cell and grain boundary formation and the deformation twinning induced by the HT shear deformation was considered as a key factor for the description of the early stages of deformation occurring in pure bcc low SFE metals, such as copper.

In materials with medium to high SFE, GNDs and SSDs develop since the early stages of plastic deformation [**52,53**]. The role of GNDs is to accommodate the shear strain gradients throughout the microstructure. SSDs are formed by tangled dislocation random trapped under uniform localized deformation. These newly introduced dislocations easily slide by cross slip by which the formation of dislocation boundaries (both low- and high-angle) is favoured with cumulative strain. The mechanism of boundary formation out of chiefly GNDs is driven by a mutual trapping, rearrangement, and annihilation process [**53,54**]. In fact, it is known that the dislocation types that do contribute to the crystal lattice rotation are the GNDs [**54**].

On the other hand, for lower SFE metals, such as copper, the formation of initially few, and then more and more volume fraction of stacking faults and twinning is favoured with cumulative straining [**55**]. Under severe plastic deformation regimes, the twinned grains contribute to accommodate the plastic deformation as well as the refining grains do. Moreover, when twinned grains have a proper crystallographic orientation respect to the external load, multiple twinning systems are activated, leading to twin-twin intersection phenomena. These, in turns, become a further strengthening mechanism for the twinned metallic material [**55,56**].

Thence, in low SFE metals the reduced dislocation mobility make the twinning deformation a necessary-like mechanism for the material to rearrange the microstructure, by strengthening it, under the applied external load. In the present study this necessary-like microstructure mechanism of twinning formation under HPT was found to occur for a strain level as low as ε_{eq} = 0.91. No traces of twinning formation was found for lower equivalent strains, where the microstructure strengthening proceeded only by formation and evolution of SSDs, GNDs, cell walls and eventually of some GB. The role of the SSDs and GNDs referring to the continuous process of cell and grain refinement induced by the HPT deformation was twofold. On one side, it was that of a microstructure source of active line defects able to thickening the newly generated boundaries, either cell or grain; on another side, it was that of contributing to rise the boundary misorientation angle as they continuously formed by the HPT action. As soon as the twins started to be generated, they behaved as a further microstructure strengthening term that did not affected the grain refining process driven by the HPT cumulative deformation.

4.2.Indentation size effect (ISE)

In nanoindentation measurements, as the indentation depths get shallow, by reducing the applied load, the obtained hardness is known to increase accordingly. This indentation size effect (ISE) was

observed in metallic materials [**32-36**]. Nix and Gao proposed a model, also known as NG-model, that relates this ISE to the generation of GNDs, whose density is proportional to the inverse indentation depth [**32**]. The additional hardening due to the GNDs is a mere effect of an indentation tip-to-the beneath indentation plastically deformed volume interaction phenomenon. Thus, ISE is particularly evident and pronounced in soft annealed metallic materials, such as the present case of annealed OFHC 99.99 purity Cu. On the contrary, ISE is typically of minimal significance in hardened metallic materials. This behaviour is directly correlated to the inner length scale of the material due to the induced increased dislocation density driven by the cumulative flow stress.
The ISE phenomenon is known to be generated by additional hardening given by the GNDs. This penetration depth sensitivity of the nanoindentation measurements is mainly based on two factors. One, is a microstructure-based factor, which is constituted by the total line length of dislocations necessary to form the permanent indented profile; the second, is geometrical-based and is related to the overall extension of the material volume in which the dislocations are stored. Indeed, both factors are strongly related to the generation of stored and necessary dislocations, *i.e.* SSDs and GNDs. A study of the ISE occurring on the early stages of HPT is here presented. To do that, nanoindentation load was almost continuously reduced from 10 mN to loads as low as ~100 μN. The obtained hardness, H, increment due to the ISE, as a function of lowering penetration depths down to few hundreds of nanometer, for strain levels of ε_{eq} = 0.40-to-3.63 is reported in **Fig. 7**. It is worth to note that the measured H variation with lowering penetration depths followed different slopes depending on the strain level to which the pure copper was subjected. It appeared that from HPT strains ε_{eq} < 0.40 / 0.91. H followed an almost continuous incremental rate as the load and penetration depth lowered. Starting from ε_{eq} = 0.91 and up to ε_{eq} = 3.63, H increment by lowering the penetration depth followed an initial almost linear trend, to drastically rise for penetration depths lower than 900-800 nm. This different ISE trend is believed to be somehow determined by the reducing grain size and the concurrent formation of twinned grains.

4.3. Twinning formation role in ISE

An ISE-driven hardness increment of ~10% was observed at indentation depths ranging 1.8-to-0.9 μm, from as-annealed to HPT strain ε_{eq} = 3.63 (**Fig. 7**). This increment can be identified as the minimal deviation from the actual H evaluation due to the ISE phenomenon and is reported in **Fig. 8**. Thus, the measured depth range to reach a H variation by 10% from the asymptotical and actual value, obtained at higher penetration depth ranges, strongly depended on the strain level and, ultimately, on the induced grain/cell size reduction. The corresponding penetration depth value is also called length scale, h^*. That is, as reported in the plot of **Fig. 8**, a direct correlation exists between the occurrence of a significant ISE and the mean grain (and cell) size of the testing metallic material. Present result appears to be in good agreement to data reported by Nix and Gao in [**32**] derived by a linear fitting of $(H/H_0)^2$ vs. h_c^{-1} in pure Cu, where a value of length scale of ISE h^* = 1.60 μm was reported. Thence, the here obtained results showed the length scale, h^*, to rise with grain, cell size reduction, and with occurrence of twinned grains. That is, the ISE appeared to anticipate by refining the grained structure of pure Cu by cumulative HPT straining. To some extent, this issue was addressed and discussed by Yang and Vehoff [**34**] who studied ISE occurring in high-purity nanocrystalline Ni with different mean grain size obtained by plastic deformation techniques. Similarly, Lapovok *et al.* [**57**] reported a certain degree of ISE initiation dependency to the level of ECAP shear straining in pure Cu. They show ISE occurring with lower penetration depth as the ECAP shear straining cumulate and thus as the resulting mean grain refined. Similar trends for commercially pure Cu were reported in [**58**] by HPT, and in [**36**] by ECAP.
Fig. 8 shows H rising trend slopes for the two strain levels above mentioned, that is, for ε_{eq} < 0.91, and for 0.91 < ε_{eq} < 2.42. It thus resulted that the H increment was slow (0.93 GPaμm^{-1}) at the earliest stages of deformation, to double (1.84 GPaμm^{-1}) for strain levels by which grain started to refine and twins started to form within the grains. This would ultimately means that a direct

correlation between the rate and amplitude of ISE and the grained structure of pure copper exists. To better understand this ISE microstructure dependency, twin spacing, λ_{Twin}, was measured for strains $0.91 < \varepsilon_{eq} < 2.42$, that is for the strain levels where twins started to form ($\varepsilon_{eq} = 0.91$) and then filled the grained structures ($\varepsilon_{eq} = 2.42$). The statistical evaluation of twin spacing, carried out for strain levels $\varepsilon_{eq} = 0.91$-to-2.42 is reported in **Fig. 9**.

The twin spacing appeared not to evolve significantly with cumulative HPT strain. Mean twin spacing was $\lambda_{Twin} \cong 32 \pm 2$ nm irrespective of the strain level throughout the range $0.91 < \varepsilon_{eq} < 2.42$. The only clear aspect that differentiated the λ_{Twin} size distribution with HPT strain was the maximum twin spacing sizes that appeared to reduced form 80 nm, at $\varepsilon_{eq} = 0.91$, down to 60 nm, at $\varepsilon_{eq} = 2.42$.

Quite similar twin spacing sizes were also reported by Yang and Vahoff [**34**] in SPD high-purity nickel and by Saldana *et al.* [**59**] in SPD same OFHC 99.99 purity copper. In particular, Saldana *et al.* accounted on thermomechanical stability in ultra-fine grained copper with high density of twin boundaries. Nanoscale network of twins within the grains are generally induced to form by SPD processes. In this sense, the here reported formation and evolution of twins induced by the HPT cumulative strain was actually expected mostly on the basis of the relative low OFHC Cu SFE. Moreover, twin boundary formation promoted by SPD (HPT in the present case) are strongly affected by the generation and evolution with strain of SSDs and GNDs. In particular, the twins formed during SPD means can have a significant high aspect ratio, that is a high length to spacing ratio). This microstructure feature was widely observed in the present study and the corresponding morphological twin evolution with SPD strain was also reported by Wang *et al.* in a nanostructured pre Cu [**60**].

Fig. 10 shows a direct comparison between the twin spacing and grain/cell evolution with cumulative HPT straining. The general refining trend of both cells and grains was accompanied by a non-significant twin spacing variation, although twin volume fraction increased to a great extent in the strain range $\varepsilon_{eq} = 1.21$-to-2.42.

4.4. Strengthening model

It is well known how strength of a metallic material can be directly related to the microstructural features, such dislocations, cell and grain boundaries (and related mean size), and, limited to the low-to-medium SFE metals, to the twin boundaries (TB). The flow stress, namely the material yield stress, can be derived as contributions aggregate of the above-mentioned strengthening terms [**61,62**]. Apart from the grain boundary strengthening which is modelled by the Hall-Petch relationship, a number of models accounted on the strength contribution coming from cell boundaries. These can actually have a low-angle, but also a very low-angle character [**14**]. The first ones are typically boundaries with misorientation angle within ~4-14°, the second ones have typical misorientation of ~2-4° and always show Moiré fringes on TEM. For the first case, the strength contribution can be modelled as to be proportional to the square root of the density of dislocation stored inside the boundaries (essentially SSDs) [**61**]. The second case corresponds to the existing tangled dislocations (TDs) [**14,62,63**]. On the other hand, the occurrence of TB from strain levels of $\varepsilon_{eq} > 0.40$, makes necessary considering this further microstructure strengthening contribution [**64,65**]. Thence, the following relationship was proposed for modelling the OFHC Cu yield stress as determined by the nanoindentation hardness measurements, Eq. (2):

$$\sigma_y = \sigma_0 + \sigma_{disl.} + \sigma_{HP} + \sigma_{TB} \qquad \text{Eq. (2)}$$

where σ_0, $\sigma_{disl.}$ is the stress due to SSDs and GNDs, σ_{HP} is the stress given by the grained structure (calculated through the Hall-Petch relationship), σ_{TB} is the stress due to the twins (twin boundaries, TB).

The dislocation contribution is the linear combination of the SSDs and of the GNDs strengthening, and they are both directly dependent on the related densities. In particular, SSDs do form very low-angle and low-angle boundaries under plastic deformation, and thus their density is expressed as, Eq. (3):

$$\rho_{SSD} = f\rho_{wall} + (1\text{-}f)\rho_{TD} \qquad \text{Eq. (3)}$$

Where f is the fraction of the SSDs that do contribute to the wall (boundary) formation, ρ_{wall} is the density of the formed walls, and ρ_{TD} represents the density of the dislocations existing in the cell and grain interiors that did not form boundaries and that are generally referred as to tangled dislocations (TD). According to [**57**] the value of f can be determined as $f = 1\text{-}(1\text{-}\lambda_{wall}/d_{cell})^3$, λ_{wall} and d_{cell} being the mean wall (cell boundary) thickness and cell size, respectively.
Thence, the dislocation strengthening contribution, $\sigma_{disl.}$, can be calculated as, Eq. (4):

$$\sigma_{disl.} = M\alpha Gb[f\rho_{wall} + (1\text{-}f)\rho_{TD} + \rho_{GND}]^{0.5} \qquad \text{Eq. (4)}$$

where $M = 3.06$ is the Taylor factor [**66**], $\alpha = 0.33$ [**66**], $G = 48.2$ GPa is the shear modulus of pure copper [**66**], $b = 0.256$ nm is the copper Burgers vector [**61,65**].
Here the walls are actually considered as the continuously generated very-low and low-angle boundaries, *i.e.* the cell boundaries.
Onset of twinning occurs whenever the slip stress reaches the minimum necessary strain to activate the twinning. The present results showed that the minimum necessary strain level to initiate the twin formation was $\varepsilon_{eq} = 0.91$. Thence, whenever formed, the twins yield a further strengthening contribution given by their boundaries (twin boundary, TB), σ_{TB}. This strengthening contribution is modelled similarly to an Hall-Petch relationship but with a constant, K_{TB}, significantly higher than that pertaining the grain boundary strengthening, K_{HP}. Thus, according to Hansen [**61,67,68**], Armstrong and Worthington [**69**] and Meyers *et al.* [**42**], $K_{TB} = 0.28$ MPa·m$^{1/2}$, compared to $K_{HP} = 0.14$ MPa·m$^{1/2}$, and the corresponding strengthening contribution can be modelled as, Eq. (5):

$$\sigma_{TB} = K_{TB}\cdot d_g^{-1/2} \qquad \text{Eq. (5)}$$

By taking into account the actual fraction of twinned grains, f_{twin}, rising with cumulative HPT straining, the following strengthening model was here proposed, Eq. (6):

$$\sigma_y = \sigma_0 + M\alpha Gb\{[f\rho_{wall} + (1\text{-}f)\rho_{TD} + \rho_{GND}]^{1/2} + [(f_{twin}\cdot K_{TB} + (1\text{-}f_{twin})\cdot K_{HP}]d_g^{-1/2}\} \qquad \text{Eq. (6)}$$

The calculated values of f_{twin} are also reported in the plot of **Fig. 10**. Referring to Eq. (6), **Fig. 11** shows a representative TEM micrograph of the microstructure at $\varepsilon_{eq} = 2.42$ in which all the strengthening features are present, *i.e.* dislocation walls, tangled dislocations, geometrically-necessary dislocations, twin boundaries, and grain boundaries.
Dislocation density, namely ρ_{wall}, ρ_{TD}, ρ_{GND}, and fraction of wall boundaries, f, were determined by TEM stereology analyses (ASM EN-112). The mean data for each experimental condition, $\varepsilon_{eq} = 0.40\text{-to-}3.63$, are reported in the following **Table 4**.
The dislocation density data obtained in the present study well agree to previously published results on severely plastic deformed pure copper by ECAP up to 16 passes [**70**]. On the other hand, Lapovok *et al.* [**70**] reported dislocation wall spacing four times lower than the cell size at the early stages of ECAP deformation. In the present case a typical spacing of the dislocation walls of almost one-order of magnitude lower than the cell spacing was found.

On the basis of the data reported in **Table 3**, for grain sizes, and **Table 4**, for dislocation densities and fraction of the dislocation walls, Eq. (6) gives a microstructure-based quantitative evaluation of the OFHC 99.99 purity Cu yield stress, as reported in **Table 5**.

The present approach founds a number of scientific support given by previously published works and models proposed for different pure metals and alloys. These include the early studies on the impact of heterogeneous nature and distribution of dislocations on the metal and alloy shear stress, which were evaluated by Mughrabi using a composite-like model [**71,72**]. Following the pioneering works by Mughrabi, several other authors applied and adapted the Mughrabi composite-like model to different metals, alloys, and plastic deformation techniques [**73-78**]. These previous works report and apply strengthening models essentially same as the one here presented and applied to the OFHC 99.99 purity Cu. Moreover, the present approach is also able to describe metals and alloys work hardening mechanisms up to flow-stress saturation, as exhaustively reported by Nes and co-workers in [**79**].

Table 5 also reports a direct comparison between the yield stress as obtained through Eq. (6), and the one derived from the nanoindentation hardness measurements, $\sigma_y^{nanoind}$. With this respect, a linear relationship is known to hold between hardness, H, and yield stress, given by $H = (\sigma_y/3)\cdot(0.1)^{m-2}$, where m is the Meyer's hardness coefficient [**80**]. With this respect several published works on different metallic materials and alloys reported a hardness-to-yield stress relationship with a narrow ratio interval of $\chi = H_V/\sigma_y$ = 2.7-3.1 [**81-83**]. In the cold-rolled metallurgical status this relationship was reported to essentially have the same ratio range of 2.8-3.1 [**80,81**]. A Meyer's hardness similar approach was recently used and applied to aluminum alloys by Tiryakioğlu in [**82**]. In this case a $\sigma_y = A\cdot H_V + B$ type relationship was used starting from a Meyer's hardness approach as: $\sigma_y = H_V /0.947\cdot C - \Delta\sigma_y$. This type of approach to determining yield stress from hardness measurements, namely nanoindentation measurements, was also used by the present author for a 6N-Al subjected to low strains by HPT [**21**]. On the other hand, Tekkaya [**83**] for cold-worked Cu-based alloys introduced a step-like variation of the yield stress-to-hardness ratio depending on the yield offset that can be taken into account. For yield offset of within 0.112% the following relationship was proposed and experimentally validated: $H_V = 2.475\cdot\sigma_y$, where H_V is the Vickers hardness number. This relationship was generalized in a form of $\sigma_y = 9.81\cdot H_V/2.475$ for yield offsets up to 0.2%. In any case, by converting the Vickers number to MPa, the two previously reported approaches (Tiryakioğlu's and Tekkaya's) can be expressed as $\sigma_y = 0.375\cdot H^{nanoind}$, that is $\chi = H_V/\sigma_y = 2.7$. Very recently, Song *et al.* [**84**] reported a rather wider variation for $\chi = H_V/\sigma_y$ = 3-4.5, this reduces down to $\chi \cong 3.24$ whenever the ultimate stress is considered instead of the yield stress. Other studies, such as the work by Zhang *et al.* [**85**] indicated values ranging 3.26-3.70 (with a mean value of $\chi = 3.5$) in pure copper subject to ECAP. In his work, Zhang *et al.* reported an overview of the factor influencing the χ ratio between H_V and σ_y for different copper alloys.

Thence, in the present study both values of $\chi = 2.9$ and $\chi = 3.5$ were taken into consideration for the identification of the more appropriate value able to meet the yield stress determined by the microstructure based model here described. It is worth to underline here that the χ = 2.9-2.8 was found to be an appropriate ratio between H_V and σ_y in metallic alloys, as well as pure metals, such aluminum ([**21,80-82**] and references therein).

The direct comparison of yield stress obtained by using both $\chi = H^{nanoind}/\sigma_y = 2.9$ and 3.5,showed a quite better agreement to the yield stress given by applying Eq. (6) with $\chi = 3.5$ rather than by using $\chi = 2.9$. Present results seem to indicate that a slight difference of the H/σ_y does exist whenever low-SFE metals (namely pure metals) or high-SFE metals subjected to SPD are considered.

To better understand this fitting ratio between the two yield stress values obtained by microstructure inspections and by indirect hardness measurements the Gao's approach was here reported and discussed. Gao's relationship between hardness and yield stress also includes the material elastic modulus, E, Eq. (7):

$$H^{nanoind} = \frac{2}{3}\sigma_y \left\{1 + \frac{3}{4}\left(\frac{1}{3}\frac{E_r}{\sigma_y}\cot(\alpha)\right)^n + \frac{1}{n}\left[\left(\frac{1}{3}\frac{E_r}{\sigma_y}\cot(\alpha)\right)^n - 1\right]\right\} \quad \text{Eq. (7)}$$

where α is the semi-angle of the indentation tip, and n is the work-hardening coefficient. This approach and equation was applied to the present case, where the reduced (local) elastic modulus was determined by the nanoindentation measurements and the semi-angle α = 65°, for a Berkovich tip. The work-hardening coefficient n can be set equals to the true strain at necking and it can be derived from nanoindentation assuming a 8-to-10% plastic strain acting during the indentation process ([**85,86**] and references therein). That is, the value of work-hardening in stress-strain curves for annealed copper was is used, n = 0.54. By putting the constant values of Eq. (7) and the obtained reduced elastic modulus values as obtained different experimental conditions here tested, the data reported in **Table 6** were obtained. **Table 6** shows a reasonably good agreement between the Gao's model data and the microstructure strengthening model for strain levels ε_{eq} > 1.21,while for lower strain levels the agreement was less evident. On the other hand, this approach seemed not to show a better result alignment to the data obtained by the strengthening model compared to simply considering the ratio $\chi = H_V/\sigma_y$ = 3.5.

5. Conclusions

In this study early stages of plastic deformation by HPT were characterized by electron microscopy inspections. A OFHC 99.99 pure copper was subjected to strain levels as low as ε_{eq} = 0.40-to-3.63. Mechanical properties were tested by nanoindentation and the indentation size effect phenomenon was correlated to the microstructure evolution induced by the cumulative straining.
The following major findings can be outlined.

1. A minimum necessary strain level to induce the formation of twins was found and it resulted to be ε_{eq} = 0.91;
2. The occurrence of twinning within the refining grains influenced the ISE as it contributed to change the hardness-to-penetration depth curves. That is, the ISE depended to some extent to the formation of twins in pure Cu. With this respect, the hardness rise due to the ISE accelerated with reducing cell and grain size and with occurrence of twins. At the same time, the penetration depth by which ISE started to occur reduced with twin formation and progressive generation within the refining grains;
3. A microstructure based strengthening model was proposed and all the meaningful strengthening contributions were taken into account. In particular, SSDs, dislocation walls, GNDs, grain boundaries and twin boundaries strengthening contributions were modelled. OFHC pure Cu yield stress given by the microstructure based model was directly compared to the yield stress as derived from the nanoindentation hardness.
4. Discussion on the different models of relationship between hardness and yield stress seemed to indicate that $\chi = H_V/\sigma_y$ = 3.5 was the more appropriate coefficient to be considered.

Declaration of Competing Interest

None.

Acknowledgements.

The author wish to thank Mr. M. Pieralisi for his assistance in performing the HPT tests.

References

[1] X.X. Huang, N. Hansen, N. Tsuji, Hardening by annealing and softening by deformation in nanostructured metals, Science 312 (2006) 249-251.
[2] I.A. Ovid'ko, R.Z. Valiev, Y.T. Zhu, Review on superior strength and enhanced ductility of metallic nanomaterials, Prog. Mater. Sci. 94 (2018) 462-540.
[3] M. Cabibbo, Nanostructured Cobalt Obtained by Combining Bottom-Up and Top-Down Approach, Metals 8(11) (2018) 962-971.
[4] I. Sabirova, M.Yu. Murashkin, R.Z. Valiev, Nanostructured aluminium alloys produced by severe plastic deformation: New horizons in development Mater. Sci. Eng. A 560 (2013) 1-24.
[5] A.P. Zhilyaev, T.G. Langdon, Using high-pressure torsion for metal processing: Fundamentals and applications, Progr. Mater. Sci. 53 (2008) 893-979.
[6] R.Z. Valiev, T.G. Langdon, Principles of equal-channel angular pressing as a processing tool for grain refinement, Progr. Mater. Sci., 51 (2006) 881-981.
[7] A. Vinogradov, Y. Estrin, Analytical and numerical approaches to modelling severe plastic deformation, Progr. Mater. Sci. 95 (2018) 172-242.
[8] Y. Cao, S. Ni, X. Liao, M. Song, Y. Zhu, Structural evolutions of metallic materials processed by severe plastic deformation, Mater. Sci. Eng. R 133 (2018) 1-59.
[9] B.L. Li, N. Tsuji, N. Kamikawa, Microstructure homogeneity in various metallic materials heavily deformed by accumulative roll-bonding, Mater. Sci. Eng. A 423 (2006) 331-342.
[10] Y. Xun, F.A. Mohamed, Refining efficiency and capability of top-down synthesis of nanocrystalline materials, Mater. Sci. Eng. A 528 (2011) 5446-5452.
[11] A.I. Almazrouee, K.J. Al-Fadhalah, S.N. Alhajeri, T.G. Langdon, Microstructure and microhardness of OFHC copper processed by high-pressure torsion, Mater. Sci. Eng. A 641 (2015) 21-28.
[12] M. Ebrahimi, C. Gode, Severely deformed copper by equal channel angular pressing, Progr. Nat. Sci.: Mater. Int.l 27 (2017) 244-250.
[13] N.Q. Chinh, T. Csanádi, J. Gubicza, T.G. Langdon, Plastic behavior of face-centered-cubic metals over a wide range of strain, Acta Mater. 58 (2010) 5015-5021.
[14] M. Cabibbo, Microstructure strengthening mechanisms in different equal channel angular pressed aluminum alloys, Mater. Sci. Eng. A560 (2013) 413-432.
[15] M. Cabibbo, A TEM Kikuchi pattern study of ECAP AA1200 via routes A, C, B_C, Mater. Character. 61 (2010) 613-625.
[16] M. Cabibbo, W. Blum, E. Evangelista, M.E. Kassner, M.A. Meyers, Transmission electron microscopy study of strain induced low- and high-angle boundary development in equal-channel angular-pressed commercially pure aluminum, Metall. Mater. Trans. A39 (2008) 181-192.
[17] C. Xu, Z. Horita, T.G. Langdon, The evolution of homogeneity in processing by high-pressure torsion, Acta Mater. 55 (2007) 203-212.
[18] G. Sakai, Z. Horita, T.G. Langdon, Grain refinement and superplasticity in an aluminum alloy processed by high-pressure torsion, Mater. Sci. Eng. A 393 (2005) 344-351.
[19] Y. Ito, K. Edalati, Z. Horita, High-pressure torsion of aluminum with ultrahigh purity (99.9999%) and occurrence of inverse Hall-Petch relationship, Mater. Sci. Eng. A 679 (2017) 428-434.
[20] D.A. Hughes, N. Hansen, D.J. Bammann, Geometrically necessary boundaries, incidental dislocation boundaries and geometrically necessary dislocations, Scripta Mater. 48 (2003) 147-153.
[21] M. Cabibbo, Minimum necessary strain to induce tangled dislocation to form cell and grain boundaries in a 6N–Al, Mater. Sci. Eng. A 77 (2020) 138420.
[22] I. Sabirov, M.Yu. Murashkin, R.Z. Valiev, Nanostructured aluminium alloys produced by severe plastic deformation: New horizons in development, Mater. Sci. Eng. A 560 (2013) 1-24.

[23] A. P. Zhilyaev, B.-K. Kim, J.A. Szpunar, M.D. Baró, T.G. Langdon, The microstructural characteristics of ultrafine-grained nickel, Mate. Sci. Eng. A 391 (2005) 377-389.
[24] G.B. Rathmayr, A. Hohenwarter, R. Pippan, Influence of grain shape and orientation on the mechanical properties of high pressure torsion deformed nickel, Mater. Sci. Eng. A 560 (2013) 224-231.
[25] K.S. Raju, M.G. Krishna, K.A. Padmanabhan, K. Muraleedharan, N.P. Gurao, G. Wilde, Grain size and grain boundary character distribution in ultra-fine grained (ECAP) nickel, Mater. Sci. Eng. A 491 (2008) 1–7.
[26] Q. Xue, I.J. Beyerlein, D.J. Alexander, G.T. Gray III, Mechanisms for initial grain refinement in OFHC copper during equal channel angular pressing, Acta Mater. 55 (2007) 655-668.
[27] A. Azushima, R. Kopp, A. Korhonen, D.Y. Yang, A. Yanagida, Severe plastic deformation (SPD) processes for metals, CIRP Annals 57 (2008) 716-735.
[28] R.Z. Valiev, Producing bulk nanostructured metals and alloys by severe plastic deformation (SPD), Nanostruct. Metals All. Chapter 1 (2011) 3-39.
[29] D. Lorenz, A. Zeckzer, U. Hilpert, P. Grau, H. Johansen, H.S. Leipner , Pop-in effect as homogeneous nucleation of dislocations during nanoindentation, Phys. Rev. B 67 (2003) 172101 1-4.
[30] A. Asenjo, M. Jaafar, E. Carrasco, J.M. Rojo, Dislocation mechanisms in the first stage of plasticity of nanoindented Au(111) surfaces, Phys. Rev. B 73 (2006) 075431 1-7.
[31] N.A. Fleck, G.M. Muller, M.F. Ashby, J.W. Hutchinson, Strain gradient plasticity: Theory and experiment, Acta Metall. Mater. 42 (1994) 475-487.
[32] W.D. Nix, H.J. Gao, Indentation size effects in crystalline materials: A law for strain gradient plasticity, Mech. Phys. Solids 46 (1998) 411-425.
[33] W. Liu, L. Chen, Y. Cheng, L. Yu, X. Yi, H. Gao, H. Duan, Model of nanoindentation size effect incorporating the role of elastic deformation, J. Mech. Phys. Solids 126 (2019) 245-255.
[34] B. Yang, H. Vehoff, Dependence of nanohardness upon indentation size and grain size – A local examination of the interaction between dislocations and grain boundaries, Acta Mater. 55 (2007) 849-856.
[35] K. Durst, M. Göken, G.M. Pharr, Indentation size effect in spherical and pyramidal indentations, J. phys. D: Appl. Phys. 41 (2008) 074005.
[36] K. Durst, B. Backes, M. Göken, Indentation size effect in metallic materials: Correcting for the size of the plastic zone, Scripta Mater. 52 (2005) 1093-1097.
[37] N.H. Polakowski, E.J. Ripling, Strength and Structure of Engineering Materials, Prentice-Hall, Englewood Cliffs, NJ, 1966.
[38] J. C. Russ, R., T. Dehoff, Practical Stereology, 2nd Ed. Springer Science & Business Media LLC New York, 2000.
[39] M. Cabibbo, P. Ricci, R. Cecchini, Z. Rymuza, J. Sullivan, S. Dub, S. Cohen, An international round-robin calibration protocol for nanoindentation measurements, Micron 43 (2012) 215-222.
[40] W.C. Oliver, G.M. Pharr, Measurement of hardness and elastic modulus by instrumented indentation: Advances in understanding and refinements to methodology, J. Mater. Res. 19 (2004) 3-20.
[41] J.H. Gong, H.Z. Miao, Z.J. Peng, Analysis of the nanoindentation data measured with a Berkovich indenter for brittle materials: effect of the residual contact stress, Acta Mater. 52 (2004) 785-793.
[42] M.A. Meyers, O. Vöhringer, V.A. Lubarda, The onset of twinning in metals: a constitutive description. Acta Mater. 49 (2001) 4025-4039.
[43] W.Z. Han, Z.F. Zhang, S.D. Wu, S.X. Li, Combined effects of crystallographic orientation, stacking fault energy and grain size on deformation twinning in fcc crystals, Phil. Mag. 88 (2008) 3011-3029.

[44] Y. Cao, Y.B. Wang, X.Z. Liao, M. Kawasaki, S.P. Ringer, T.G. Langdon, Y.T. Zhu, Applied stress controls the production of nano-twins in coarse-grained metals. Appl. Phys.Lett. 101 (2012) 231903.
[45] G. Laplanche, A. Kostka, O.M. Horst, G. Eggeler, E.P. George, Microstructure evolution and critical stress for twinning in the CrMnFeCoNi high-entropy alloy. Acta Mater. 118 (2016) 152-163.
[46] Y.S. Li, Y. Zhang, N.R. Tao, K. Lu, Effect of the Zener-Hollomon parameter on the microstructures and mechanical properties of Cu subjected to plastic deformation. Acta Mater. 57 (2009) 761-772.
[47] L.E. Murr, M.A. Meyers, C.S. Niou, Y.J. Chen, S. Pappu, C. Kennedy, Shock-induced deformation twinning in tantalum. Acta Mater. 45 (1997) 157-175.
[48] I.J. Beyerlein, L.S. Tóth, Texture evolution in equal-channel angular extrusion. Progr. Mater. Sci. 54 (2009) 427-510.
[49] M.F. Ashby, The deformation of plastically non-homogeneous materials. Phil. Mag. 21 (1970) 399-424.
[50] D.A. Hughes, N. Hansen, D.J. Bammann, Geometrically necessary boundaries, incidental dislocation boundaries and geometrically necessary dislocations. Scripta Mater. 48 (2003) 147-153.
[51] P. Li, S.X. Li, Z.G. Wang, Z.F. Zhang, Fundamental factors on formation mechanism of dislocation arrangements in cyclically deformed fcc single crystals. Progr. Mater. Sci. 56 (2011) 328-377.
[52] D. Kuhlmann-Wilsdorf, Theory of plastic deformation: properties of low energy dislocation structures. Mater. Sci. Eng, A 113 (1989) 1-41.
[53] X.H. An, Q.Y. Lin, S. Qu, G. Yang, S.D. Wu, Z.F. Zhang, Influence of stacking-fault energy on the accommodation of severe shear strain in Cu-Al alloys during equal-channel angular pressing. J. Mater. Res. 24 (2009) 3636-3646.
[54] A.A.S. Mohammed, E.A. El-Danaf, A.A.Radwan, A criterion for shear banding localization in polycrystalline FCC metals and alloys and critical working conditions for different microstructural variables. J. Mater. Process. Technol. 186 (2007) 14-21.
[55] P. Müllner, A.E. Romanov, Internal twinning in deformation twinning. Acta Mater. 48 (2000) 2323-37.
[56] J.W. Christian, S. Mahajan, Deformation twinning. Progr. Mater. Sci. 39 (1995) 1-157.
[57] R. Lapovok, F.H. Dalla Torre, J. Sandlin, C.H.J. Davies, E.V. Pereloma, P.F. Thomson, Y. Estrin, Gradient plasticity constitutive model reflecting the ultrafine micro-structure scale: the case of severely deformed copper, J. Mech. Phys. Solids 53 (2005) 729-747.
[58] Y. Estrin, A. Molotnikov, C.H.J. Davies, R. Lapovok, Strain gradient plasticity modelling of high-pressure torsion, J. Mech. Phys. Solids 56 (2008) 1186-1202.
[59] C. Saldana, A.H. King, S. Chandrasekar, Thermal stability and strength of deformation microstructures in pure copper, Acta Mater 60 (2012) 4107-4116.
[60] H.L. Wang, Z.B. Wang, K. Lu, Interfacial diffusion in a nanostructured Cu produced by means of dynamic plastic deformation, Acta Mater. 59 (2011) 1818-1828.
[61] N. Hansen, Hall–Petch relation and boundary strengthening, Scripta Mater. 51 (2004) 801-806.
[62] S. Nemat-Nasser, Y. Li, Flow stress of f.c.c. polycrystals with application to OFHC Cu, Acta Mater. 46 (1998) 565-577.
[63] M. Cabibbo, Microstructure strengthening mechanisms in an Al–Mg–Si–Sc–Zr equal channel angular pressed aluminium alloy, Appl. Surf. Sci. 281 (2013) 38-43.
[64] W. Han, S. Wu, C. Huang, S. Li, Z. Zhang, Orientation design for enhancing deformation twinning in Cu single crystal subjected to equal channel angular pressing, Adv. Eng. Mater. 10 (2008) 1110-1113.
[65] S.D. Antolovich, R.W. Armstrong, Plastic strain localization in metals: origins and consequences, Progr. Mater. Sci. 59 (2014) 1-160.

[66] F. Dalla Torre, R. Lapovok, J. Sandlin, P.F. Thomson, C.H.J. Davies, E.V. Pereloma, Microstructures and properties of copper processed by equal channel angular extrusion for 1–16 passes, Acta Mater. 52 (2004) 4819-4832.
[67] N. Hansen, X. Huang, G. Winther, Grain orientation, deformation microstructure and flow stress, Mater. Sci. Eng. A 494 (2008) 61-67.
[68] N. Hansen, X. Huang, Microstructure and flow stress of polycrystals and single crystals, Acta Mater. 46 (1998) 1827-1836.
[69] R.W. Armstrong, P.J. Worthington, in Metallurgical Effects at High Strain Rates, ed. R.W. Rohde, B.M. Butcher, J.R. Holland, C.H. Karnes. Plenum Press, New York, USA (1973) 401-414.
[70] R. Lapovok, F.H. Dalla Torre, J. Sandlin, C.H.J. Davies, E.V. Pereloma, P.F. Thomson, Y. Estrin, Gradient plasticity constitutive model reflecting the ultrafine micro-structure scale: the case of severely deformed copper, J. Mech. Phys. Solids 53 (2005) 729-747.
[71] H. Mughrabi, Dislocation wall and cell structures and long-range internal stresses in deformed metal crystals, Acta Metall. 31 (1983) 1367-1379.
[72] H. Mughrabi, A two-parameter description of heterogeneous dislocation distributions in deformed metal crystals, Mater. Sci. Eng. A 85 (1987) 15-31.
[73] F.R.N. Nabarro, Work hardening and dynamical recovery of F.C.C. metals in multiple glide, Acta Metall. 37 (1989) 1521-1546.
[74] T. Ungár, L.S. Tóth, J. Illy, I. Kovács, Dislocation structure and work hardening in polycrystalline ofhc copper rods deformed by torsion and tension, Acta Metall. 34 (1986) 1257-1267.
[75] A.S. Argon, P. Haasen, A new mechanism of work hardening in the late stages of large strain plastic flow in F.C.C. and diamond cubic crystals, Acta Metall. Mater. 11 (1993) 3289-3306.
[76] Y.Estrin, L.S. Tóth, A. Molinari, Y. Bréchet, A dislocation-based model for all hardening stages in large strain deformation, Acta Mater. 46 (1998) 5509-5522.
[77] X. Feaugas, P. Pilvin, A Polycrystalline Approach to the Cyclic Behaviour of f.c.c. Alloys – Intra- Granular Heterogeneity, Adv. Eng. Mater. 11 (2009) 703-709.
[78] M.E. Kassner, P. Geantil, L.E. Levine, Long range internal stresses in single-phase crystalline materials, Int. J. Plast. 45 (2013) 44-60.
[79] E. Nes, T. Pettersen, K. Marthinsen, On the mechanisms of work hardening and flow-stress saturation, Scripa Mater. 43 (2000) 55-62.
[80] J.R. Cahoon, W.H. Broughton, A.R. Kutzak, The determination of yield strength from hardness measurements, Mater. Trans. 2 (1971) 1979-1983.
[81] E. Broitman, Indentation Hardness Measurements at Macro-, Micro-, and Nanoscale: A Critical Overview, Tribol. Lett. 65 (2017) 23-41.
[82] M. Tiryakioğlu, On the relationship between Vickers hardness and yield stress in Al–Zn–Mg–Cu Alloys, Mater. Sci. Eng. A 633 (2015) 17-19.
[83] A.E. Tekkaya, An Improved Relationship between Vickers Hardness and Yield Stress for Cold Formed Materials and its Experimental Verification, Annals CIRP 49 (2000) 205-208.
[84] M. Song, C. Sun, Y. Chen, Z. Shang, J. Li, Z. Fan, X. Zhang, Grain refinement mechanisms and strength-hardness correlation of ultrafine grained grade 91 steel processed by equal channel angular extrusion, Int.l J. Press. Vess. Piping 172 (2019) 212-219.
[85] P. Zhang, S.X. Li, Z.F. Zhang, General relationship between strength and hardness, Mater. Sci. Eng. A 529 (2011) 62-73.
[86] X.-L. Gao, An expanding cavity model incorporating strain-hardening and indentation size eff ects, Int. J. Solids Struct. 43 (2006) 6615-6629.

Figures and Tables captions

Fig. 1. Microstructure of the as annealed OFHC Cu.

Fig. 2. To scale scheme of HPT showing the location of extraction of the TEM discs.

Fig. 3. Microstructure evolution with cumulative HPT shear strain, at ε_{eq} = 0.40, a); ε_{eq} = 0.91, b); ε_{eq} = 1.21, c); ε_{eq} = 1.81, d); ε_{eq} = 2.42, e); ε_{eq} = 3.63, f). In b) the dark-field (DF) micrograph shows the early formation of low-angle boundaries (cells) from tangled dislocations (GNDs). Inset in b) is the indexed SAEDP. DF g-vector was g = [02-2]. By selecting this crystallographic plane the existing tangled dislocations and cell boundaries within the grains were almost entirely visible as they mostly lying in the [022] planes and (022) directions.

Fig. 4. Twinning formation induced by the HPT strain, ε_{eq} = 0.91, a); ε_{eq} = 1.81, b); ε_{eq} = 3.63, c). Cu crystals were oriented along [011]-zone axis to properly reveal the twin boundaries and lines; related indexed SAEDP is reported in d).

Fig. 5. Nanoindentation load-displacement curves, *P*-*h*, using a load *P* = 10 mN, for HPT OFHC 99.99% purity Cu at ε_{eq} = 0.40, 0.91, 1.21, 181, 2.42, and 3.63. The annealed OFHC Cu nanoindentation curve, ε_{eq} = 0, is reported for comparison.

Fig. 6. Plot of hardness, *H*, and reduced elastic modulus, E_r, vs. cumulative HPT straining, ε_{eq} = 0.40 to 3.63. Error bars were determined by averaging the obtained values from the 64 individual nanoindentation measurements that were performed at each experimental condition.

Fig. 7. The ISE phenomenon. Hardness, *H*, vs. indentation depth, h_c, for ε_{eq} = 0.40-to-3.63; the as-annealed curve is reported for comparison to the HPT experimental conditions.

Fig. 8. Minimum nanoindentation load to initiate ISE vs. mean grain and cell size produced by HPT of the OFHC 99.9% purity Cu.

Fig. 9. Evolution of twin mean spacing, λ_{Twin}, for HPT strains $0.91 < \varepsilon_{eq} < 2.42$.

Fig. 10. Grain size, d_{grain}, cell size, d_{cell}, twin spacing, λ_{Twin}, and twinned grain volume fraction, $f_{twinned\ grains}$, evolution with HPT strains ε_{eq} = 0.40-to-3.63.

Fig. 11. BF-TEM at ε_{eq} = 2.42 showing dislocation walls (DW), tangled dislocations (TD), geometrically-necessary dislocations (GND), twin boundaries (TB), and grain boundaries (GB).

Table 1. Chemical composition of the OFHC 99.99% purity copper (wt.%x1000), as reported by the supplier (purity standard identified as DIN1706-NFA51050 / CuC1, source FRW^{TM}).

Table 2. Equivalent strain ε_{eq} obtained by the different HPT experimental parameters at *N* = 1/18 (lowest) to 1/2 turns (highest), at radial distances *r* = 2 mm (almost mid-radius) from disc thick-center.

Table 3. Mean grain, d_g, and cell size, d_{cell}, of OFHC CU subjected to HPT at ε_{eq} = 0.40 to 3.63. These mean values were determined out of 3 different areas of the TEM thin discs accounting of some 0.56-to-0.74 mm^2 per each experimental condition.

Table 4. Dislocation density and dislocation wall volume fraction, *f*, for ε_{eq} = 0.40-to-3.63.

Table 5. Yield stress as calculated by the model of Eq. (6), σ_y^{model}, and as derived from the nanoindentation Hardness measurements, $\sigma_y^{nanoind}$. In this latter case, two different approaches are here proposed, one according to [**21**] in which a factor of χ = 2.9 was considered as *H* to σ_y ratio; a second according to [**82**] in which the ratio χ = 3.5. Data refers to ε_{eq} = 0.40, 0.91, 1.21, 1.81, 2.42, and 3.63.

Table 6. Gao's model of Eq. (7) applied to the microstructure strengthening model of the present study at ε_{eq} = 0.40, 0.91, 1.21, 1.81, 2.42, and 3.63.

Figure 1

Click here to download high resolution image

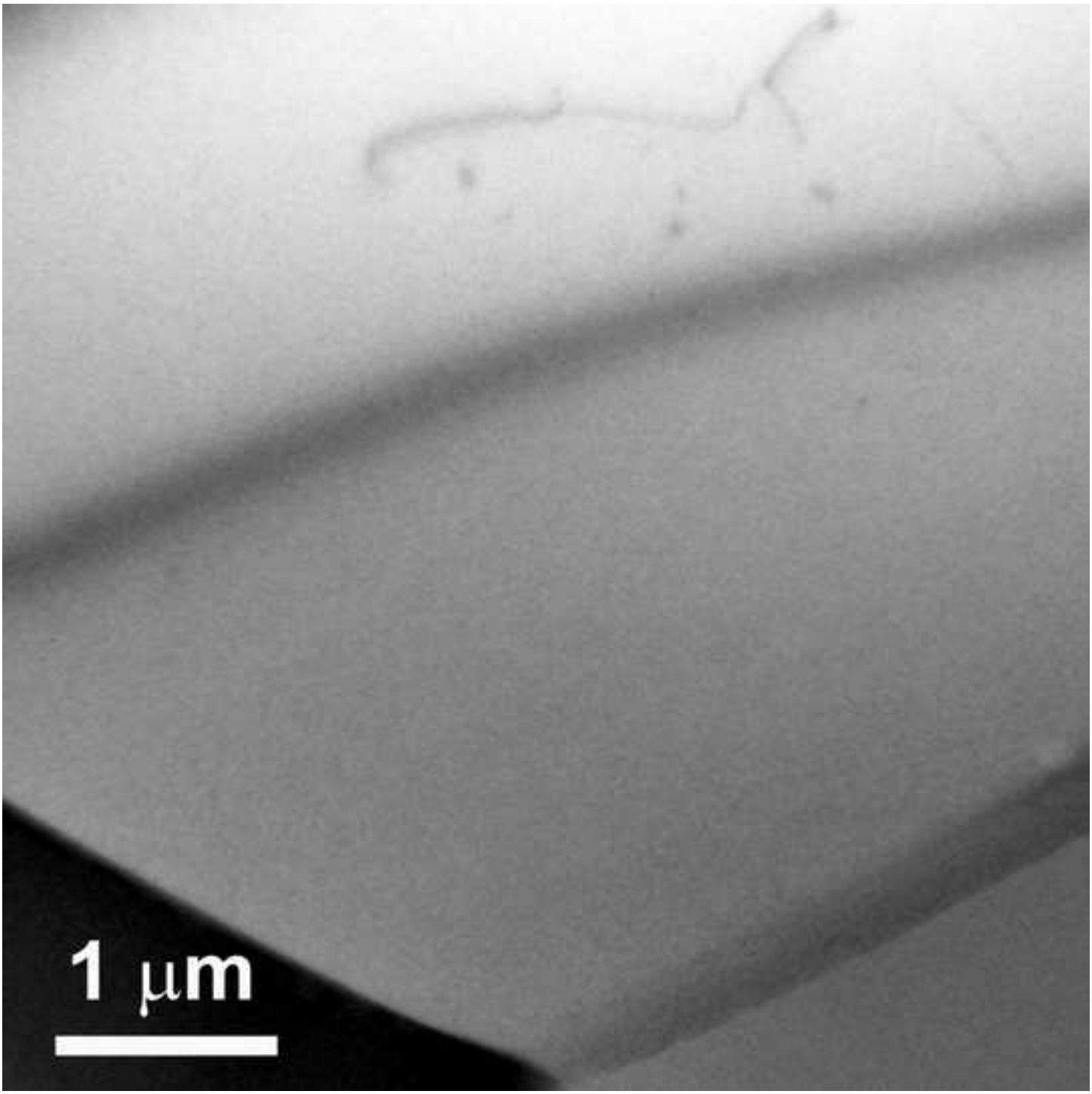

Figure 2

Click here to download high resolution image

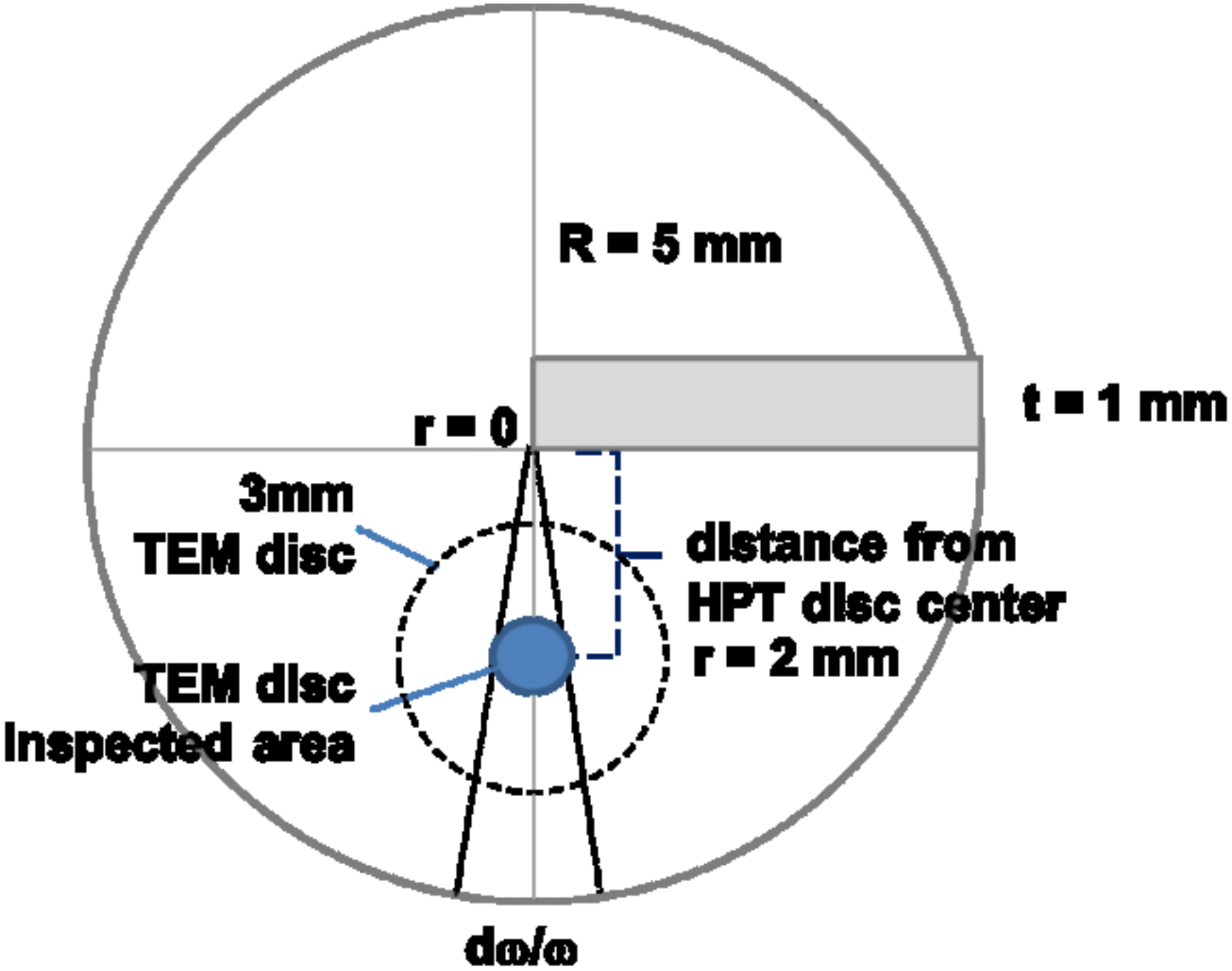

Figure 3a
Click here to download high resolution image

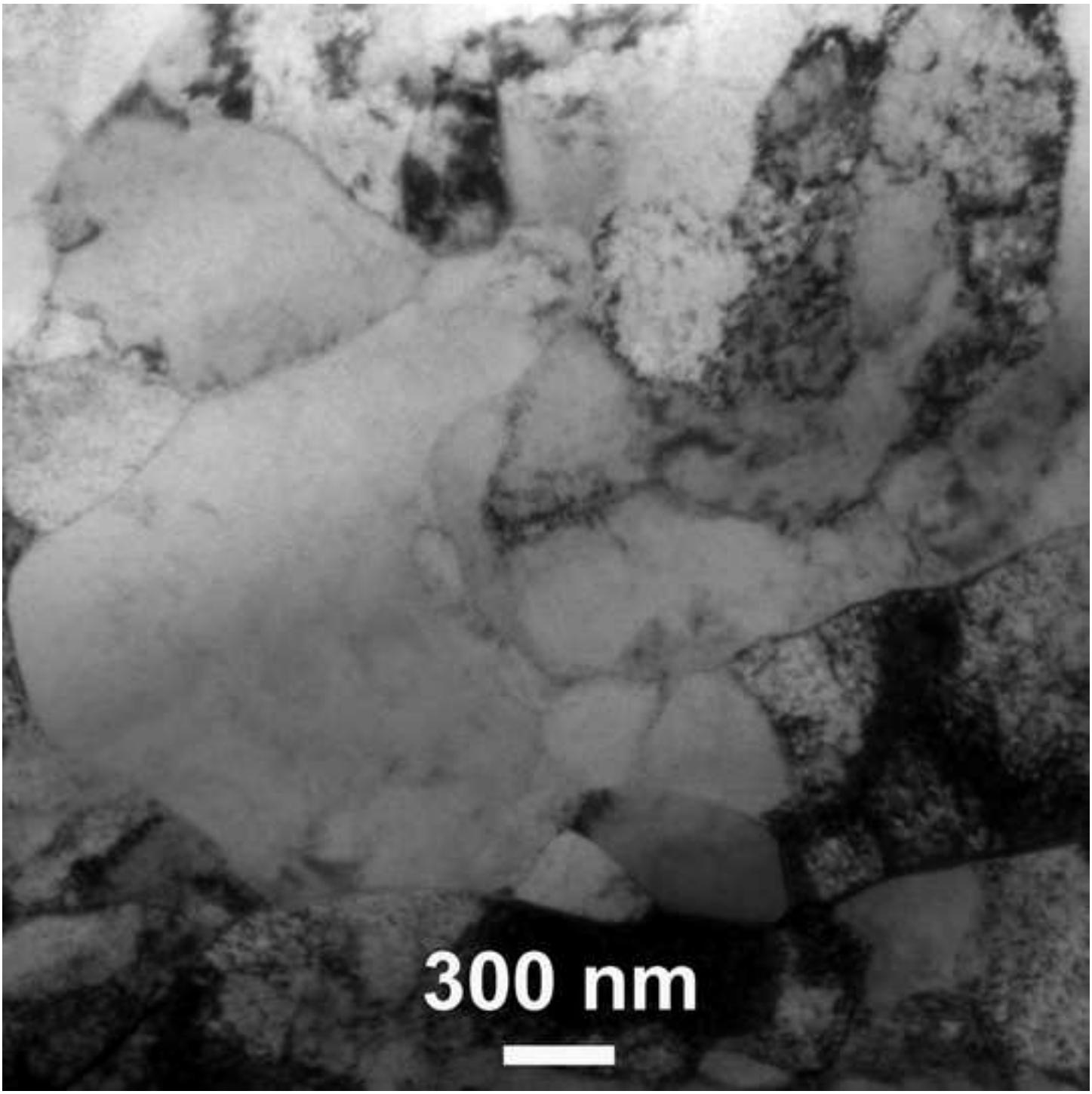

Figure 3b

Click here to download high resolution image

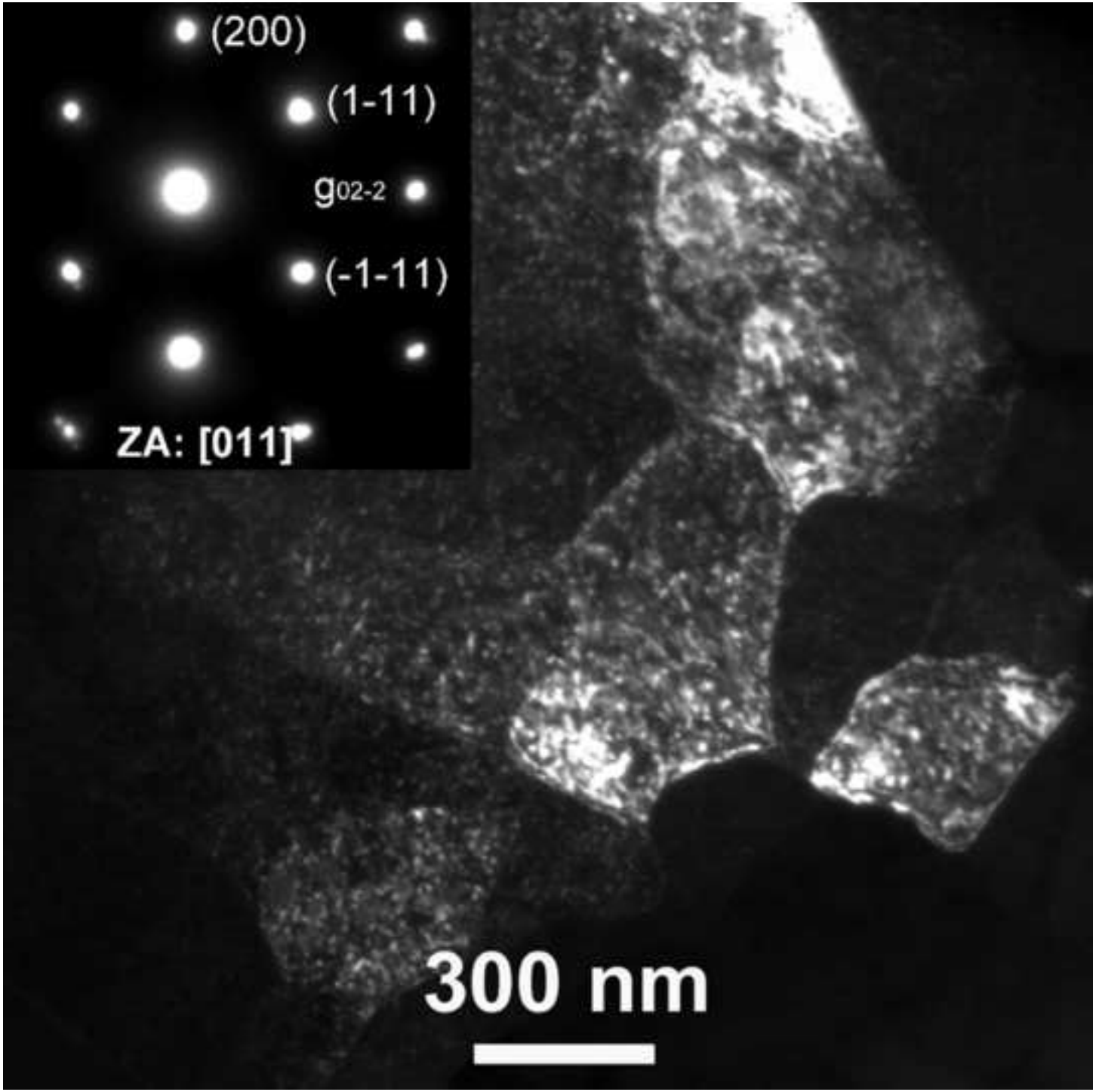

Figure 3c
Click here to download high resolution image

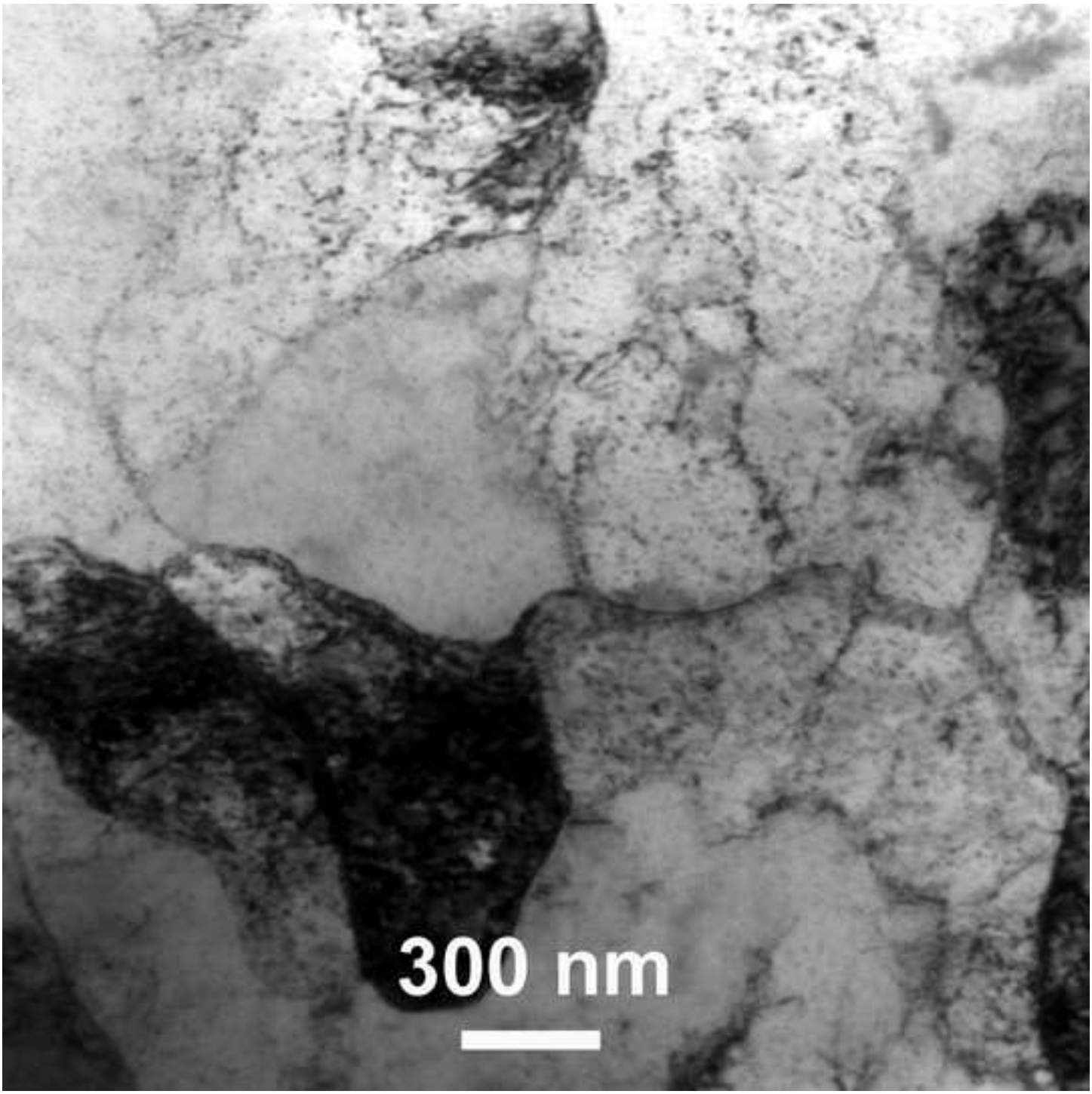

Figure 3d

Click here to download high resolution image

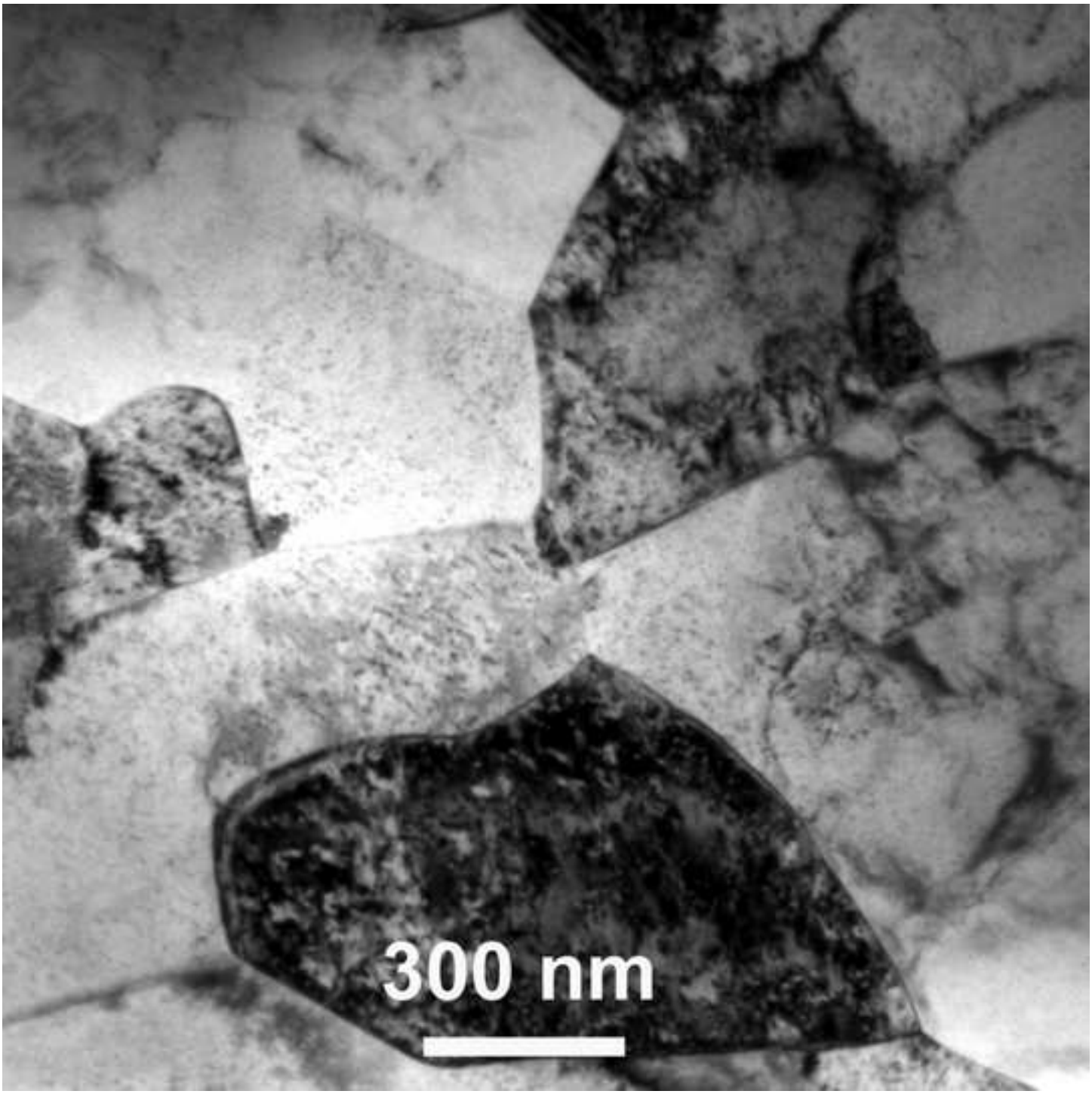

Figure 3e
Click here to download high resolution image

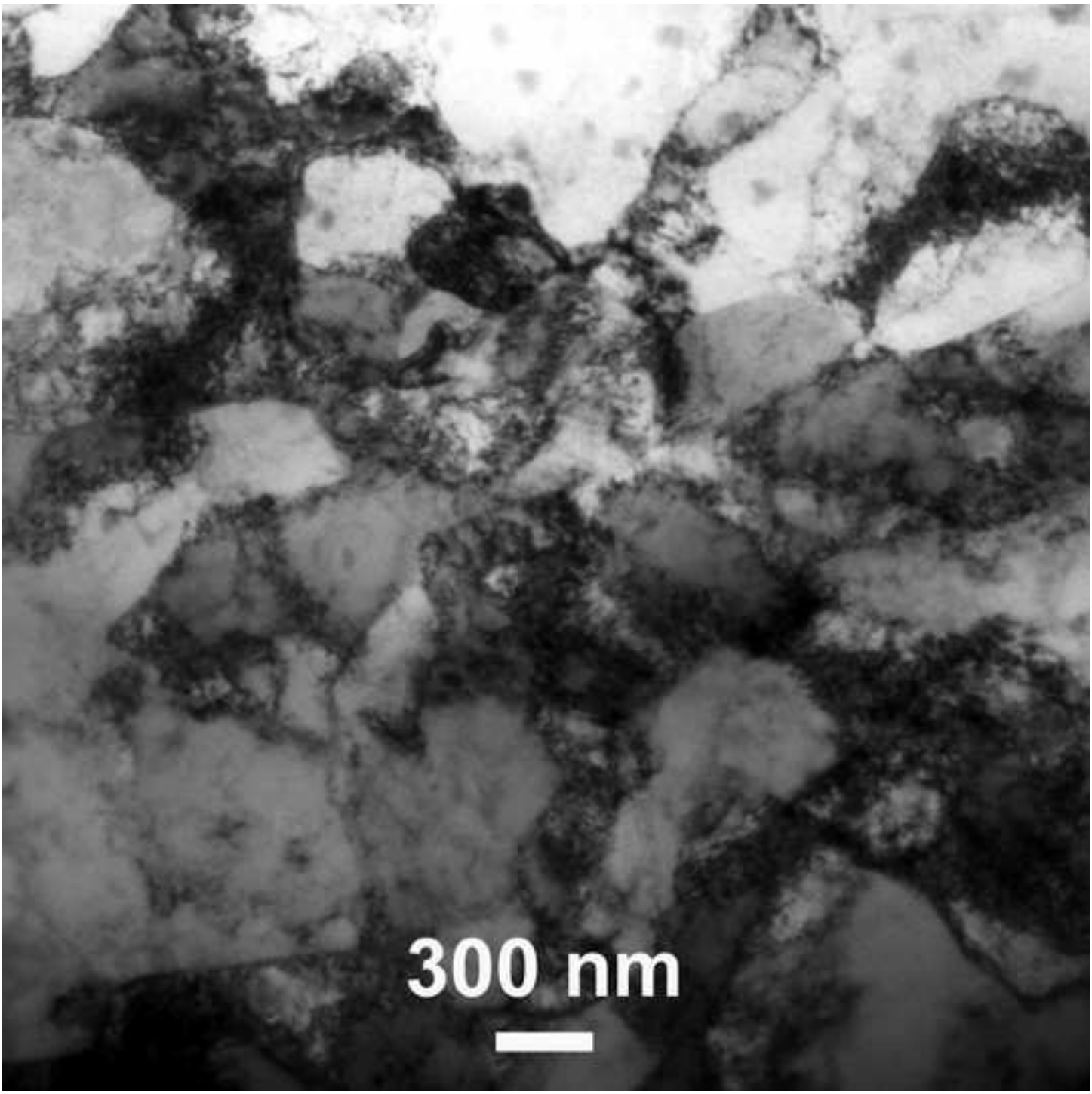

Figure 3f

Click here to download high resolution image

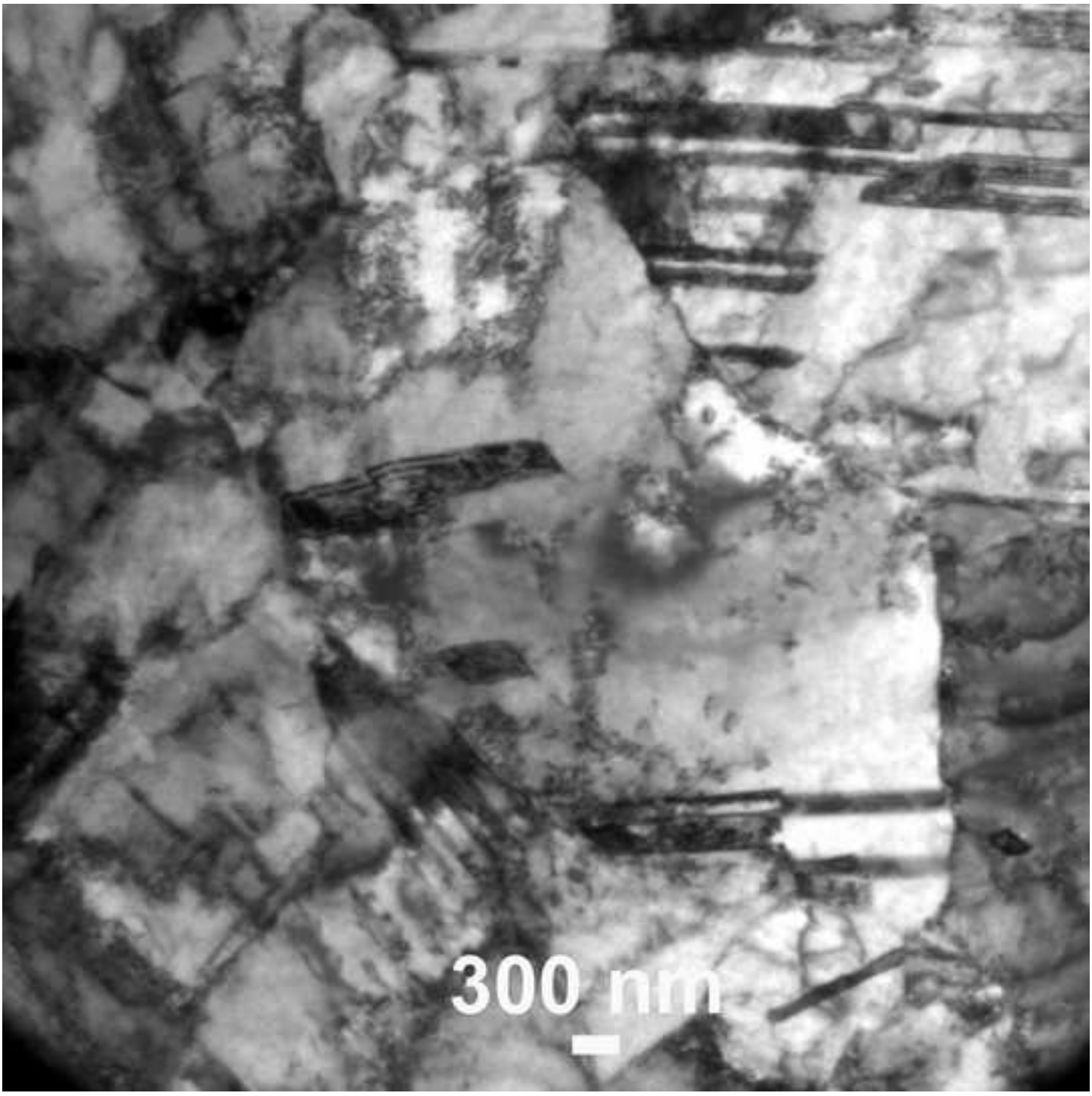

Figure 4a
Click here to download high resolution image

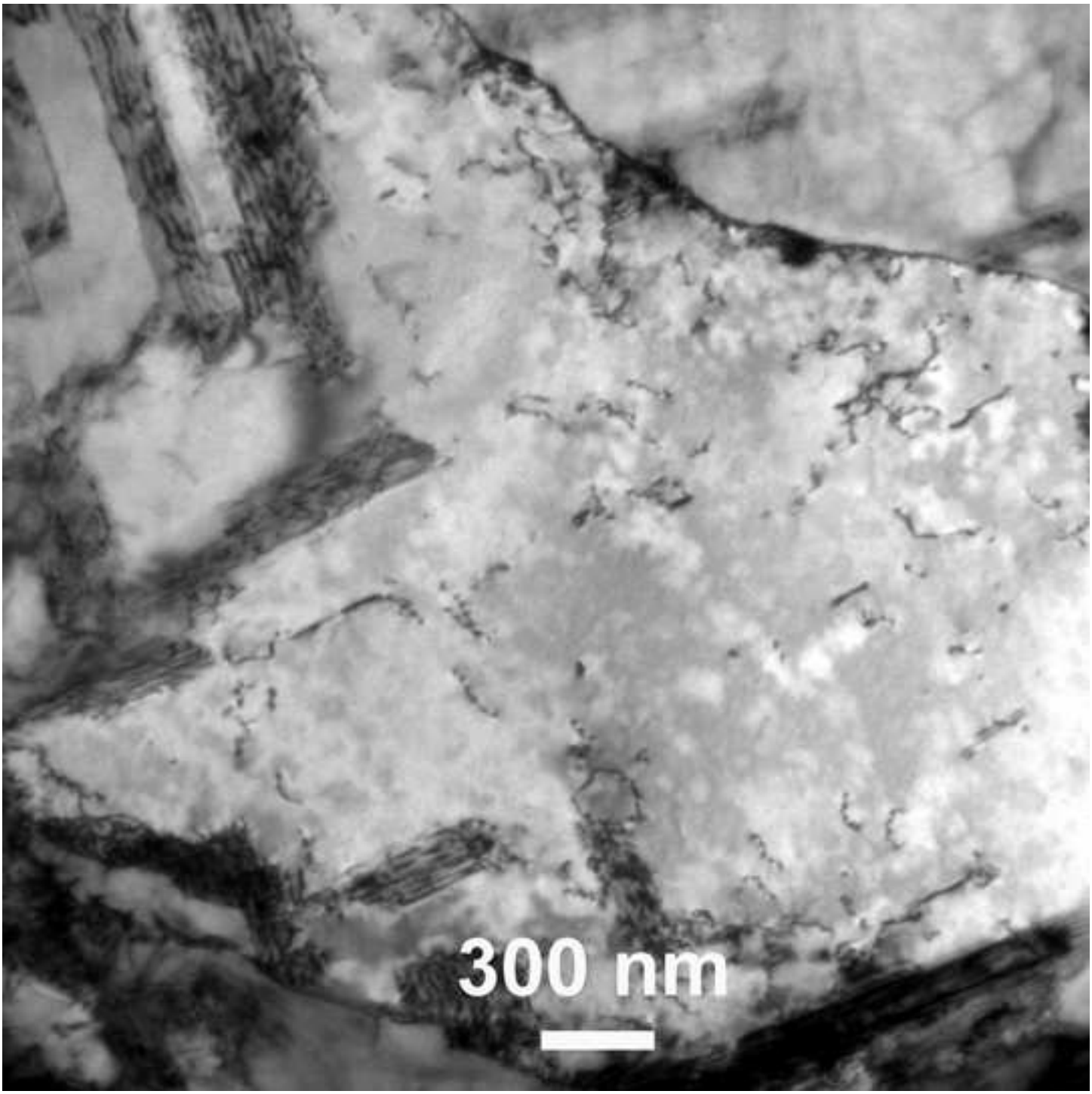

Figure 4b
Click here to download high resolution image

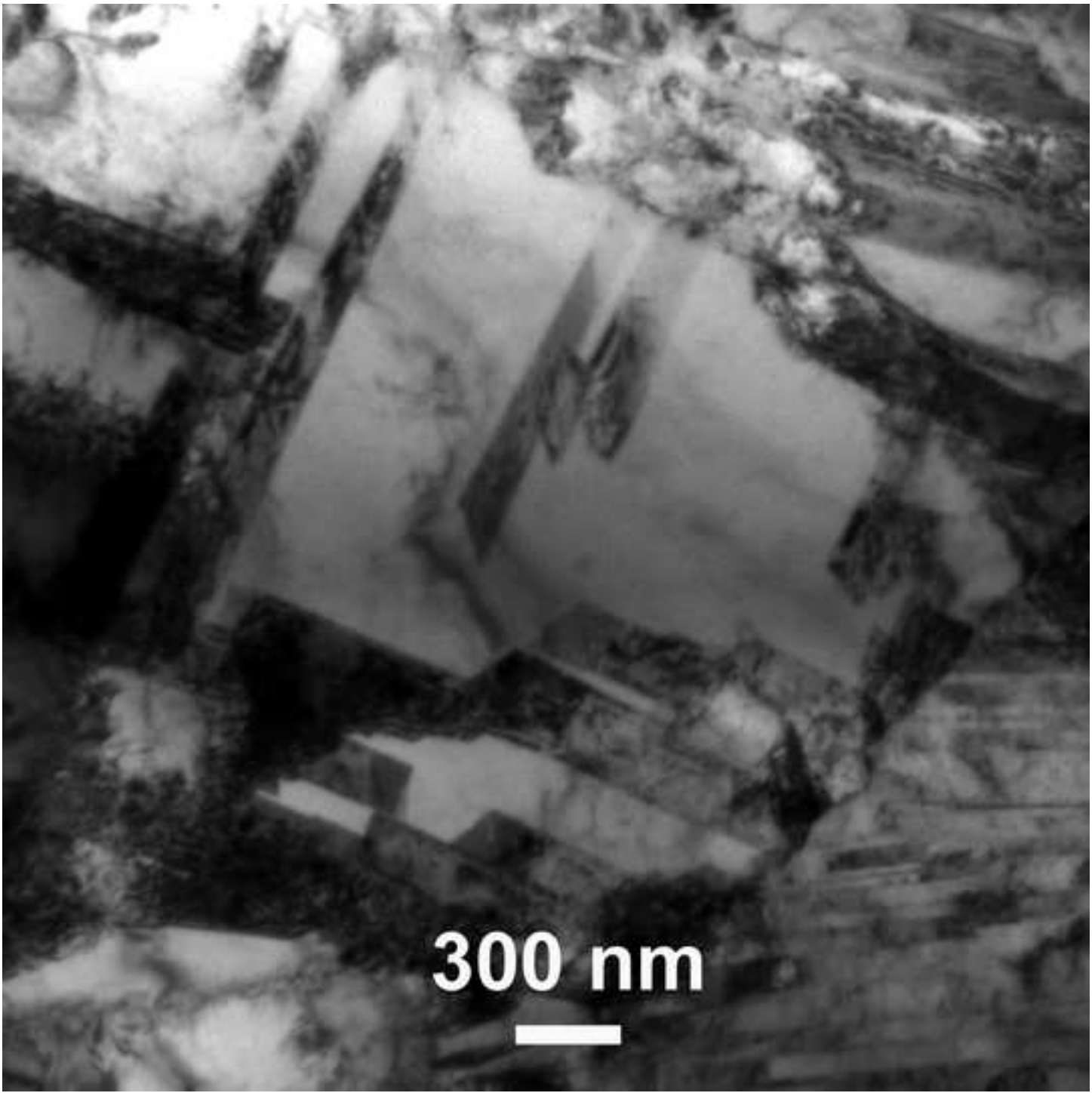

Figure 4c

Click here to download high resolution image

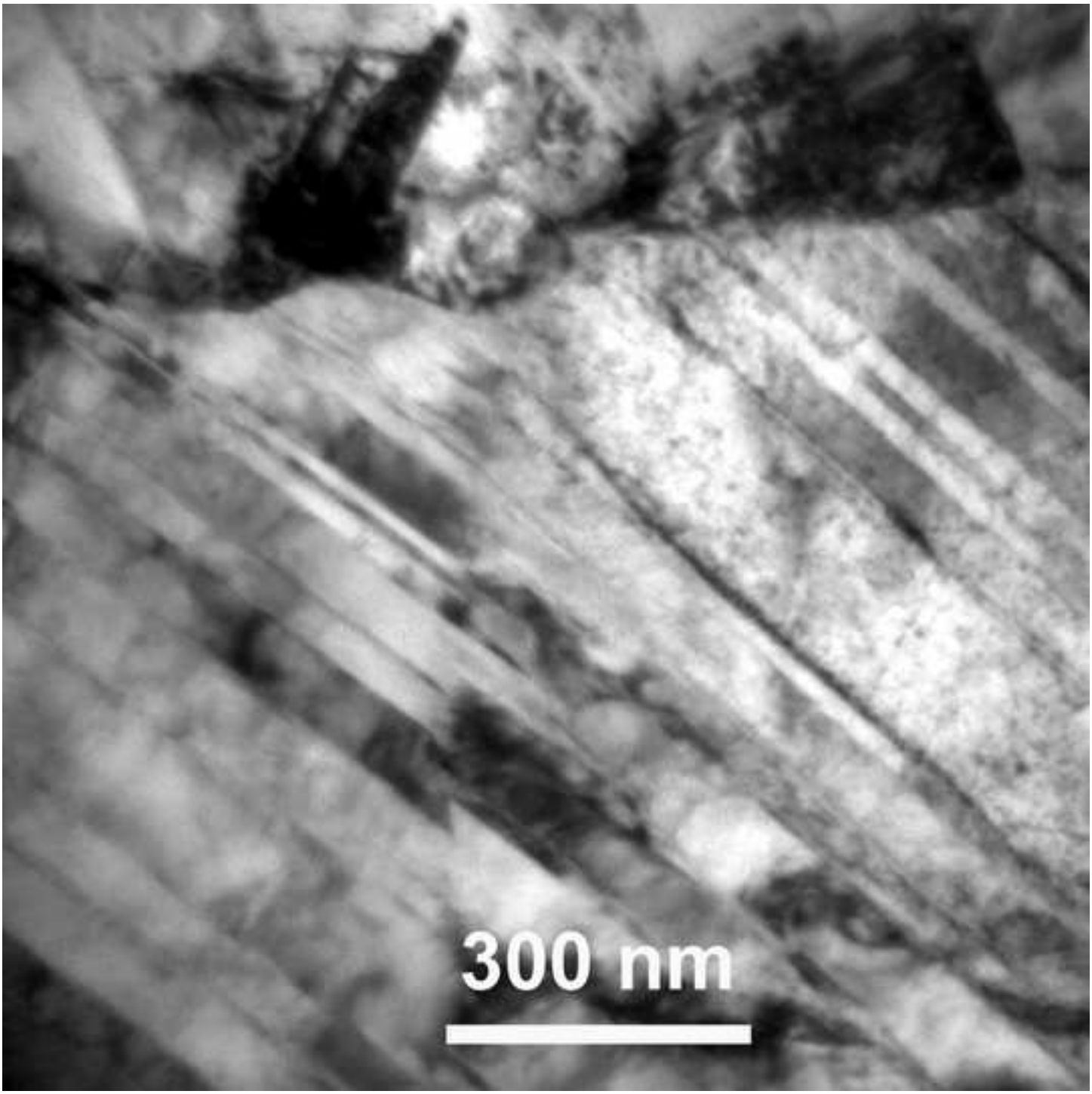

Figure 4d

Click here to download high resolution image

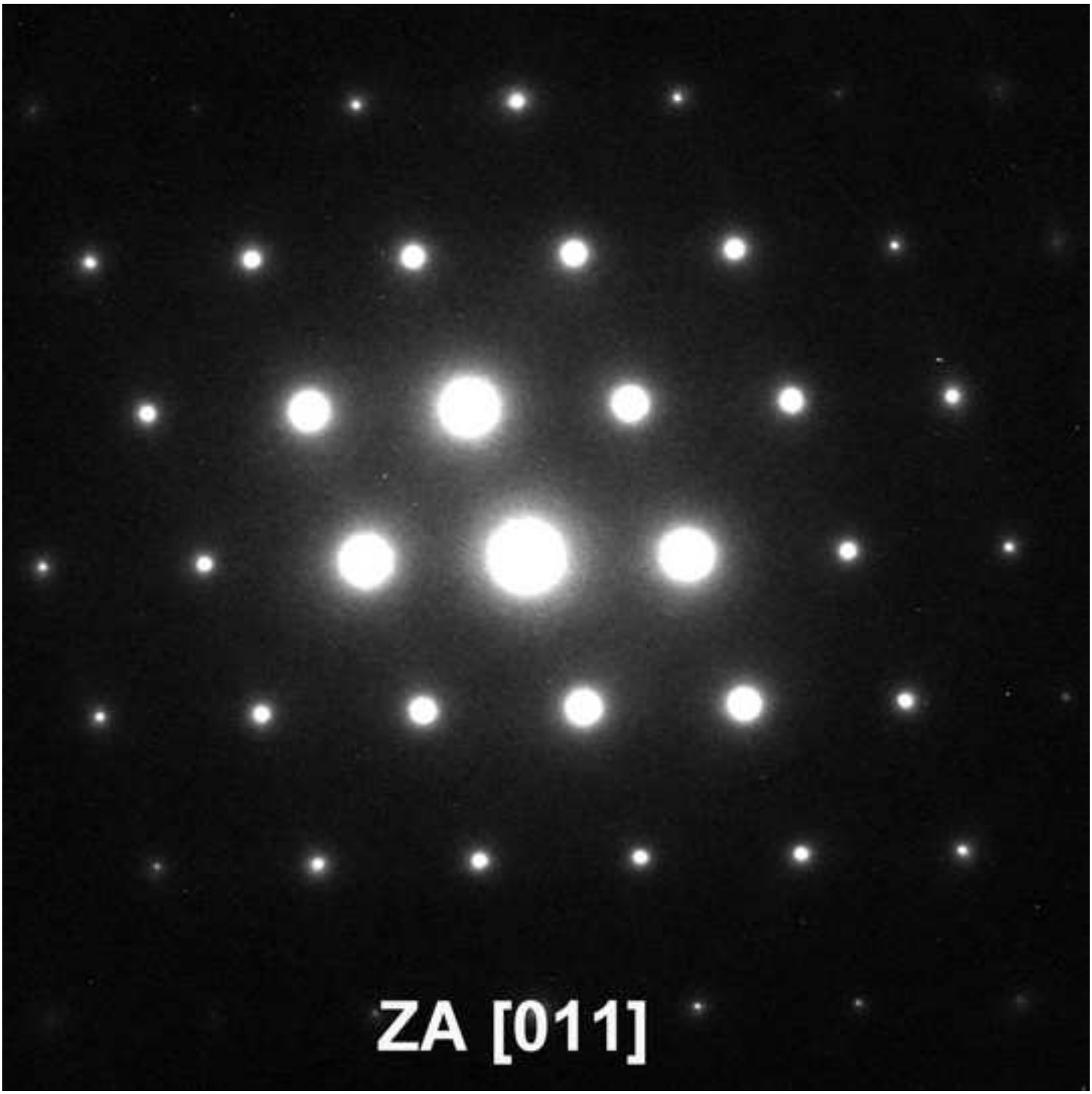

Figure 5

Click here to download high resolution image

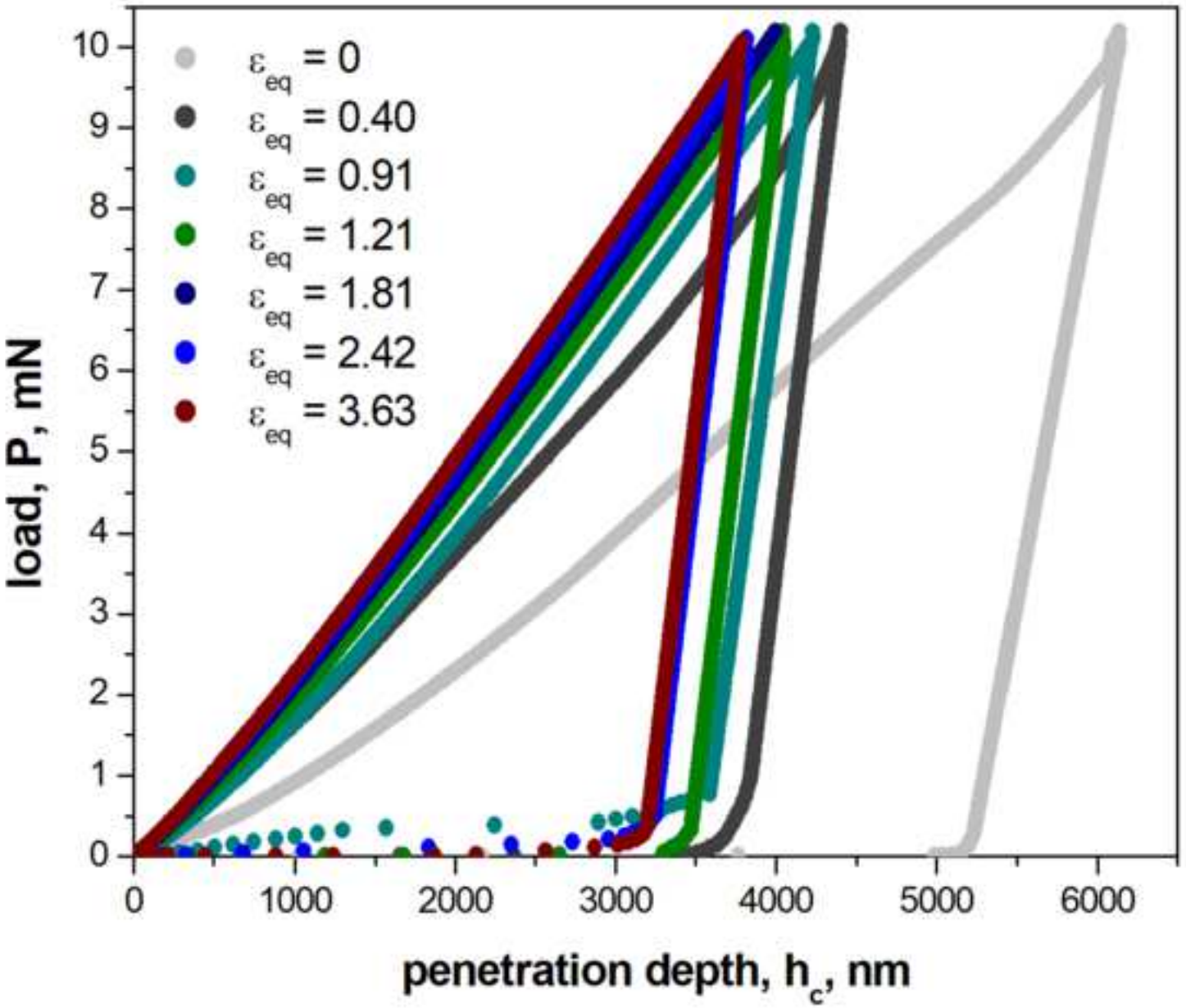

Figure 6

Click here to download high resolution image

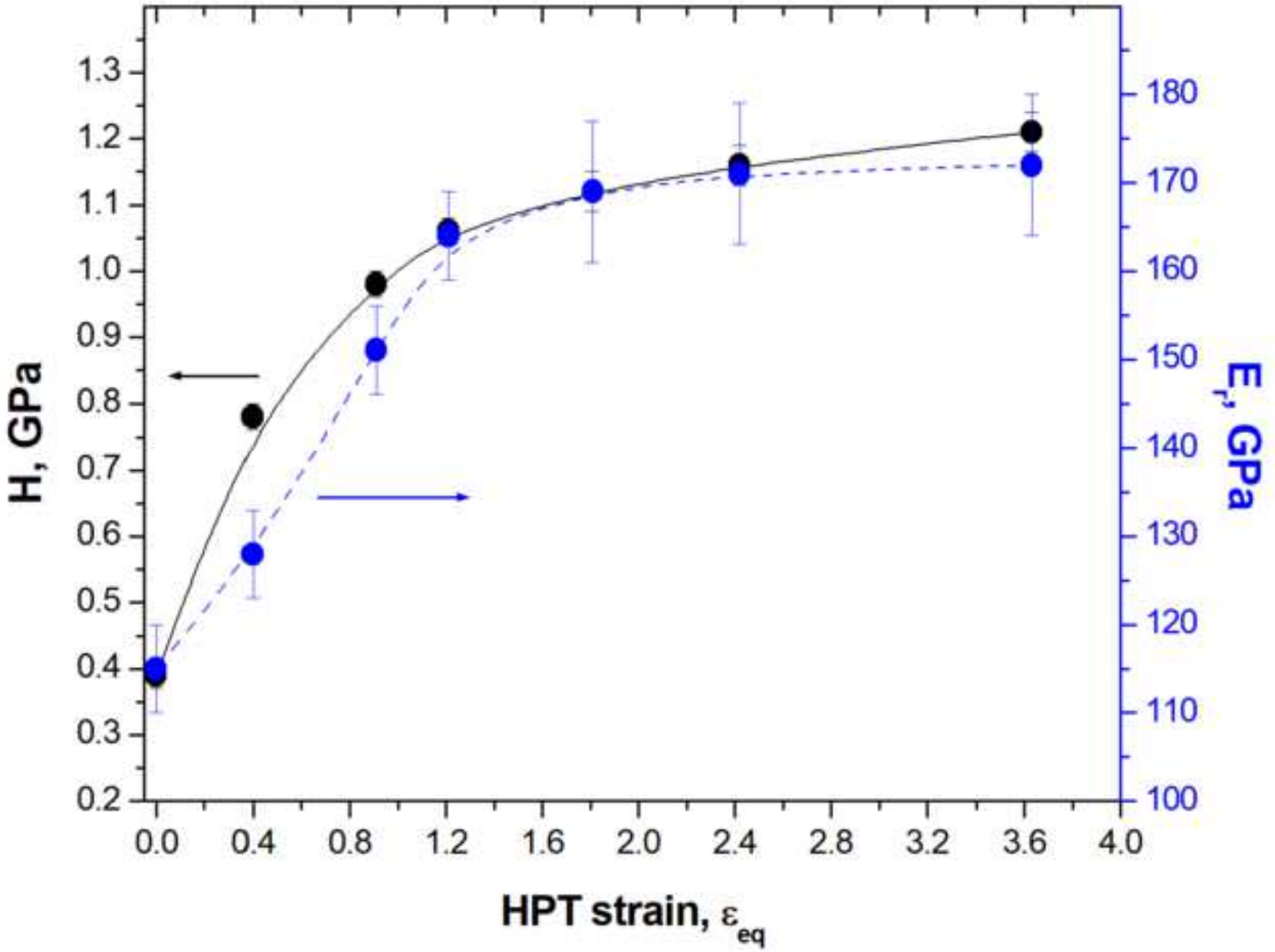

Figure 7

Click here to download high resolution image

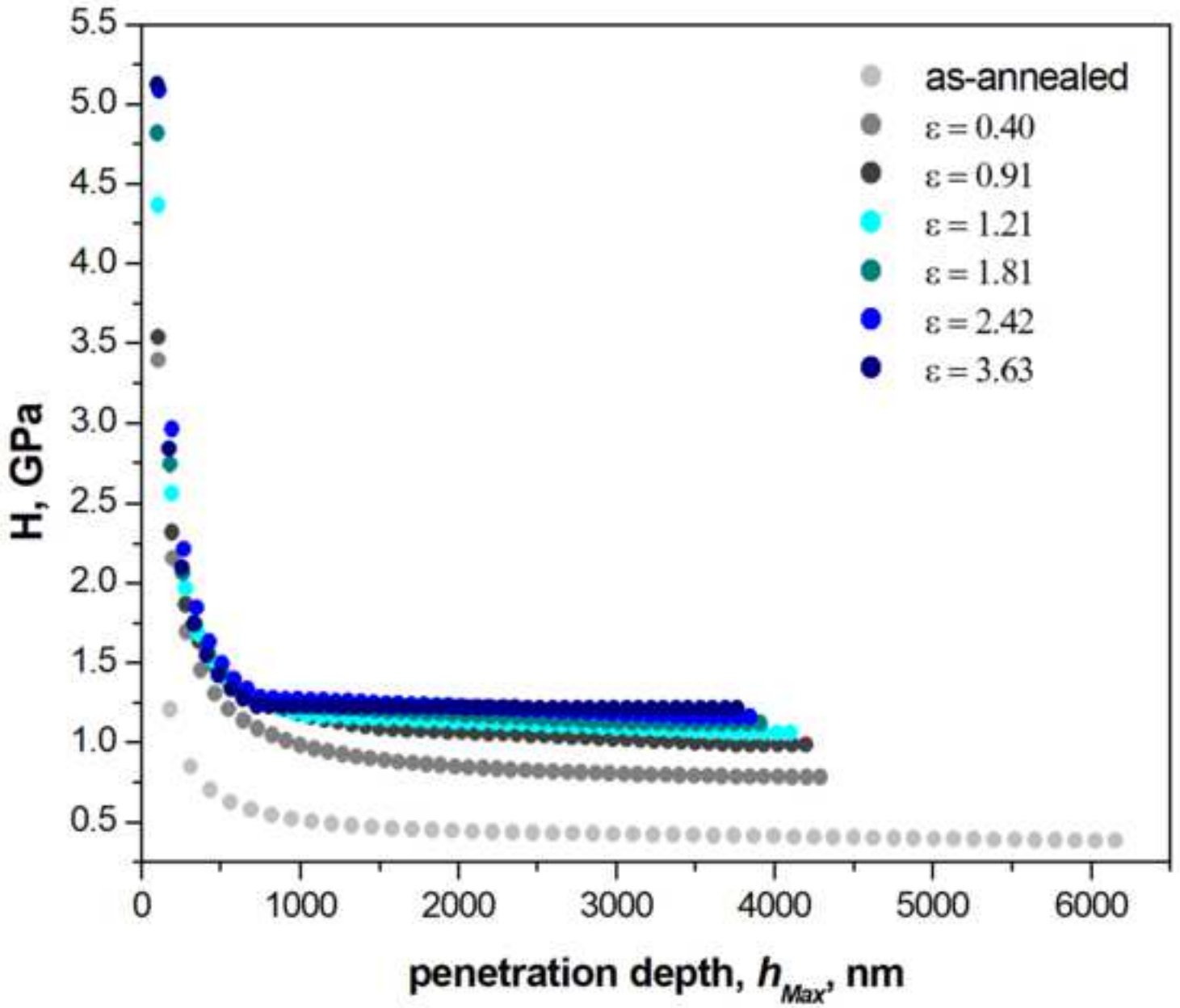

Figure 8

Click here to download high resolution image

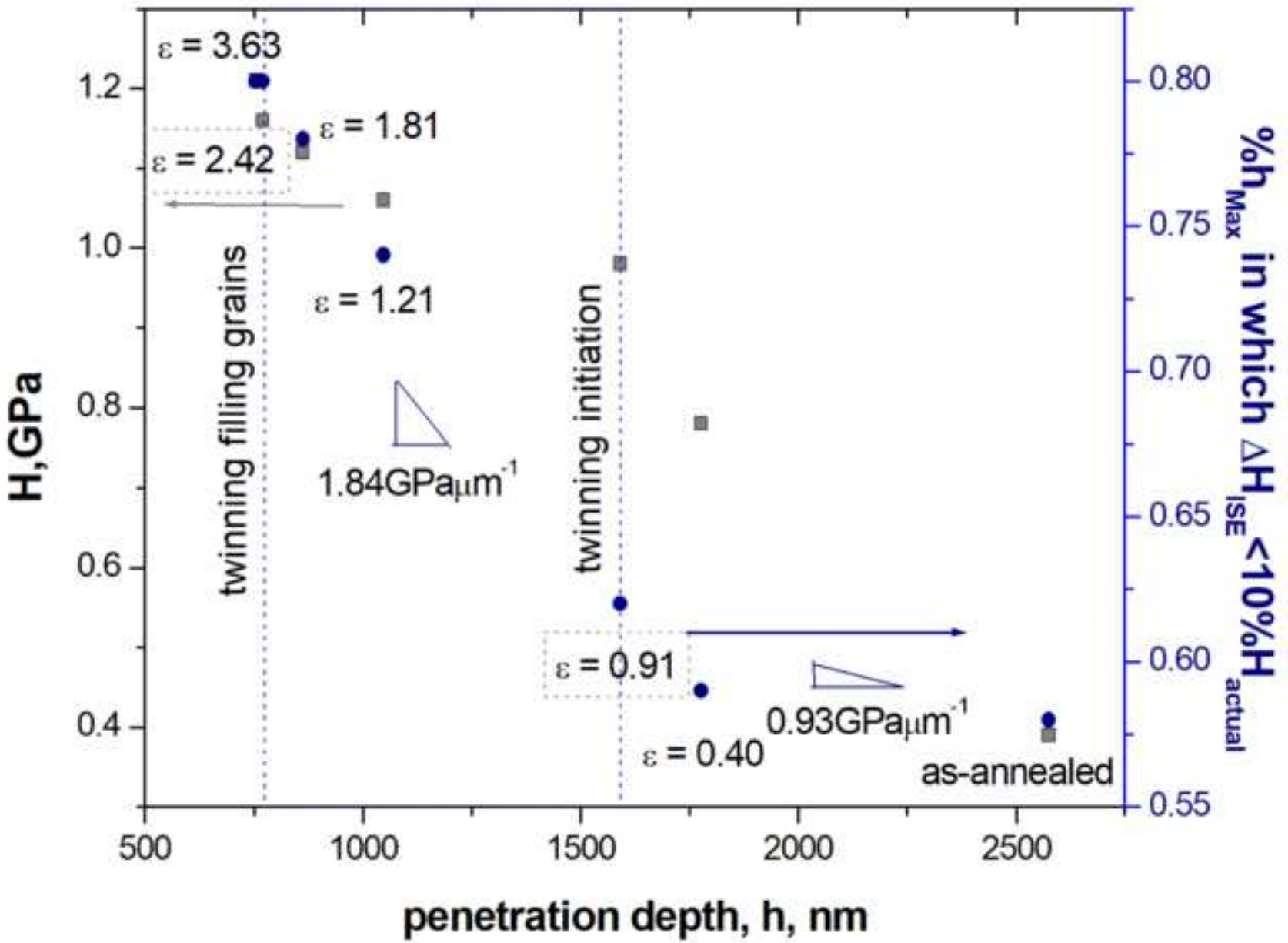

Figure 9

Click here to download high resolution image

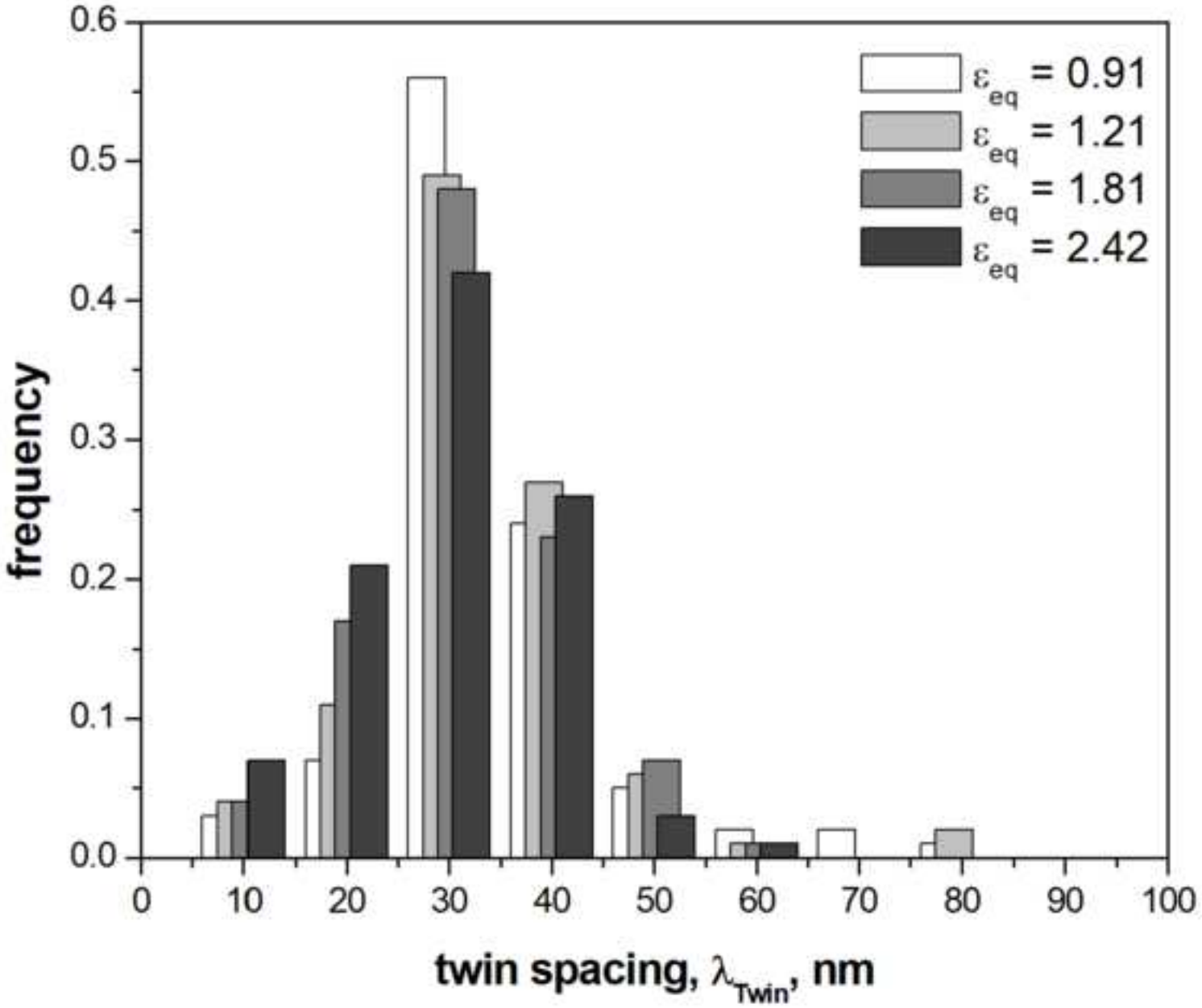

Figure 10

Click here to download high resolution image

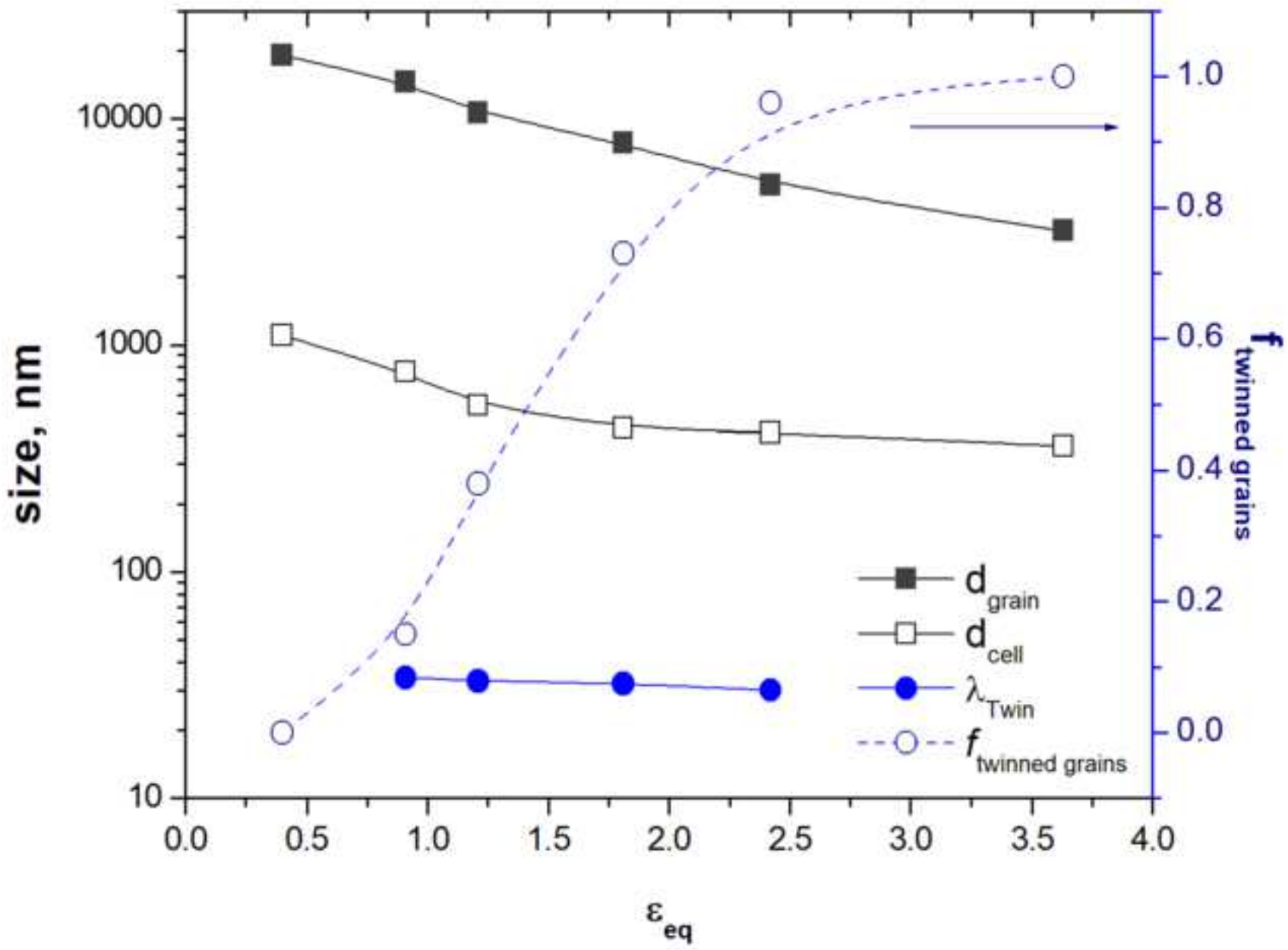

Figure 11
Click here to download high resolution image

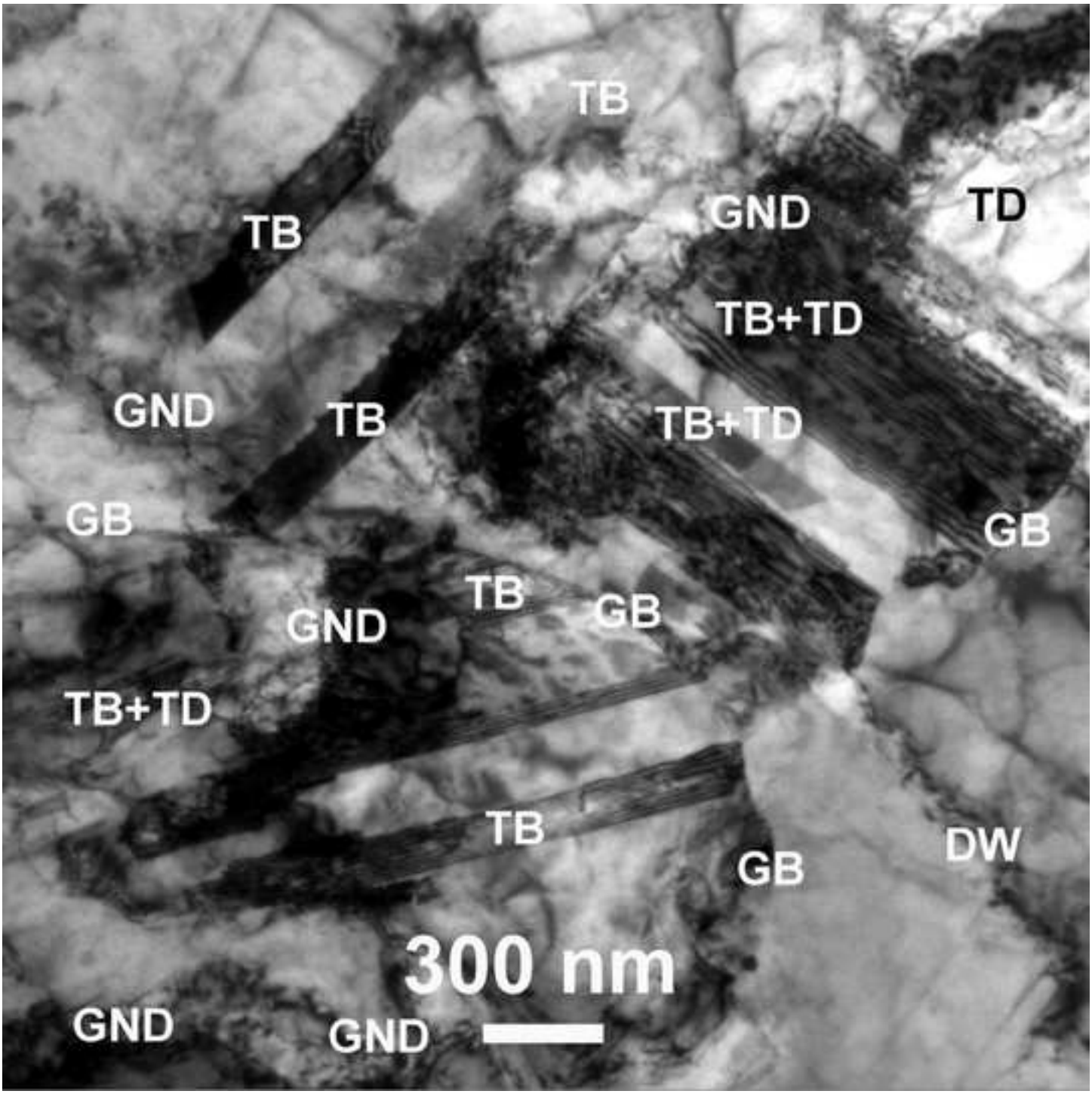

Table 1

Ag	Pb+S	Fe	O	P	Cd	Mn	others	Cu
2.2	2.2	1.5	0.5	0.4	0.2	0.05	0.9	99992

Table 1. Chemical composition of the OFHC 99.99% purity copper (wt.%x1000), as reported by the supplier (purity standard identified as DIN1706-NFA51050 / CuC1, source FRW™).

Table 2

	rotational angle, θ°, and number of turns, (N)					
	20 (1/18)	45 (1/8)	60 (1/6)	90 (1/4)	120 (1/3)	180 (1/2)
ε_{eq}	0.40	0.91	1.21	1.81	2.42	3.63

Table 2. Equivalent strain ε_{eq} obtained by the different HPT experimental parameters at N = 1/18 (lowest) to 1/2 turns (highest), at radial distances r = 2 mm (almost mid-radius) from disc thick-center.

Table 3

	ε_{eq}					
cell / grain mean size	0.40	0.91	1.21	1.81	2.42	3.63
d_g, µm	19 ± 1	14.5 ± 0.5	10.6 ± 0.5	7.8 ± 0.5	5.1 ± 0.5	3.2 ± 0.4
d_{cell}, nm	1100 ± 100	760 ± 50	540 ± 50	430 ± 40	410 ± 40	360 ± 30

Table 3. Mean grain, d_g, and cell size, d_{cell}, of OFHC CU subjected to HPT at ε_{eq} = 0.40 to 3.63. These mean values were determined out of 3 different areas of the TEM thin discs accounting of some 0.56-to-0.74 mm^2 per each experimental condition.

Table 4

Table 4. Dislocation density and dislocation wall volume fraction, *f*, for ε_{eq} = 0.40-to-3.63.

dislocation data measured by TEM	ε_{eq} = 0.40	ε_{eq} = 0.91	ε_{eq} = 1.21	ε_{eq} = 1.81	ε_{eq} = 2.42	ε_{eq} = 3.63
ρ_{wall} , 10^{12} m^{-2}	105 ± 10	130 ± 20	165 ± 20	225 ± 30	295 ± 30	330 ± 30
f (wall), 10^{-2}	4	6	7	7	5	5
ρ_{TD} , 10^{12} m^{-2}	25 ± 5	35 ± 5	40 ± 5	65 ± 10	70 ± 10	60 ± 10
ρ_{GND} , 10^{12} m^{-2}	95 ± 5	110 ± 5	120 ± 10	115 ± 10	120 ± 10	110 ± 10

Table 5

Table 5. Yield stress as calculated by the model of Eq. (5), σ_y^{model}, and as derived from the nanoindentation Hardness measurements, $\sigma_y^{nanoind}$. In this latter case, two different approaches are here proposed, one according to [**21**] in which a factor of $\chi = 2.9$ was considered as H to σ_y ratio; a second according to [**82**] in which the ratio $\chi = 3.5$. Data refers to $\varepsilon_{eq} = 0.40$, 0.91, 1.21, 1.81, 2.42, and 3.63.

yield stress, MPa	$\varepsilon_{eq} = 0.40$	$\varepsilon_{eq} = 0.91$	$\varepsilon_{eq} = 1.21$	$\varepsilon_{eq} = 1.81$	$\varepsilon_{eq} = 2.42$	$\varepsilon_{eq} = 3.63$
σ_y^{model}	217	237	256	288	324	362
$\sigma_y^{nanoind}(\chi = 2.9)$ [**21**]	269	338	366	386	400	417
deviation ($\chi = 2.9$), %	19	30	30	26	19	13
$\sigma_y^{nanoind}(\chi = 3.5)$ [**82**]	223	280	303	320	331	346
deviation ($\chi = 3.5$), %	3	18	18	11	2	5

Table 6

Table 6. Gao's model of Eq. (6) applied to the microstructure strengthening model of the present study at ε_{eq} = 0.40, 0.91, 1.21, 1.81, 2.42, and 3.63.

yield stress, MPa	ε_{eq} = 0.40	ε_{eq} = 0.91	ε_{eq} = 1.21	ε_{eq} = 1.81	ε_{eq} = 2.42	ε_{eq} = 3.63
σ_y^{model}	217	237	256	288	324	362
σ_y (Gao'smodel)	281	325	337	351	362	376
deviation, %	23	27	24	18	10	4

***Credit Author Statement**

Credit author statement

Marcello Cabibbo: Conceptualization, Methodology, Microscopy and Nanoindentation investigations, Data curation, Manuscript preparation, Validation, Reviewing and Editing,

Highlights

- OFHC pure Cu was subjected to low-strain levels by HPT;
- A minimum necessary HPT strain to induce twin formation was identified;
- Nanometric-scale twin width influenced the occurrence of nanoindentation ISE;
- TEM-based strengthening model was compared to σ_y as determined by nanoindentation;
- The ratio $\chi = H_V/\sigma_y$ was discussed.

***Declaration of Interest Statement**

Declaration of interests

☒ The authors declare that they have no known competing financial interests or personal relationships that could have appeared to influence the work reported in this paper.